NRL Memorandum Report 3077

Localization and Dynamics Determinations over Spherical Surfaces

ALBERT A. GERLACH

Advanced Projects Group
Acoustics Division

June 1975

NAVAL RESEARCH LABORATORY
Washington, D.C.

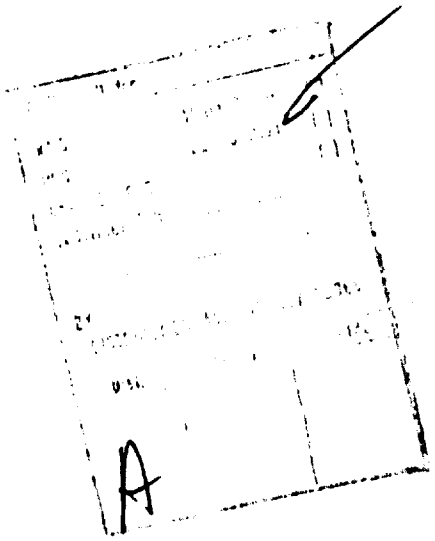
A

SECURITY CLASSIFICATION OF THIS PAGE (When Data Entered)

REPORT DOCUMENTATION PAGE

READ INSTRUCTIONS BEFORE COMPLETING FORM

1. REPORT NUMBER: NRL Memorandum Report 3077
2. GOVT ACCESSION NO.
3. RECIPIENT'S CATALOG NUMBER

4. TITLE (and Subtitle): LOCALIZATION AND DYNAMICS DETERMINATIONS OVER SPHERICAL SURFACES
5. TYPE OF REPORT & PERIOD COVERED: An interim report on a continuing NRL problem.
6. PERFORMING ORG. REPORT NUMBER

7. AUTHOR(s): Albert A. Gerlach
8. CONTRACT OR GRANT NUMBER(s)

9. PERFORMING ORGANIZATION NAME AND ADDRESS: Naval Research Laboratory, Washington, D.C. 20375
10. PROGRAM ELEMENT, PROJECT, TASK AREA & WORK UNIT NUMBERS: NRL Problem S01-61; ARPA Order-2275

11. CONTROLLING OFFICE NAME AND ADDRESS: Defense Advanced Research Projects Agency, Arlington, VA 22209
12. REPORT DATE: June 1975
13. NUMBER OF PAGES: 93

14. MONITORING AGENCY NAME & ADDRESS (if different from Controlling Office)
15. SECURITY CLASS. (of this report): Unclassified
15a. DECLASSIFICATION/DOWNGRADING SCHEDULE

16. DISTRIBUTION STATEMENT (of this Report)

Approved for public release; distribution unlimited.

NRL-S01-61

17. DISTRIBUTION STATEMENT (of the abstract entered in Block 20, if different from Report)

DDC AUG 9 1975 D

18. SUPPLEMENTARY NOTES

19. KEY WORDS (Continue on reverse side if necessary and identify by block number)

Position (location)
Tracking
Navigation
Motional dynamics
Surveillance
Spherical geometry
Analysis

20. ABSTRACT (Continue on reverse side if necessary and identify by block number)

Algorithms providing the location and dynamics (course and speed) of a moving vehicle are derived for application to navigation and localization systems on a global basis. The basic measures, used for computing the location and vehicle dynamics, are obtained from signals propagated over great-circle paths between the vehicle in question and two (or more) pairs of receiving sensors. The measured signal parameters are the time register (or time delay) and the time scale-factor (or doppler) shift, between pairs of receiving sensors.

(Continues)

DD FORM 1 JAN 73 1473 EDITION OF 1 NOV 65 IS OBSOLETE
S/N 0102-014-6601

SECURITY CLASSIFICATION OF THIS PAGE (When Data Entered)

20. Abstract (Continued)

Algorithms and graphs are presented to further provide the resolution in localization and vehicle dynamics achievable for any given system geometry. These resolution (or error) data are given in terms of the resolution in the basic measures of time register and time scale-factor shift. The central idea of the report is to provide, in convenient and usable form, algorithms and data which yield on a global-system basis the location and the dynamics of a transiting vehicle and the confidence limits for these parameters.

Examples are provided for both electromagnetic signal propagations and underwater acoustic propagations to illustrate the feasibility and broad applicability of the resulting data. Optimum and near optimum system geometries are derived for both a worldwide global navigation system and for a more limited surveillance area. The results indicate that a high degree of resolution in both localization and dynamics is achievable over extremely long ranges, provided reliable propagation conditions exist. An interesting aspect of the spherical geometry is that it provides a natural propagation convergence zone on the opposite side of the globe from the signal source. This phenomena results in localization and dynamics resolutions at extremely long ranges which are equivalent to the resolutions achievable in the near sensor field.

It is concluded that fully automatized signal-processing implementations for the precise navigation or localization and tracking of air, sea, and land vehicles on a global scale is realizable in the near future.

CONTENTS

PAGE

List of Illustrations v
List of Tables vi

I. INTRODUCTION AND SUMMARY 1

1.0 INTRODUCTION 1
2.0 BASIC SYSTEM CONCEPT 2
3.0 DISCUSSION AND SUMMARY 3
4.0 CONCLUDING REMARKS 6

II. SOURCE LOCALIZATION OVER SPHERICAL SURFACES 7

1.0 PROBLEM FORMULATION FOR A RECEIVING SENSOR PAIR . . . 7
1.1 Fundamental Equations 9
1.2 Polynomial Equations in χ 10
2.0 PROBLEM SOLUTION FOR A RECEIVING SENSOR PAIR 11
2.1 General Algorithms. 11
2.2 Sign Determination 15
2.3 Divisions of Symmetry 16
3.0 PROPERTIES OF THE SOLUTION 17
3.1 Longitudinal Alignment of the Sensors 17
3.2 Equatorial Alignment of the Sensors 23
4.0 SOURCE LOCALIZATION ALGORITHMS 26
4.1 Simultaneous Equations 26
4.2 General Approaches to the Solution 27
4.3 Iterative Algorithm 28

III. SOURCE DYNAMICS DETERMINATION OVER SPHERICAL SURFACES . . . 30

1.0 PROBLEM FORMULATION FOR A RECEIVING SENSOR PAIR . . . 30
2.0 DETERMINATION OF THE PROPAGATION VECTORS 32
3.0 SOURCE DYNAMICS ALGORITHMS 35

IV. RESOLUTION IN SOURCE LOCALIZATION 38

1.0 PROBLEM FORMULATION FOR A RECEIVING SENSOR PAIR . . . 38
1.1 Fundamental Equations 38
1.2 Graphical Interpretation of the Error Vector . . 40
2.0 SOLUTION OF THE BASIC ERROR EQUATIONS 40
2.1 General Solution 40
2.2 Solution for Small θ_x 42
3.0 TRANSFORMATION OF THE COORDINATE FRAME OF REFERENCE . 43
3.1 Transformation Equations 43
3.2 Solution for the Parameter μ 44
4.0 SOLUTION OF THE ERROR VECTOR FOR A RECEIVING SENSOR PAIR 46
4.1 Near (and Convergent Zone) Field Solution 46
4.2 Far Field Solution 48

PAGE

5.0 SOURCE LOCALIZATION ERROR ALGORITHMS 51
5.1 General Description of the System Geometry . . . 51
5.2 Error Vector Data Abstraction 54
5.3 Construction of the Localization Error Parallelogram 54
6.0 EXAMPLES OF THE USE OF THE LOCALIZATION ERROR DATA . . 57
6.1 Electromagnetic Localization Applications 57
6.2 Underwater Acoustic Localization Applications . . 59
7.0 OPTIMUM LOCALIZATION RESOLUTION SYSTEMS. 61
7.1 Channel Navigation Applications 62
7.2 Global Navigation Applications 63

V. RESOLUTION IN SOURCE DYNAMICS 65

1.0 BASIC RELATIONS 65
1.1 Source Velocity Relation 65
1.2 Source Heading Relation 66
2.0 RELATIONS EXPRESSED IN INTERPRETABLE FORM 66
2.1 Definition of Geometric Parameters 67
2.2 Dynamic Error Relations 68
2.3 Properties of the Dynamic Error 70
3.0 DYNAMIC ERROR MEASURE STATISTICS 71
3.1 Probability Density Function for the Dynamic Error Measures 71
3.2 Standard Deviation of the Dynamic Error Measures 72
3.3 Properties of the Standard Deviations 72
4.0 EXAMPLES OF THE USE OF THE DYNAMIC ERROR DATA 81
4.1 Electromagnetic Source Applications 82
4.2 Underwater Acoustic Applications. 83
5.0 OPTIMUM DYNAMICS RESOLUTION SYSTEMS. 85

ILLUSTRATIONS

Fig. No.		Page
1	Geometry of the Two Sensor Problem	7
2	Graphical Plot of the Near Field Solution for $\theta_x \ll 1$	21
3	Graphical Plot of the Far Field Solution for $\theta_x \ll 1$	22
4	Solution of θ as a Function of ϕ for $\theta_x = 30°$	24
5	Vector Geometry of the Problem	31
6	Graphical Plot of the Error Magnitude for the Near (and Convergence Zone) Field	49
7	Graphical Plot of the Angle α_u for the Near (and Convergence Zone) Field	50
8	Graphical Plot of the Error Magnitude for the Far Field	52
9	Graphical Plot of the Angle α_u for the Far Field	53
10	Determination of the Localization Error Geometry from the System Geometry and Error Vectors	55
11	Dependence of Localization Resolution on the Angle φ	58
12	Geometric Diagram Illustrating the Significant Parameters Involved in the Source Dynamics Error Relations	69
13	Graphical Plot of the Source Dynamics Standard Deviations (b=1.0)	75
14	Graphical Plot of the Source Dynamics Standard Deviations (b=0.866)	76
15	Graphical Plot of the Source Dynamics Standard Deviations (b=0.707)	77
16	Graphical Plot of the Source Dynamics Standard Deviations (b=0.50)	78
17	Graphical Plot of the Source Dynamics Standard Deviations (b=0.316)	79
18	Optimum Sensor Geometry for a Localized Area Coverage	86

TABLES

Table No.		Page
1	Interrelations Between Variables	44
2	Results of Three EM Localization Examples	60
3	Results of Three Underwater Acoustic Localization Examples	61
4	Interpretation of Abscisa Scales on the Accompanying Graphs	74
5	Results of Four EM Dynamics Examples	83
6	Results of Four Underwater Acoustic Dynamics Examples	84

LOCALIZATION AND DYNAMICS DETERMINATIONS OVER SPHERICAL SURFACES

I
INTRODUCTION AND SUMMARY

1.0 INTRODUCTION

Navigation or localization of a transiting vehicle over a wide expanse of the earth's surface has been a problem of interest to man since the beginning of recorded history. Over the years, new techniques for this purpose have been employed as the relevant technology advanced. At the present time, technology is sufficiently advanced to permit localization on a global scale to well within one square mile, using energy sensors (or transmitters) far removed from the point under surveillance. The major problems, today, consist not in seeking new technology but, in determining how to most effectively utilize the available technology, and in establishing and improving the reliability of any advanced navigation or localization and tracking system.

In the subject paper we shall address the navigation or localization and tracking problem from the standpoint of exploiting the signal properties of long range propagations which travel over, essentially, great circle paths between an unknown location on the surface of a sphere (presumably the earth) and several known locations on the same sphere. The approach to be taken, in the subject analyses, is to postulate a source emanating signal energy from the unknown point in question, and assume that the signal is being received and processed at several receiving sensors whose locations are precisely known. Under these circumstances, the basic information about the source is remote from the unknown point in question. When approached from this standpoint, the problem is usually termed localization. The problem is, however, fully reversible. That is, the same analysis is applicable to the situation where a common source signal is transmitted from some several precisely known locations and received at the unknown point in question. In this latter case, the information is available at the point in question to determine its own location. Under such a situation, the self-localization determination is generally termed as navigation. Thus, from a purely theoretical standpoint, the problem of localization and navigation can

Note Manuscript submitted May 29, 1975

be considered reversible. And the results of the analyses to be presented in this paper will be applicable to either the remote localization and tracking of an unknown located signal source, or to the navigation (self-localization) of a vehicle transiting the surface of the sphere. The reversible feature comes about as a result of interchanging the role of transmitting source and receiving sensors.

2.0 BASIC SYSTEM CONCEPT

The basic navigation or localization concept, as studied in the subject paper, consists of exploiting the signal measures of time register, τ, and time scale-factor shift, b, between several known signal locations. Consider, if you will, a signal emanating from a moving source and propagating over great circle paths to several fixed receiving stations. In principle, the signal received at the various fixed stations will be identical except for two possible factors. The one factor is; the received signals may be out of time register (translated in time with respect to each other) depending on the difference in great circle range (between the source and the several receiving stations) and the velocity of signal propagation in the medium. Thus, if one can consider that the average signal propagation velocity is constant and known, the measure of the time register (time shift) between the signals received at two receiving stations will provide a measure of the difference in great circle range between the two receiving stations and the source. And, as will be shown later, the acquisition of two such time register measures (from two pairs of receiving stations) is sufficient (in a practical sense) to uniquely locate the source on the surface of the sphere.

The second factor (or difference in the temporal structure of the signals received at the several receiving stations) is a difference in time scale-factor. This difference in signal structure will result when the motional range-rate of the source, (along the great circle rays emanating from the source to the receiving stations) is different. The resulting time scale-factor difference is manifested as a slight time compression (or expansion) of the one signal relative to the other. This slight shift in time scale factor results in what is commonly termed a "doppler" shift, when the signal in question is very narrow banded in its

power spectrum. Thus, if one measures the time scale-factor (or doppler) shift between the signals received at two receiving stations, he will have a measure of the difference in range-rate of the source along the two rays emanating from the source to the two receiving stations. And, as will be shown later, the acquisition of two such time scale-factor shift measures (from two pairs of receiving stations) is sufficient to uniquely determine the source dynamics (heading and speed).

The above concept, for determining localization and dynamics information on the transiting vehicle, is realizable and has been implemented in a number of specific applications over generally relatively short ranges. A variety of techniques are available to the system designer for achieving the measures of time register, τ, and time scale-factor shift, δ, for a given application. Depending on the characteristics of the transmitted signal and the methods of achieving the τ and δ measures, there will exist an inherent resolution in the measure of these critical parameters. That is, in a "real-life" situation, there will always exist some fundamental limit on the accuracy with which the time-register measure, τ, and the time scale-factor shift measure, δ, can be relied upon. And, this accuracy (or resolution) in the measures of τ and δ is generally known to a reasonable degree of precision. It is the effect of this imprecision (in the measure of τ and δ) on the accuracy of the computed source localization and dynamics which is of great interest to the system designer.

In the subject paper, we intend to exploit the use of time register measures and time scale-factor shift measures, between several receiving sensors, to determine the location and target dynamics (heading and speed) of an unknown signal source located on the surface of a sphere. In addition, we intend, further, to determine the accuracy (or resolution) of the resulting location, heading, and speed in terms of the (presumably) known errors (or standard deviations) in the measures of τ and δ. Such will be the object of the sections to follow.

3.0 DISCUSSION AND SUMMARY

The material to be presented is divided into four main sections to cover the four logical steps of; (1) source localization, (2) source dynamics determination, (3) localization resolution, and (4) dynamics

resolution. The four main sections are reasonably autonomous, and can be read in any order. However, as one might expect, the sections on resolution do build, somewhat, on the results from the earlier analyses.

The subject material is presented in a concise logical manner, in order to provide the reader with a thorough understanding of the underlying physical and/or geometric principles involved. Lengthy mathematical proofs and derivations are avoided, so as not to detract from the principal theme of the paper. The central idea of the paper is to provide, in convenient and usable form, algorithms and data which yield; (1) the location, (2) the dynamics, and (3) the confidence limits for these parameters, for a transiting vehicle over a global surface. The assumed system inputs are; (1) the precise locations of several receiving sensors, (2) the measures of the signal physics parameters τ and δ, and (3) the resolution of these signal physics parameters (standard deviation of the τ and δ measures). From the analysis and data provided, one will also be able to synthesize a system geometry which will be optimum for navigation, or localization and tracking, in a specified region of the globe.

In the first two sections (Sections II and III), the algorithms are developed for; first, the source location, and then the source dynamics (heading and speed). These are given in terms of the known locations of the fixed sensor positions, and the measured values of time register, τ, or time scale-factor shift, δ. A number of graphs are presented which display the significant geometric properties of the problem. In this way, the reader may obtain an insight into the way in which the system geometry influences the computed source location and dynamics results.

In the later two sections (Sections IV and V), algorithms and data are developed which provide the measures of confidence that can be placed in the earlier computations. These are given in terms of the system geometry and the resolution (or standard deviation) in the measures of τ and δ. A number of graphs are provided; whereby, one may quickly ascertain the confidence in the computed source location and dynamics. In effect, one may readily construct a parallelogram about the computed source location;

within which, the source will be known to exist with a prescribed level of confidence. Also, the heading and speed of the source will be known within prescribed standard deviation limits.

Two interesting sidelights resulting from the subject analysis are worthy of special mention in this brief summary. The first of these concerns the fact that the spherical geometry results in a natural propagation convergence zone on the diametric opposite side of the globe from the source location. That is, rays emanating from the source and following great circle paths, will first diverge and then subsequently converge as the signal propagates around the globe. This leads to some very interesting results from the standpoint of accuracy in navigation or localization and dynamics determinations. Under normal circumstances, one would expect that; as a vehicle is located more and more remote from any measurement sensor configuration, the precision with which that vehicle can be located and its dynamics determined will degrade. And such is the case, up to the point where the vehicle is one-quarter of the distance around the globe from the sensor configuration. However, beyond this point, the navigation or localization and dynamics precision will start to improve again. This improvement will continue until the vehicle reaches the extreme far-field, on the opposite side of the globe from the sensor configuration. In this extreme far-field, the localization and dynamics resolution will be the same as if the vehicle were located in the image near-field of the sensor configuration. This convergence phenomenon has some very interesting practical implications. It implies that if we can achieve reliable propagation over the surface of the globe, we can very accurately determine the location, heading, and speed of a vehicle on the far side of the globe from a simple configuration of transmitters (in the case of navigation) or receiving sensors (in the case of localization and dynamics). Typical resolutions in localization and dynamics for several sensor configurations are given in the examples discussed in Sections IV, 6.0 and V, 4.0.

The second interesting sidelight, resulting from the subject investigation, concerns the design of an optimum sensor (or transmitter) configuration for a global navigation system. It turns out that the localization and dynamics resolution can be minimized for a geometric configuration of transmitters located on three orthogonal globe axes over the surface of the sphere.

Thus, if reliable propagation can be achieved over the surface of the globe, optimum resolution in the navigation parameters is realizable. Also, over any given region of the globe's surface, a more confined geometry of sensors can be designed which will result in a resolution of the navigation parameters which is near optimum. Thus, over a limited area (such as an ocean basin) the geometric spacing of the sensors (or transmitters) need not be greater than the diameter of the area under surveillance. These optimum and near optimum configurations are discussed in some detail in Sections IV, 7.0 and V, 5.0.

4.0 CONCLUDING REMARKS

The global localization and dynamics study, presented in this report, represents an extension of techniques successfully employed over relatively short distances, assuming planar geometry. The results are relevant to a variety of applications in the general areas of navigation and localization and tracking from remote sensor configurations. The basic measures are readily derived from the signal structure of energy transmissions which propagate over, essentially, great circle paths around the surface of the globe. As such, the results are applicable to both underwater accustic propagations, and to the lower frequency electromagnetic emissions which follow (or are ducted around) the surface of the earth. Current technology is amenable today, to realize both; (1) the time register and time scale-factor measurement aspects, and (2) the automatic computational aspects, of a precise global navigation or localization and tracking system. There remains to be investigate in some detail, the deleterious effects of certain long range propagation anomalies which may degrade system performance over that predicted under more idealized conditions. It can be concluded that fully automatized signal processing implementations for the precise navigation or localization and tracking of air, sea, and land vehicles on a global scale is realizable in the near future.

II

SOURCE LOCALIZATION OVER SPHERICAL SURFACES

In this section, we shall develop the algorithms for the localization of an emitter source whose location on a spherical surface (presumably the surface of the earth) is unknown. In the analyses to follow, it shall be assumed that the source is emitting energy which propagates in great circle paths over the spherical surface, and which is detectable at two (or more) pairs of receiving sensors whose positions on the surface of the sphere are precisely known. For convenience, the spherical surface shall be assumed to be the earth, and all location coordinates shall be given in angular units of North Latitude and West Longitude.

1.0 PROBLEM FORMULATION FOR A RECEIVING SENSOR PAIR

Consider that a signal source is located on the surface of a sphere at location (θ_o, ϕ_o), and that a pair of receiving sensors are detecting the source signal at known locations (θ_x, ϕ_x) and (θ_y, ϕ_y). The geometry of the problem is illustrated in Figure 1.

In the subject problem, it will be assumed that the two sensor stations, x and y, can measure the time register (or time difference in arrival) between the source signals which arrive at the two receiving stations. Under these circumstances, and with a-priori knowledge of the signal propagation velocity, the range difference ΔR_{yx} is readily determined as,

$$\Delta R_{yx} = R_y - R_x = c\tau_{yx} \tag{1-1}$$

where,

- ΔR_{yx} is the great circle range difference between the source to the y receiving station and the source to the x receiving station
- R_x = R_{ox} is the great circle range from the source to the x receiving station
- R_y = R_{oy} is the great circle range from the source to the y receiving station
- τ_{yx} is the time difference in signal propagation between the R_y path and the R_x path
- c is the mean signal propagation velocity over the great circle paths

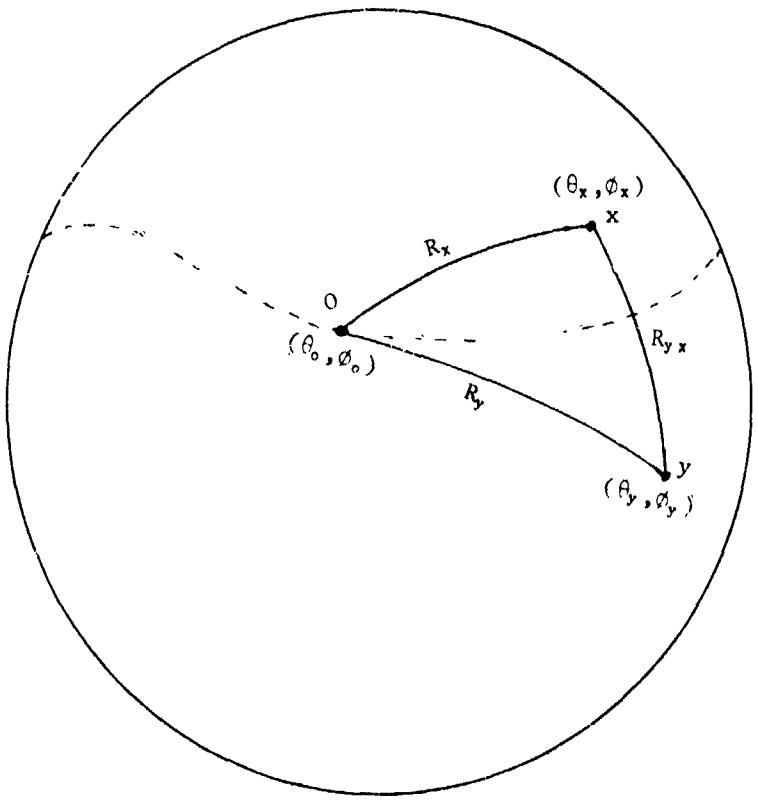

FIG. 1 GEOMETRY OF TWO SENSOR PROBLEM

Since, now, R_x and R_y will be a function of the two unknown variables, θ_o and ϕ_o, a unique solution to the source location will not be possible by a simple measure of ΔR_{yx} (or τ_{yx}). What equation (1-1) provides is a locus of points (or curve) over the surface of the sphere; such that, a signal source located anywhere on the curve would provide the measure τ_{yx}. That is, the indicated curve maps out the locus of points on the surface of the sphere where the great circle range difference, ΔR_{yx} is constant. (This curve is depicted in Fig. 1 as a dashed line.) To obtain a unique solution for the source location, two such pairs of receiving sensor stations will be required. Each pair will provide a locus of points (curve) over the surface of the sphere, indicative of the time register measure. The location of the source will be the point where the two curves intersect. (NOTE: Since, in fact, the two curves will intersect at two points on the surface

of [illegible]ere, [illegible]ty does exist. However, practical considerations c[illegible]rally be employed to rule out one of the two points in a real-life [illegible]stion.)

1.1 Fundamental Equations:

The equation which describes the relevant curve for a given measure of ΔR_{yx} (between the two sensor locations x and y) may take a variety of forms. We shall now derive several of these forms which provide a reasonably clear insight into the physical geometry of the problem.

It can readily be shown that the chord or straight line distance between two arbitrary points, (θ_1,ϕ_1) and (θ_2,ϕ_2) on the surface of a sphere, may be expressed as,

$$R_{12} = 2\rho\sqrt{\tfrac{1}{2}[1-\sin\theta_1\sin\theta_2-\cos\theta_1\cos\theta_2\cos(\phi_1-\phi_2)]}$$

$$= 2\rho\sqrt{\sin^2\tfrac{1}{2}(\theta_1-\theta_2)\cos^2\tfrac{1}{2}(\phi_1-\phi_2)+\sin^2\tfrac{1}{2}(\theta_1+\theta_2)\sin^2\tfrac{1}{2}(\phi_1-\phi_2)}$$

$$= 2\rho\sin\tfrac{1}{2}\Psi_{12} \qquad (1\text{-}2)$$

where,

R_{12} is the chord length between points (θ_1,ϕ_1) and (θ_2,ϕ_2) on the surface of the sphere

ρ is the radius of the sphere

Ψ_{12} is the angle subtending the two vectors which emanate from the center of the sphere to the two points in question

and where all θ's and all ϕ's are expressed in angular units of Latitude and Longitude respectively.

For convenience, we shall define a new variable, χ, as follows. Let,

$$\chi_{12}(\theta_1,\phi_1;\theta_2,\phi_2) = \tfrac{1}{2}[1-\sin\theta_1\sin\theta_2-\cos\theta_1\cos\theta_2\cos(\phi_1-\phi_2)]$$

$$= \sin^2\tfrac{1}{2}(\theta_1-\theta_2)\cos^2\tfrac{1}{2}(\phi_1-\phi_2)+\cos^2\tfrac{1}{2}(\theta_1+\theta_2)\sin^2\tfrac{1}{2}(\phi_1-\phi_2)$$

$$= \sin^2\left[\tfrac{1}{2}\Psi_{12}(\theta_1,\phi_1;\theta_2,\phi_2)\right] \qquad (1\text{-}3)$$

It will also prove convenient to define two parameters, μ and λ as follows. Let,

$$\left.\begin{aligned} \mu_{yx} &= \frac{\Delta R_{yx}}{R_{yx}} = \frac{c\tau_{yx}}{\rho \sin^{-1}\sqrt{\chi_{xy}}} \\ \text{and,} \quad \lambda_{yx} &= \sin(\mu_{yx}\sin^{-1}\sqrt{\chi_{xy}}) = \sin(c\tau_{yx}/2\rho) \end{aligned}\right\} \tag{1-4}$$

Since $|\Delta R_{yx}|$ will, necessarily, be less than or equal to R_{yx}, the value of μ will range over $-1 \leq \mu \leq 1$.

From (1-2), it is evident that the great circle range between any two points, (θ_1,ϕ_1) and (θ_2,ϕ_2), on the surface of the sphere will be,

$$R_{12}(\theta_1,\phi_1;\theta_2,\phi_2)=2\rho \sin^{-1}(R_{12}/2\rho)=2\rho \sin^{-1}\sqrt{\chi_{12}} \tag{1-5}$$

Using the above relations in (1-1), then, gives,

$$\Psi_y(\theta,\phi;\theta_y,\phi_y)-\Psi_x(\theta,\phi;\theta_x,\phi_x)=\mu_{yx}\Psi_{xy}(\theta_x,\phi_x;\theta_y,\phi_y) \tag{1-6}$$

or,

$$\sin^{-1}\left[\chi_y^{\frac{1}{2}}(\theta,\phi;\theta_y,\phi_y)\right]-\sin^{-1}\left[\chi_x^{\frac{1}{2}}(\theta,\phi;\theta_x,\phi_x)\right] = \mu_{yx}\frac{R_{xy}}{2\rho}$$

$$= \mu_{yx}\sin^{-1}\left[\chi_{xy}^{\frac{1}{2}}(\theta_x,\phi_x;\theta_y,\phi_y)\right] \tag{1-7}$$

1.2 Polynomial Equations in χ:

Although the equations given in (1-6) and (1-7) display the geometry of the problem in simple form, they are far too cumbersome for numerical analysis. By taking the sine of both sides of equation (1-7) and using the parameter λ defined in (1-4), the relation may be transformed to,

$$\sqrt{\chi_y(1-\chi_x)} - \sqrt{\chi_x(1-\chi_y)} = \lambda_{yx} \tag{1-8}$$

And by a further process of squaring and collecting terms, the resulting equation can be reduced to the following polynomial equation in χ_x and χ_y,

$$(\chi_y-\chi_x)^2-2\lambda_{yx}^2(\chi_x+\chi_y-2\chi_x\chi_y)+\lambda_{yx}^4 = 0 \tag{1-9}$$

or,

$$(\chi_y - \lambda_{yx}^2)^2 - 2(1-2\lambda_{yx}^2)\chi_x\chi_y + (\chi_x - \lambda_{yx}^2)^2 = \lambda_{yx}^4 \qquad (1\text{-}10)$$

The above equations are still implicit functions of the two variables θ and ϕ, but they are in a form suitable for the solution of θ as an explicit function of the variable ϕ.

2.0 PROBLEM SOLUTION FOR A RECEIVING SENSOR PAIR

The solution to equations (1-9) or (1-10) is rather involved and tedious; so that, the details will not be provided here. We shall be content to provide only the final results and demonstrate the use of these results in some specific examples which illustrate the general properties of the solution.

2.1 General Algorithms:

For the sake of simplicity the pertinent relations are given in a nested sequence of equations which start with the final format of θ expressed as a function of ϕ, and work backwards to the basic coefficients which are simple functions of the sensor location parameters (θ_x, ϕ_x) and (θ_y, ϕ_y).

2.1.1 Format of Solution: The general solution of the subject problem may be expressed as,

$$\theta = \tan^{-1}\left\{ \frac{\mathcal{J}_{xy}(\phi;\lambda_{yx}^2)}{\pm \lambda_{yx}\sqrt{\mathcal{K}_{xy}(\phi;\lambda_{yx}^2) - \mathcal{L}_{xy}(\phi;\lambda_{yx}^2)}} \right\} \qquad (2\text{-}1)$$

where the angles θ and ϕ are expressed in angular units of North Latitude and West Longitude respectively, and where λ_{yx} is defined in (1-4). In the subject application,

$$\chi_{xy} = \sin^2\tfrac{1}{2}(\theta_x - \theta_y)\cos^2\tfrac{1}{2}(\phi_x - \phi_y) + \cos^2\tfrac{1}{2}(\theta_x + \theta_y)\sin^2\tfrac{1}{2}(\phi_x - \phi_y) \qquad (2\text{-}2)$$

2.1.2 Functions of Longitude: The three basic functions of the angle ϕ, given in (2-1) are,

$$\mathfrak{F}_{xy}(\phi;\lambda^2_{yx}) = f_{s(x,y)}(\lambda^2_{yx})\sin^2\phi + 2f_{sc(x,y)}(\lambda^2_{yx})\sin\phi\cos\phi$$

$$+ f_{c(x,y)}(\lambda^2_{yx})\cos^2\phi - f_o(\lambda^2_{yx}) \qquad (2\text{-}3)$$

$$\mathfrak{G}_{xy}(\phi;\lambda^2_{yx}) = g_{s(x,y)}(\lambda^2_{yx})\sin\phi + g_{c(x,y)}(\lambda^2_{yx})\cos\phi \qquad (2\text{-}4)$$

$$\mathfrak{K}_{xy}(\phi;\lambda^2_{yx}) = h_{s(x,y)}(\lambda^2_{yx})\sin^2\phi + 2h_{sc(x,y)}(\lambda^2_{yx})\sin\phi\cos\phi$$

$$+ h_{c(x,y)}(\lambda^2_{yx})\cos^2\phi + h_{o(x,y)}(\lambda^2_{yx}) \qquad (2\text{-}5)$$

All of the coefficients of the trigonometric functions of ϕ, in the above expressions, are polynomial functions of the parameter, λ^2_{yx} .

2.1.3 Polynomial Function Coefficients: The sets of polynomial coefficients given in (2-3), (2-4), and (2-5) are,

$$\left.\begin{aligned} f_{s(x,y)}(\lambda^2_{yx}) &= A_{s(x,y)} + B_{s(x,y)}\lambda^2_{yx} \\ f_{c(x,y)}(\lambda^2_{yx}) &= A_{c(x,y)} + B_{c(x,y)}\lambda^2_{yx} \\ f_{sc(x,y)}(\lambda^2_{yx}) &= A_{sc(x,y)} + D_{(x,y)}\lambda^2_{yx} \\ f_o(\lambda^2_{yx}) &= \lambda^2_{yx}(1-\lambda^2_{yx}) \end{aligned}\right\} \qquad (2\text{-}6)$$

$$\left.\begin{aligned} g_{s(x,y)}(\lambda^2_{yx}) &= E_{s(x,y)} + F_{s(x,y)}\lambda^2_{yx} \\ g_{c(x,y)}(\lambda^2_{yx}) &= E_{c(x,y)} + F_{c(x,y)}\lambda^2_{yx} \end{aligned}\right\} \qquad (2\text{-}7)$$

$$\left.\begin{aligned} h_{s(x,y)}(\lambda^2_{yx}) &= G_{s(x,y)} + H_{s(x,y)}\lambda^2_{yx} - B_{s(x,y)}\lambda^4_{yx} \\ h_{c(x,y)}(\lambda^2_{yx}) &= G_{c(x,y)} + H_{c(x,y)}\lambda^2_{yx} - B_{c(x,y)}\lambda^4_{yx} \\ h_{sc(x,y)}(\lambda^2_{yx}) &= G_{sc(x,y)} + H_{sc(x,y)}\lambda^2_{yx} - D_{(x,y)}\lambda^4_{yx} \\ h_{o(x,y)}(\lambda^2_{yx}) &= J_{(x,y)} - K_{(x,y)}\lambda^2_{yx} + L_{(x,y)}\lambda^4_{yx} - \lambda^6_{yx} \end{aligned}\right\} \qquad (2\text{-}8)$$

where, the coefficients of the above polynomials in λ^2 are exclusive functions of the receiving sensor locations, (θ_x, ϕ_x) and (θ_y, ϕ_y).

2.1.4 Fixed Parameter Coefficients: Prior to giving the functional relations for the fixed parameter coefficients, the following fundamental parameters will be defined where all angles θ and ϕ are given in North Latitude and West Longitude coordinates. Let,

$$\left.\begin{aligned} M_{(x,y)} &= 1 - \sin\theta_x \sin\theta_y \\ N_{(x,y)} &= \tfrac{1}{2}(\sin\theta_x - \sin\theta_y) \\ P_{s(x,y)} &= \tfrac{1}{2}(\cos\theta_x \sin\phi_x - \cos\theta_y \sin\phi_y) \\ P_{c(x,y)} &= \tfrac{1}{2}(\cos\theta_x \cos\phi_x - \cos\theta_y \cos\phi_y) \end{aligned}\right\} \quad (2\text{-}9)$$

The coefficients of the polynomial functions given in (2-6), (2-7), and (2-8), are then,

$$A_{s(x,y)} = P^2_{s(x,y)} \quad (2\text{-}10)$$

$$A_{c(x,y)} = P^2_{c(x,y)} \quad (2\text{-}11)$$

$$A_{sc(x,y)} = P_{s(x,y)} P_{c(x,y)} \quad (2\text{-}12)$$

$$B_{s(x,y)} = \cos\theta_x \cos\theta_y \sin\phi_x \sin\phi_y \quad (2\text{-}13)$$

$$B_{c(x,y)} = \cos\theta_x \cos\theta_y \cos\phi_x \cos\phi_y \quad (2\text{-}14)$$

$$D_{(x,y)} = \tfrac{1}{2}\cos\theta_x \cos\theta_y \sin(\phi_x + \phi_y) \quad (2\text{-}15)$$

$$E_{s(x,y)} = N_{(x,y)} P_{s(x,y)} \quad (2\text{-}16)$$

$$E_{c(x,y)} = N_{(x,y)} P_{c(x,y)} \quad (2\text{-}17)$$

$$F_{s(x,y)} = \tfrac{1}{2}(\cos\theta_x \sin\theta_y \sin\phi_x + \sin\theta_x \cos\theta_y \sin\phi_y) \tag{2-18}$$

$$F_{c(x,y)} = \tfrac{1}{2}(\cos\theta_x \sin\theta_y \cos\phi_x + \sin\theta_x \cos\theta_y \cos\phi_y) \tag{2-19}$$

$$G_{s(x,y)} = M_{(x,y)} A_{s(x,y)} + N_{(x,y)} [2P_{s(x,y)} F_{s(x,y)} - N_{(x,y)} B_{s(x,y)}] \tag{2-20}$$

$$G_{c(x,y)} = M_{(x,y)} A_{c(x,y)} + N_{(x,y)} [2P_{c(x,y)} F_{c(x,y)} - N_{(x,y)} B_{c(x,y)}] \tag{2-21}$$

$$G_{sc(x,y)} = M_{(x,y)} A_{sc(x,y)} + N_{(x,y)} [P_{s(x,y)} F_{c(x,y)} + P_{c(x,y)} F_{s(x,y)} - N_{(x,y)} D_{(x,y)}] \tag{2-22}$$

$$H_{s(x,y)} = F^2_{s(x,y)} + M_{(x,y)} B_{s(x,y)} - A_{s(x,y)} \tag{2-23}$$

$$H_{c(x,y)} = F^2_{c(x,y)} + M_{(x,y)} B_{c(x,y)} - A_{c(x,y)} \tag{2-24}$$

$$H_{sc(x,y)} = F_{s(x,y)} F_{c(x,y)} + M_{(x,y)} D_{(x,y)} - A_{sc(x,y)} \tag{2-25}$$

$$J_{(x,y)} = N^2_{(x,y)} \tag{2-26}$$

$$K_{(x,y)} = M_{(x,y)} + J_{(x,y)} \tag{2-27}$$

$$L_{(x,y)} = 1 + M_{(x,y)} \tag{2-28}$$

The above, fixed parameter coefficients, are dependent only on the location of the fixed sensor receiving stations, and independent of both the source location and the measurement parameter λ. For any set of fixed sensor locations, x and y, the above parameters may be computed in advance and stored in memory. It is further easy to verify that, if $Q_{(x,y)}$ represents any of the parameters given in (2-10) through (2-28), then,

$$Q_{(x,y)} = Q_{(y,x)} \tag{2-29}$$

That is, the fixed parameter values are symmetric with respect to the location subscripts x and y. As a consequence, the subscripts, x and y, may be transposed without affecting the results.

With preknowledge of a set of receiving station locations, the fixed parameter coefficients can be computed and tabulated (or stored in computer memory) for any given sensor geometry.

2.2 Sign Determination

The function defined by (2-1) describes a family of curves for θ as a function of ϕ in angular coordinates of North Latitude and West Longitude. The family of curves is generated by reason of the measurement parameter λ . Thus, when λ is fixed at some specified value, equation (2-1) is expected to generate a single closed curve over the surface of the sphere. But it is evident that some ambiguity exists as a result of the "$\pm$ sign" in the denominator of equation (2-1). Unfortunately, this ambiguity cannot be resolved without placing some restrictions on the location of the two receiving sensor stations. This fact arises as a result of the possible bi-valued nature of the independent variable θ in (2-1). Consequently, some judgment will be required on the part of the user of the subject algorithms if they are to be applied in any physical application.

The basic property to look for (in a test for bi-valuedness) is to determine whether or not the function $\mathcal{N}_{xy}(\phi;\lambda^2)$ can become negative for some value of ϕ, after the value of λ is specified. If so, then bi-valuedness of θ is implied for those values of ϕ where $\mathcal{N}_{xy}(\phi;\lambda^2)$ is positive. If not, then θ will be a single valued function of ϕ (for the specified λ) and only either the "+ sign" or the "- sign" need be used in (2-1), with the selection of λ carrying its own "sign". To determine the appropriate "sign" to use, in this latter case, the following rule can be employed.

$$\text{for } \theta_x < \theta_y \text{ use the "+ sign"}$$

$$\text{for } \theta_y < \theta_x \text{ use the "- sign"} \qquad (2\text{-}30)$$

In the former case (where bi-valuedness for θ is indicated), both the "+ sign" and the "- sign" will need to be employed to describe the appropriate curve. The physical geometry of the sensor station locations, (θ_x,ϕ_x) and (θ_y,ϕ_y), will dictate over what range of the variable ϕ the appropriate curve will occur for a given choice of the parameter λ .

In general, when $|\phi_x-\phi_y| \ll |\theta_x-\theta_y|$, the subject family of curves will be single valued over much of the range of λ. On the other hand, when $|\theta_x-\theta_y| \ll |\phi_x-\phi_y|$, the subject family of curves will be bi-valued over much of the range of λ.

2.3 Divisions of Symmetry

Due to the physical geometry of the subject problem, the family of curves (over the surface of the sphere) described by (2-1), can be expected to exhibit symmetry about three mutually orthogonal planes which pass through the center of the sphere. These planes will intersect the surface of the sphere in great circles. One such great circle curve will pass through the two sensor locations (θ_x,ϕ_x) and (θ_y,ϕ_y). A second great circle of symmetry (orthogonal to the first) will bisect the great circle arc between the two sensor locations. The third great circle of symmetry will, of course, be unique in that it is orthogonal to the other two.

The equations for the great circles of symmetry are of interest and may be readily be derived, in the case of the first two.

2.3.1 Algorithm for the Great Circle Arc Passing Through Two Fixed Points, (θ_x,ϕ_x) and (θ_y,ϕ_y): It can readily be shown that the great circle curve which passes through two points, (θ_x,ϕ_x) and (θ_y,ϕ_y) is described by the following algorithm,

$$\theta = \tan^{-1}\left\{\frac{\tan\theta_y \sin(\phi-\phi_x)+\tan\theta_x \sin(\phi_y-\phi)}{\sin(\phi_y-\phi_x)}\right\} \qquad (2\text{-}31)$$

where all θ's and all ϕ's are expressed in North Latitude and West Longitude coordinates respectively. (Note that for $\phi=\phi_x, \theta=\theta_x$ and for $\phi=\phi_y, \theta=\theta_y$).

2.3.2 Algorithm for the Great Circle Arc which Bisects and is Orthogonal to the Great Circle Arc Joining Two Fixed Points, (θ_x,ϕ_x) and (θ_y,ϕ_y): To determine the subject curve, we need merely to employ (2-1), letting the parameter $\lambda_{yx}=0$. When this is done we obtain, simply,

$$\vartheta = \tan^{-1}\left\{\frac{\cos\theta_x\cos(\phi-\phi_x)-\cos\theta_y\cos(\phi_y-\phi)}{\sin\theta_y-\sin\theta_x}\right\} \tag{2-32}$$

The above great circle curve will be orthogonal to the great circle curve defined by (2-31) and will intersect this curve at a point midway between the two fixed points (θ_x,ϕ_x) and (θ_y,ϕ_y).

3.0 PROPERTIES OF THE SOLUTION

To study the properties and characteristics of the family of curves derived for the sensor pair configuration, it will be convenient to transform the coordinate axes of the sphere in a manner which will provide a simple analytical solution. It should be evident that the relative geometry of the family of curves remains invarient with a simple set of rotations of the axes of the sphere, and only the analytical form of the curves change. (NOTE: For notational simplicity, the subscripts will be dropped from the parameters μ and λ in this section. It should be kept in mind, however, that the indicated subscripts are a proper part of these parameters).

3.1 Longitudinal Alignment of the Receiving Sensors:

We now propose a simple set of rotations on the spherical axes; such that, the transformed coordinate points of the receiving sensor stations will be aligned along the zero Longitudinal axis and equidistant about the equator. That is, let

$$\theta_y = -\theta_x$$
$$\phi_y = \phi_x = 0 \tag{3-1}$$

Under these circumstances, the equation for the family of curves given by (2-1) becomes,

$$\theta = \tan^{-1}\left\{\frac{\lambda}{\sqrt{1-\lambda^2}}\sqrt{\frac{(1-\lambda^2)-\cos^2\theta_x\cos^2\phi}{\sin^2\theta_x\cdot\lambda^2}}\right\}$$
$$= \tan^{-1}\left\{\frac{\lambda}{\sqrt{1-\lambda^2}}\sqrt{1+\frac{\cos^2\theta_x\sin^2\phi}{\sin^2\theta_x-\lambda^2}}\right\} \tag{3-2}$$

Now, from (3-4) and (2-2), we may write,

$$\left.\begin{aligned} \chi_{xy} &= \sin^2\theta_x \\ \lambda &= \sin\mu\theta_x \end{aligned}\right\} \qquad (3\text{-}3)$$

Using (3-3) in (3-2) gives,

$$\theta = \tan^{-1}\left\{\sqrt{1+\frac{\cos^2\theta_x\sin^2\phi}{\sin^2\theta_x-\sin^2\mu\theta_x}}\ \tan\mu\theta_x\right\}$$

$$= \tan^{-1}\left\{\sqrt{1+\frac{\cos^2\theta_x\sin^2\phi}{\sin(1+\mu)\theta_x\sin(1-\mu)\theta_x}}\tan\mu\theta_x\right\} \qquad (3\text{-}4)$$

3.1.1 Case When $\theta_x = \pi/2$: In the particular case where $\theta_x = \pi/2$, equation (3-4) reduces to, simply,

$$\theta = \mu\pi/2 \qquad (3\text{-}5)$$

In other words, the subject family of curves degenerate to simple Latitude circles over the surface of the sphere. This is not surprising; since, for receiving sensors located at the two poles, the circles of constant Latitude represent the locus of points (on the surface of the sphere) whose difference in great circle path length to the two poles is a constant.

3.1.2 Symmetrical Properties: An examination of equation (3-2) reveals that

$$\begin{aligned} \theta(-\phi;\lambda) &= \theta(\phi;\lambda) \\ \theta(\pi-\phi,\lambda) &= \theta(\phi;\lambda) \\ \theta(\phi;-\lambda) &= -\theta(\phi;\lambda) \end{aligned} \qquad (3\text{-}6)$$

Therefore, the family of curves defined in (3-4) is symmetric about each of three mutually orthogonal planes which pass through the center of the sphere. In this particular coordinate system, the three planes intersect the surface of the sphere in the three orthogonal great circles which form the zero and 180 degree Longitudinal curves, the ± 90 degree Longitudinal curves and the

zero Latitude curve (equator). This symmetrical property of the subject family of curves had been forecast in Section 2.3 .

3.1.3 Maxima and Minima of $|\theta|$: From (3-4) it may readily be observed that the minima and maxima of the absolute value of $\theta(\phi;\lambda)$ will occur for ϕ equal to zero (and 180 degrees) and $\pm \pi/2$ (or $\pm$ 90 degrees) respectively. The minimum absolute value of θ will, therefore, be

$$\theta_m = \mu\theta_x \tag{3-7}$$

and the maximum absolute value of θ becomes,

$$\theta_M = \tan^{-1}\left\{\frac{\sin\mu\theta_x}{\sqrt{\sin^2\theta_x - \sin^2\mu\theta_x}}\right\}$$

$$= \tan^{-1}\left\{\frac{\sin\mu\theta_x}{\sqrt{\sin(1+\mu)\theta_x \sin(1-\mu)\theta_x}}\right\} \tag{3-8}$$

3.1.4 Case When $\theta_x \ll 1$: When θ_x is sufficiently small so that $\sin\theta_x$ and $\tan\theta_x$ can be replaced by θ_x without significant error, equations (3-4) and (3-8) can be approximated as,

$$\theta_M \approx \tan^{-1}\left\{\frac{\mu}{\sqrt{1-\mu^2}}\right\} = \sin^{-1}\mu \tag{3-9}$$

and

$$\theta = \tan^{-1}\left\{\sqrt{\theta_x^2\cos^2\theta_M + \sin^2\phi}\,\tan\theta_M\right\} \tag{3-10}$$

The above system will now be examined in the near field (relatively close proximity to the receiving sensors), in the relatively far field (remote from the receiving sensor stations), and in the extreme far field (the image of the near field on the opposite side of the sphere).

When θ and ϕ are sufficiently small; such that, tan θ and sin ϕ can be replaced by the respective angles without significant error, then equation (3-10) can be approximated as,

$$\frac{\theta^2}{\mu^2\theta_x^2} - \frac{\phi^2}{(1-\mu^2)\theta_x^2} = 1 \qquad (3\text{-}11)$$

The above relation is the equation for a family of hyperbolas in the θ,ϕ plane. This is just what one would expect, since the solution for the basic phenomena in planar geometry results in a hyperbolic family of curves. A graphical plot of (3-11) for the near field solution is illustrated in Figure 2.

The relatively far field behavior of the family of curves can be obtained from (3-10) through the artifice of taking the limit as $\theta_x \to 0$. Thus,

$$\lim_{\theta_x \to 0} \theta = \tan^{-1}\left\{\frac{\mu}{\sqrt{1-\mu^2}}\sin\phi\right\}$$

$$= \tan^{-1}\{\tan\theta_M \sin\phi\} \qquad (3\text{-}12)$$

A plot of the resulting family of curves is illustrated in Figure 3.

An interesting facet of the spherical geometry is that, in the extreme far field (the surface area on the opposite side of the sphere from the receiving sensor location), there exists a convergence zone where the ray paths converge to form a propagation field identical to the field in the near-sensor region. As a consequence, the equations and curves given for the near field are equally applicable to the extreme far field region. This fact has important practical implications; in that, it tells us that the resolution for localizing a source (or, conversely, the accuracy of navigation) in the extreme far field (on the opposite side of the sphere) is just as good as in the near field. This is a consequence of the propagation ray convergence in the extreme far field zone.

3.1.5 Case When θ_x is large: To study the behavior of the curves for the case when θ_x is relatively large, we shall let θ_x be equal to $\pi/6$ (30 degrees). In this event, equation (3-4) becomes,

$$\theta = \tan^{-1}\left\{\sqrt{1 + \frac{3\sin^2\phi}{1-4\sin^2(\mu\pi/6)}}\tan(\mu\pi/6)\right\} \qquad (3\text{-}13)$$

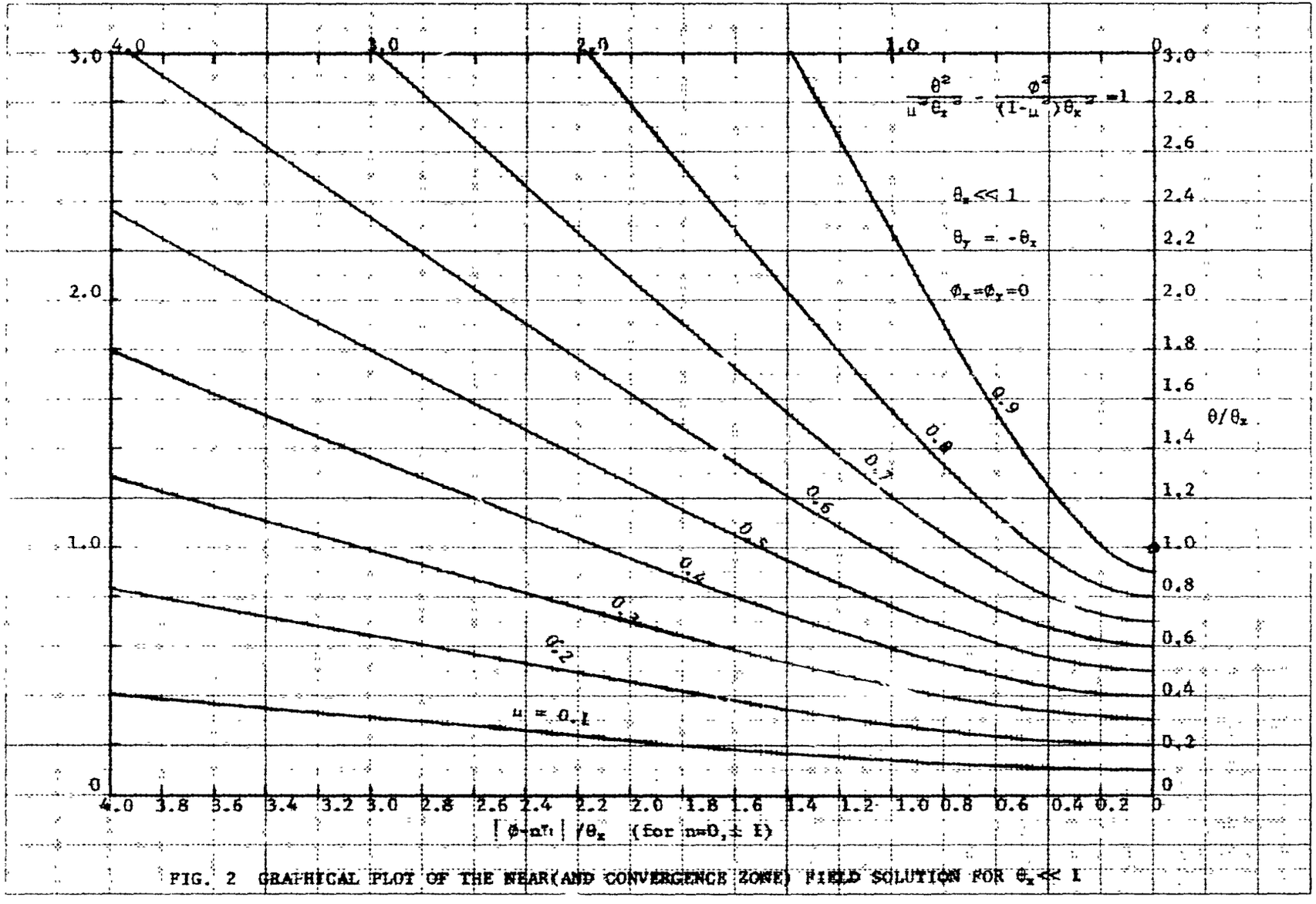

FIG. 2 GRAPHICAL PLOT OF THE NEAR(AND CONVERGENCE ZONE) FIELD SOLUTION FOR $\theta_x \ll 1$

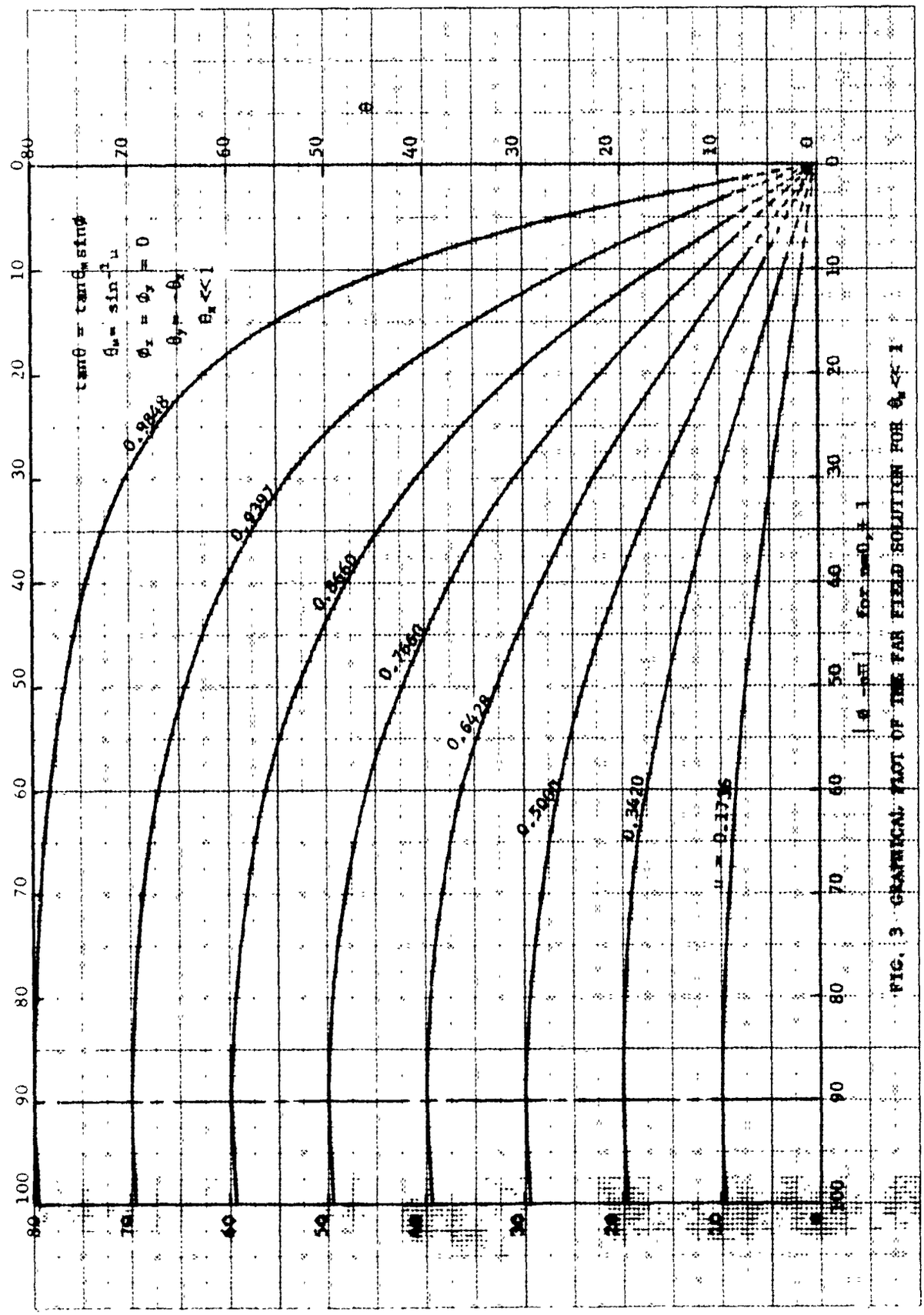

FIG. 3 GRAPHICAL PLOT OF THE FAR FIELD SOLUTION FOR $\theta_x \ll 1$

A graphical presentation of these curves is illustrated in Figure 4. The family of curves is plotted over the entire range of Longitude, and for both positive and negative values of the measurement parameter μ. The illustration vividly demonstrates the three dimensions of symmetry over the surface of the sphere. The location of the two receiving sensors are depicted as small circles located at $\theta = \pm 30°$ and $\phi = 0$. In a sense, the family of curves take on the appearance of flexible Latitude circles which have been pinched (or compressed) toward the equator ($\theta=0$), at $\phi=0$ and $\phi=180°$, due to the presence of the two sensors. The closer the two sensors are spaced, the greater will be the compression of the family of curves at the two relevant Longitudinal positions.

3.1.6 Slope of the Curves: To determine the slope of the family of curves given by (3-4) we may proceed as follows,

$$\text{Slope} = \frac{1}{\cos\theta}\ \frac{d\theta}{d\phi}$$

$$= \frac{\cos^2\theta_x \sin\mu\theta_x \sin\phi\cos\phi}{\sqrt{(\cos^2\mu\theta_x - \cos^2\theta_x\cos^2\phi)(\sin^2\theta_x\cos^2\mu\theta_x - \cos^2\theta_x\sin^2\mu\theta_x\cos^2\phi)}} \qquad (3\text{-}14)$$

When θ_x is small this approximates,

$$\text{Slope} = \frac{\mu\sin\phi\cos\phi\ (1-\theta_x^2)}{\sqrt{[1-\mu^2(\cos^2\phi+\theta_x^2\sin^2\phi)][\sin^2\phi+\theta_x^2(\cos^2\phi-\mu^2)]}} \qquad (3\text{-}15)$$

And, in the limit, as $\theta_x \to 0$,

$$\text{Slope} = \frac{\mu\cos\phi}{\sqrt{1-\mu^2\cos^2\phi}} \qquad (3\text{-}16)$$

Thus, for $\phi \ll 1$, the slope becomes equal to $\mu/\sqrt{1-\mu^2}$, which is the slope asymptote for the plane geometry case (see Figure 2).

3.2 Equatorial Alignment of the Receiving Sensors

As an alternate to aligning the receiving sensors in a longitudinal orientation, we could have transformed the coordinate axes of the sphere to

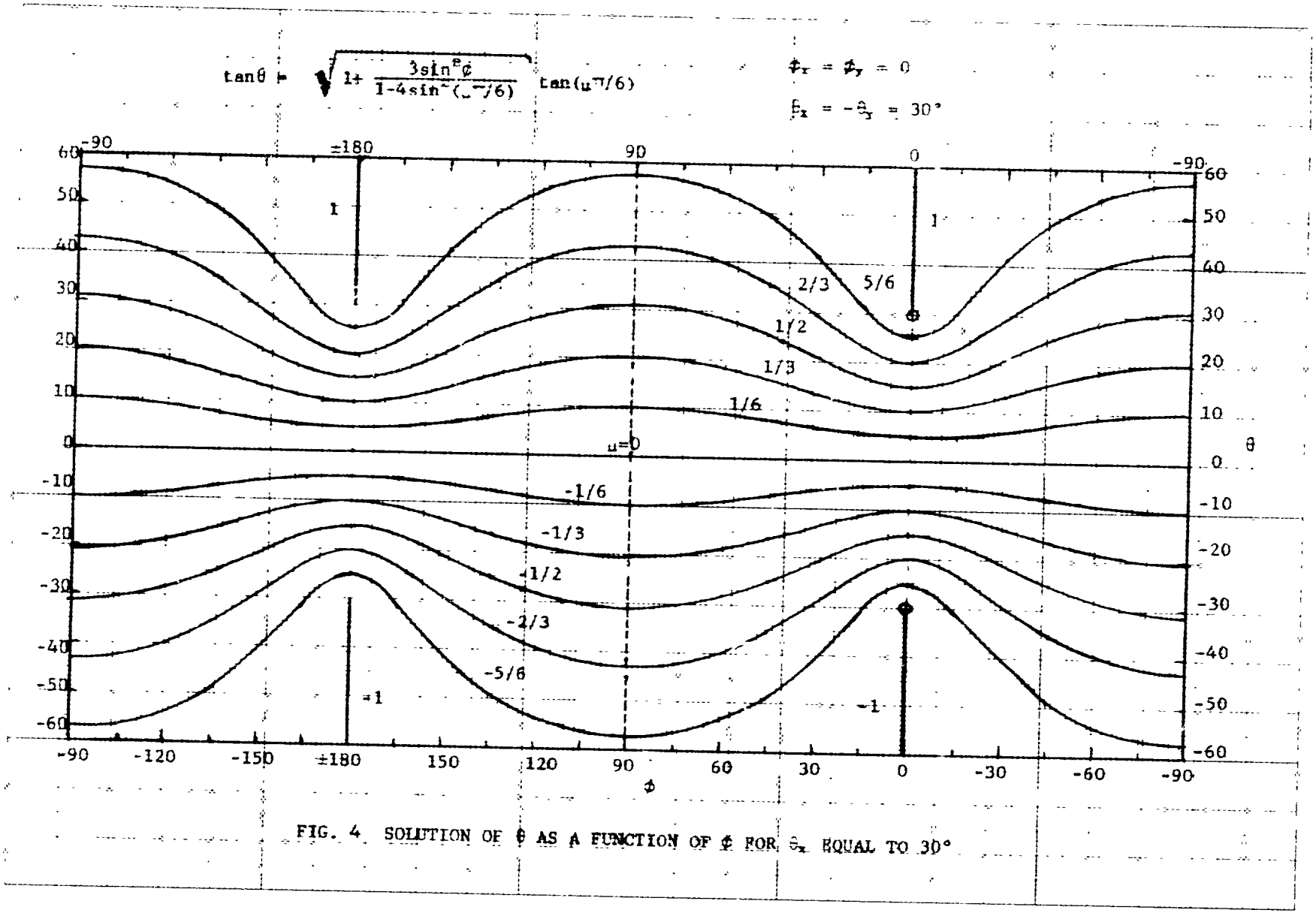

FIG. 4 SOLUTION OF θ AS A FUNCTION OF ϕ FOR β_x EQUAL TO 30°

a new set where the receiving sensors were located on the equator, equidistant about the zero Longitudinal axis. That is, let,

$$\left.\begin{aligned} \theta_y &= \theta_x = 0 \\ \phi_y &= -\phi_x \end{aligned}\right\} \tag{3-17}$$

Under these circumstances, the equation for the family of curves given by (2-1) becomes,

$$\theta = \pm \tan^{-1}\left\{\frac{1}{\lambda}\sqrt{\frac{(\sin^2\phi_x-\lambda^2)(\sin^2\phi-\lambda^2)}{1-\lambda^2}}\right\} \tag{3-18}$$

Now, from (1-4) and (2-2), we may write,

$$\left.\begin{aligned} \chi_{xy} &= \sin^2\phi_x \\ \lambda &= \sin\mu\phi_x \end{aligned}\right\} \tag{3-19}$$

Using (3-19) in (3-18) gives

$$\theta = \pm \tan^{-1}\left\{\frac{\sqrt{(\sin^2\phi_x-\sin^2\mu\phi_x)(\sin^2\phi-\sin^2\mu\phi_x)}}{\sin\mu\phi_x\cos\mu\phi_x}\right\}$$

$$= \pm \tan^{-1}\sqrt{\left(\frac{\sin^2\phi_x}{\sin^2\mu\phi_x}-1\right)\left(\frac{\sin^2\phi}{\cos^2\mu\phi_x}-\tan^2\mu\phi_x\right)} \tag{3-20}$$

The resulting family of curves given by the above expression is identical to the family of curves given in (3-4). The only difference between the two is a change in the coordinate frame of reference. As a consequence, all of the properties developed in Section 3.1 will be applicable to the above curves. It is important to realize that the geometric properties of the family of curves are independent of any linear transformation on the frame of reference over the surface of the sphere. However, it should be noted that an appropriate linear transformation in the coordinate frame of reference can greatly simplify the resulting analytical representation of the family of curves.

The coordinate frames of reference chosen in the last two sections provide the simplest forms for the analysis of the geometric properties of the subject family of curves. In fact, the coordinate frame of reference chosen in Section 3.1 is superior to this later choice since the ambiguity relative to the "sign" of the parameter u was removed. This was evident in (3-4) where the "± sign" was not present. (The parameter u can carry its own "sign" when $\phi_x = \phi_y$). In (3-20), on the other hand, it was necessary to incorporate the "± sign" in order to completely map the curve for any fixed value of the parameter u. In this latter case, one would select the curve for positive values of ϕ when u_{yx} is positive, and the curve for negative values of ϕ when u_{yx} is negative. In the more general case, given by (2-1), some care will need to be taken (in this regard) if ambiguity in the location of the proper curve is to be avoided.

4.0 SOURCE LOCALIZATION ALGORITHMS

In the earlier analyses we have determined that a simple measure of range (or time) difference between a source and two known receiving sensor stations is insufficient, by itself, in determining the location of the source. Such a measure will, however, provide a closed curve over the surface of the sphere on which the source is known to be located. Consequently, if the range (or time) difference between two (or more) pairs of known receiving sensor locations can be established, then the location of source will be known to exist at the intersection of the two (or more) resulting closed curves. Since two closed curves will intersect at two deterministic locations on the surface of the sphere, bivalued ambiguity still exists in principle. However, one can generally rule out one of the locations on the basis of purely physical considerations. As a consequence, the localization of an unknown source is, for all practical purposes, realizable in physical applications.

4.1 Simultaneous Equations:

What is involved in the localization problem, is the simultaneous solution of two equations of the form given in (2-1) for each of two sensor pairs. Thus, the location (in North Latitude and West Longitude coordinates) of the source will be the set (θ_o, ψ_o) which satisfies the following relations,

$$\left.\begin{aligned}\theta_o &= \tan^{-1}\left\{\frac{\mathcal{T}_{xy}(\phi_o;\lambda_{yx}^2)}{\pm\lambda_{yx}\sqrt{\mathcal{K}_{xy}(\phi_o;\lambda_{yx}^2)-\mathcal{L}_{xy}(\phi_o;\lambda_{yx}^2)}}\right\}\\ &= \tan^{-1}\left\{\frac{\mathcal{T}_{zw}(\phi_o;\lambda_{wz}^2)}{\pm\lambda_{wz}\sqrt{\mathcal{K}_{zw}(\phi_o;\lambda_{wz}^2)-\mathcal{L}_{zw}(\phi_o;\lambda_{wz}^2)}}\right\}\end{aligned}\right\} \qquad (4\text{-}1)$$

where, the known locations of the receiving sensors are (θ_x,ϕ_x), (θ_y,ϕ_y), (θ_z,ϕ_z) and (θ_w,ϕ_w). (It should be noted that only three receiving sensor locations are necessary, since two pairs can readily be derived from only three sensor stations. In this event, z can be made equal to y in the above relations.)

4.2 General Approaches to the Solution

Now, there are a number of ways for solving the above relations. One simple technique is to maintain a graphical plot of the family of curves resulting from the two sensor pairs. Upon obtaining the measures for μ_{yx} and μ_{wz}, one may then identify and follow the trace for these two parameters on the graphical plots until the appropriate point of intersection is obtained. Although the graphical technique is rather crude and generally not too accurate (unless extremely large graphs are maintained with quite small increments in μ), it can be employed advantageously to provide a first approximation to the source location. To obtain a more accurate fix on the source location, the two equations, incorporated in (4-1), can be treated separately, and independently solved for θ as a function of ϕ based upon some initial estimate of ϕ_o. Using an initial estimate of ϕ_o (say ϕ_1), then two independent values of θ will be obtained from (4-1). By observing the two values for θ, and noting which value is the larger, a second estimate for ϕ_o may be made. Again two values for θ will be obtained and these can be compared with each other, and with the earlier results obtained for ϕ_1, to arrive at a still more refined estimate of ϕ_o. In this iterative manner, the solution for θ_o and ϕ_o can be converged upon in a relatively short time with the aid of high speed digital computers.

Although one might solve equation (4-1) explicitly for ϕ_o, this process

would result in an extremely cumbersome relation for all except the most simple geometry. Therefore, this procedure is not recommended. What is recommended is to consider the relation, given in (4-1), as two independent equations for θ as a function of ϕ, and solve these equations for various estimates of ϕ until the resulting θ solutions converge to the same value (viz. θ_o). An algorithm for rapidly converging to the desired solution (θ_o, ϕ_o) will now be given.

4.3 Iteration Algorithm

To begin the iterative solution, we shall first require an estimate of the value ϕ_o. This estimate need not be too accurate and may be obtained from a rather crude graphical plot of the solution as described earlier. One should then choose two values of ϕ equally spaced about the best estimate of ϕ_o. For convenience, we shall call these two choices, ϕ_1 and ϕ_2. Using these values for ϕ, we then compute $\theta_{1,1}$ and $\theta_{2,1}$ (for $\phi=\phi_1$) and $\theta_{1,2}$ and $\theta_{2,2}$ (for $\phi=\phi_2$), using the two equations given in (4-1). Based on the results for the first two choices for ϕ (viz. ϕ_1 and ϕ_2), we then compute the best estimate for ϕ_o as ϕ_3 where,

$$\phi_3 = \frac{(\theta_{2,2}-\theta_{1,2})\phi_1-(\theta_{2,1}-\theta_{1,1})\phi_2}{(\theta_{2,2}-\theta_{1,2})-(\theta_{2,1}-\theta_{1,1})}$$

$$= \phi_2 - \frac{(\theta_{2,2}-\theta_{1,2})(\phi_2-\phi_1)}{(\theta_{2,2}-\theta_{1,2})-(\theta_{2,1}-\theta_{1,1})} \qquad (4\text{-}2)$$

Using the estimate ϕ_3 in (4-1), then, the values for $\theta_{1,3}$ and $\theta_{2,3}$ are computed, and a further estimate for ϕ_o is obtained. This iterative process is continued; whereby, newer and more refined estimates for ϕ_o are obtained from the general formula,

$$\phi_{n+1} = \phi_n - \frac{(\theta_{2,n}-\theta_{1,n})(\phi_n-\phi_{n-1})}{(\theta_{2,n}-\theta_{1,n})-(\theta_{2,n-1}-\theta_{1,n-1})}$$

$$= \phi_n + (-1)^{n-1}(\phi_2-\phi_1)\prod_{i=2}^{n}\frac{\theta_{2,i}-\theta_{1,i}}{(\theta_{2,i}-\theta_{1,i})-(\theta_{2,i-1}-\theta_{1,i-1})} \qquad (4\text{-}3)$$

Subsequent to each estimate of ϕ_o, one may test the result against a predetermined tolerance $\Delta\phi$ and $\Delta\theta$ as follows,

$$\begin{aligned} &| \phi_{n+1} - \phi_n | < \Delta \phi \\ &| \theta_{2,n+1} - \theta_{1,n+1} | < \Delta \theta \end{aligned} \tag{4-4}$$

When the above criterion is met, the process may be terminated and the value of (θ_o, ϕ_o) selected as,

$$(\theta_o, \phi_o) = (\theta_{n+1}, \phi_{n+1}) \tag{4-5}$$

That such a solution will converge in the limit as $n \to \infty$ should be evident from the general geometry and from (4-3). For most practical applications the convergence should be quite rapid, requiring only several iterations (dependent, of course, on the tolerence values $\Delta\theta$ and $\Delta\phi$ and the problem geometry).

III

SOURCE DYNAMICS DETERMINATION OVER SPHERICAL SURFACES

It is well known that the first order effect of relative motion, on the temporal structure of a signal being propagated through a transmission medium, is manifested as a time scale-factor change on the signal being transmitted. That is, the signal is either compressed or expanded in time (usually by a very small fraction) as a result of the relative motion between the source and the receiving sensor. Receiving sensors in the transmission medium will, then, measure the compressed (or expanded) signal instead of the true signal which was transmitted. And the signal measured at each receiving station will vary, depending on the velocity of the source and the angle between the velocity vector and the transmission vector to the receiving sensor. By measuring and noting the difference in time scale-factor shift (doppler shift in the case of CW signals) between two (or more) pairs of receiving stations, it is then possible to uniquely determine the dynamics (course and speed) of the source.

The purpose of the present section will be to develop the algorithms which express the source dynamics (course and speed) in terms of the time scale-factor shifts which are measured between two pairs of receiving sensors. The geometry hypothesized will be a spherical surface (presumably the surface of the earth) on which the source and receiving stations are located.

1.0 PROBLEM FORMULATION FOR A RECEIVING SENSOR PAIR

Figure 5 depicts the relative geometry of the source dynamics vector and the propagation vectors to a pair of receiving sensors located on the surface of a sphere. The locations of the source and receiving sensor stations are presumed known and the signal transmission paths are assumed to be great circle routes.

The time scale-factor shift, δ_α, realized at the α^{th} receiving sensor

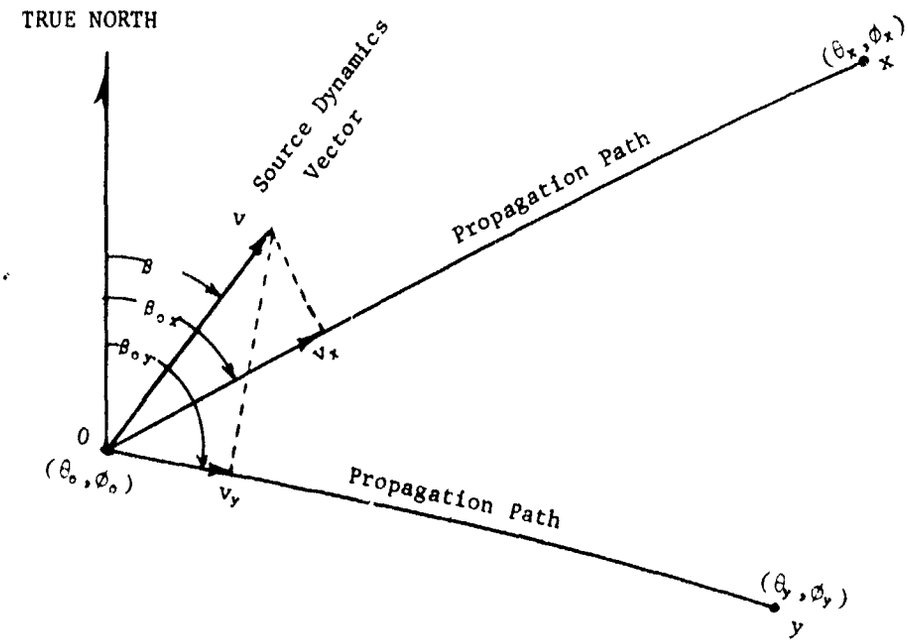

FIG. 5 VECTOR GEOMETRY OF THE PROBLEM

(due to source motion) will be,*

$$\delta_x = \frac{v_x}{c} = \frac{v}{c} \cos(\beta_{ox} - \beta) \qquad (1\text{-}1)$$

where,

v is the speed of the so in the transmission medium

β is the course of the source relative to true North

β_{ox} is the direction of the great circle path between the source and the x^{th} receiving sensor (relative to true North)

c is the velocity of propagation in the medium

(The above approximate relation will be highly accurate providing that $v << c$.)

---

* see, for example, A. A. Gerlach "Theory and Applications of Statistical Wave-Period Processing", Gordon and Breach Science Publishers Inc., Vol. I, Chap. 3, p. 98; 1970.

The difference in time scale-factor shift that will be measured between any two receiving sensor stations y and x, will therefore be,

$$\delta_{yx}(v,\beta;\beta_{ox},\beta_{oy}) = \delta_y - \delta_x$$

$$\approx \frac{v}{c}\,[\cos(\beta_{oy}-\beta)-\cos(\beta_{ox}-\beta)]$$

$$= 2\,\frac{v}{c}\,\sin\tfrac{1}{2}(\beta_{ox}-\beta_{oy})\sin[\tfrac{1}{2}(\beta_{ox}+\beta_{oy})-\beta] \qquad (1\text{-}2)$$

The above relation contains two unknowns, v and β, and, therefore, cannot be employed to uniquely determine the source dynamics. However, the one unknown can be explicitly solved for in terms of the other to determine the relationship between the two. Thus, we may obtain from (1-2),

$$v = \frac{c\ \delta_{yx}}{2\ \sin\tfrac{1}{2}(\beta_{ox}-\beta_{oy})\sin[\tfrac{1}{2}(\beta_{ox}+\beta_{oy})-\beta]} \qquad (1\text{-}3)$$

and

$$\beta = \tfrac{1}{2}(\beta_{ox}+\beta_{oy})-\sin^{-1}\left\{\frac{c\ \delta_{yx}}{2v\sin\tfrac{1}{2}(\beta_{ox}-\beta_{oy})}\right\} \qquad (1\text{-}4)$$

As a consequence, if one or the other of the unknowns can be reasonably well estimated, the other can be computed from either (1-3) or (1-4). However, it will be observed that bivalued ambiguity does exist (in the case of β) on account of the anti-trigonometric relation. In certain applications this ambiguity might be removed by physical considerations. In any event, two (or more) pairs of receiving sensors will be required to uniquely solve for the source dynamics.

2.0 DETERMINATION OF THE PROPAGATION VECTORS

Before proceeding with the unique solution of the source dynamics, it will be well to develop the relations for the great circle propagation vectors, β_{ox}, between two points (θ_o,ϕ_o) and (θ_x,ϕ_x).

To determine the angle of propagation between the two relevant points on the surface of the sphere we will first compute the slope of the great circle path between the two points. From equation (2-31) in Section II,

we may write the equation for the great circle curve through the two points (θ_o, ϕ_o) and (θ_x, ϕ_x) as,

$$\vartheta = \tan^{-1}\left\{\frac{\tan\theta_o \sin(\phi-\phi_x)+\tan\theta_x \sin(\phi_o-\phi)}{\sin(\phi_o-\phi_x)}\right\} \tag{2-1}$$

where the angles θ_o, θ_x and ϕ_o, ϕ_x are given in North Latitude and West Longitude coordinates respectively.

Now, the slope of this curve may be readily shown to be,

$$\tan[\alpha(\phi;\theta_o,\phi_o,\theta_x,\phi_x)] = \frac{1}{\cos\theta}\ \frac{d\theta}{d\phi}$$

$$= \frac{\tan\theta_o \cos(\phi-\phi_x)-\tan\theta_x \cos(\phi_o-\phi)}{\sqrt{\sin^2(\phi_o-\phi_x)+[\tan\theta_o \sin(\phi-\phi_x)+\tan\theta_x \sin(\phi_o-\phi)]^2}} \tag{2-2}$$

Therefore, the angle α, of the propagation vector at the source location (relative to the Latitude parallel), will be,

$$\alpha(\phi_o) = \tan^{-1}\left\{\frac{\sin\theta_o \cos(\phi_o-\phi_x)-\cos\theta_o \tan\theta_x}{\sin(\phi_o-\phi_x)}\right\} \tag{2-3}$$

Since, now, α will range over ± 90 degrees we shall need to incorporate the following additional algorithm for the computation of the propagation angle β_{ox} (relative to true North),

$$\beta_{ox} = \left\{\begin{array}{l}\alpha(\phi_o)+90^\circ \text{ when } \phi_x < \phi_o \\ \alpha(\phi_o)+270^\circ \text{ when } \phi_o < \phi_x\end{array}\right\} \tag{2-4}$$

It will be of interest to compute the direction of the propagation vector, β_{xo}, from the x^{th} receiving station toward the source. From (2-2) we have,

$$\alpha(\phi_x) = \tan^{-1}\left\{\frac{\cos\theta_x \tan\theta_o-\sin\theta_x \cos(\phi_o-\phi_x)}{\sin(\phi_o-\phi_x)}\right\} \tag{2-5}$$

and, the angle β_{xo} (relative to true North) becomes,

$$\beta_{xo} = \left\{\begin{array}{l}\alpha(\phi_x) + 270^\circ \text{ when } \phi_x < \phi_o \\ \alpha(\phi_x) + 90^\circ \text{ when } \phi_o < \phi_x\end{array}\right\} \tag{2-6}$$

For the particular situation when $\phi_x = \phi_o$, the following algorithms apply,

$$\beta_{ox} = \left\{ \begin{array}{ll} 180^\circ & \text{when } \theta_x < \theta_o \\ 0^\circ & \text{when } \theta_o < \theta_x \end{array} \right\} \tag{2-7}$$

and,

$$\beta_{xo} = \left\{ \begin{array}{ll} 0^\circ & \text{whe } \theta_x < \theta_o \\ 180^\circ & \text{when } \theta_o < \theta_x \end{array} \right\} \tag{2-8}$$

It is significant to note that, in general, the angle β_{xo} is not simply equal to the angle β_{ox} minus 180°. As a matter-of-fact, under special circumstances, β_{xo} will be equal to β_{ox}. This apparent dilemma is due to the nature of the great circle arc over the surface of the sphere.

Some symmetries, relative to the above propagation vectors, are as follows:

From (2-3), it may readily be shown that,

$$\alpha\left\{(180+\phi_x)-(\phi_o-\phi_x);-\theta_o,(180+\phi_x)-(\phi_o-\phi_x),\theta_x,\phi_x)\right\}$$

$$= \alpha(\phi_o;\theta_o,\phi_o,\theta_x,\phi_x) \tag{2-9}$$

$$\alpha\left\{\phi_x-(\phi_o-\phi_x);\theta_o,\phi_x-(\phi_o-\phi_x),\theta_x,\phi_x)\right\}$$

$$= -\alpha(\phi_o;\theta_o,\phi_o,\vartheta_x,\phi_x) \tag{2-10}$$

$$\alpha\left\{\phi_o;\vartheta_o,\phi_o-\theta_x,\phi_x+180\right\}$$

$$= \alpha(\phi_o;\theta_o,\phi_o,\theta_x,\phi_x) \tag{2-11}$$

and,

$$\alpha\left\{\phi_o;\theta_o,\phi_o,\theta_x,\phi_x+2(\phi_o-\phi_x)\right\}$$

$$= -\alpha(\phi_o;\theta_o,\phi_o,\theta_x,\phi_x) \tag{2-12}$$

And from (2-5), it can be shown that,

$$\alpha\{\phi_x ; -\theta_o, (180+\phi_x)-(\phi_o-\phi_x), \theta_x, \phi_x\}$$

$$= -\alpha(\phi_x ; \theta_o, \phi_o, \theta_x, \phi_x) \tag{2-13}$$

$$\alpha\{\phi_x ; \theta_o, \phi_x-(\phi_o-\phi_x), \theta_x, \phi_x\}$$

$$= -\alpha(\phi_x ; \theta_o, \phi_o, \theta_x, \phi_x) \tag{2-14}$$

$$\alpha\{\phi_x+180 ; \theta_o, \phi_o, -\theta_x, \phi_x+180\}$$

$$= -\alpha(\phi_x, \theta_o, \phi_o, \theta_x, \phi_x) \tag{2-15}$$

and,

$$\alpha\{\phi_x+2(\phi_o-\phi_x) ; \theta_o, \phi_o, \theta_x, \phi_x+2(\phi_o-\phi_x)\}$$

$$= -\alpha(\phi_x ; \theta_o, \phi_o, \theta_x, \phi_x) \tag{2-16}$$

Equations (2-9) and (2-11) demonstrate the convergence zone property of the spherical geometry for a source located in the extreme far field. Thus, the apparent sensor pair aperture angle for a source located in the extreme far field (on the opposite side of the hemisphere from the sensor locations) will be the same as for a source located in the corresponding image position on the near side of the hemisphere. This convergent zone property will permit the source dynamics measures, of a source located in the extreme far field, to be resolved with the same precision as would be realized in the corresponding image location in the near hemisphere. More will be said about this feature of the spherical geometry in Section V.

3.0 SOURCE DYNAMICS ALGORITHMS

In the earlier analyses we determined that the computation for the source dynamics (course and speed) would require the solution of two sets of nonlinear simultaneous equations of the form given in (1-2). Thus, if we assume that two pairs of receiving sensors were receiving and simultaneously measuring the time scale-factor shift from the transmitted source

signal, the two resulting nonlinear equations involving the unknown dynamic variables, v and β, would be,

$$\left\{ \begin{array}{l} \delta_{yx} = 2\,\frac{v}{c}\,\sin\tfrac{1}{2}(\beta_{ox}-\beta_{oy})\sin[\tfrac{1}{2}(\beta_{ox}+\beta_{oy})-\beta] \\ \\ \delta_{wz} = 2\,\frac{v}{c}\,\sin\tfrac{1}{2}(\beta_{oz}-\beta_{ow})\sin[\tfrac{1}{2}(\beta_{oz}+\beta_{ow})-\beta] \end{array} \right\} \qquad (3\text{-}1)$$

where the two pairs of receiving sensors are at the known locations (θ_x,ϕ_x), (θ_y,ϕ_y) and (θ_z,ϕ_z),(θ_w,ϕ_w), and the corresponding propagation vector angles are β_{ox},β_{oy} and β_{oz},β_{ow}, respectively.

For convenience, we shall let,

$$\left\{ \begin{array}{l} b_{yx} = \sin\tfrac{1}{2}(\beta_{oy}-\beta_{ox}) \\ \\ b_{wz} = \sin\tfrac{1}{2}(\beta_{ow}-\beta_{oz}) \end{array} \right\} \qquad (3\text{-}2)$$

and,

$$\left\{ \begin{array}{l} \xi = \tfrac{1}{4}(\beta_{ox}+\beta_{oy}+\beta_{oz}+\beta_{ow}) \\ \\ \eta = \tfrac{1}{2}(\beta_{oz}+\beta_{ow}-\beta_{ox}-\beta_{oy}) \end{array} \right\} \qquad (3\text{-}3)$$

From (3-1), (3-2), and (3-3) then,

$$\left\{ \begin{array}{l} v\,\sin(\xi-\beta-\eta) = -c\delta_{yx}/2b_{yx} \\ \\ v\,\sin(\xi-\beta+\eta) = -c\delta_{wz}/2b_{wz} \end{array} \right\} \qquad (3\text{-}4)$$

Making use of the identity, $\sin(a\pm b) = \sin a\cos b \pm \cos a \sin b$, the above expression reduces to, simply,

$$\left\{ \begin{array}{l} v\,\sin(\xi-\beta) = -\,\frac{c}{4}\,\frac{b_{yx}\delta_{wz}+b_{wz}\delta_{yx}}{b_{yx}b_{wz}\cos\eta} \\ \\ v\,\cos(\xi-\beta) = -\,\frac{c}{4}\,\frac{b_{yx}\delta_{wz}-b_{wz}\delta_{yx}}{b_{yx}b_{wz}\sin\eta} \end{array} \right\} \qquad (3\text{-}5)$$

The above two nonlinear equations in the unknown variables, v and β, may be readily solved to give,

$$\beta = \begin{matrix} \\ \end{matrix} -\tan^{-1}\left\{ \frac{b_{yx}\delta_{wz}+b_{wz}\delta_{yx}}{b_{yx}\delta_{wz}-b_{wz}\delta_{yx}} \tan\eta \right\} \tag{3-6}$$

and

$$v = c\,\frac{\sqrt{(b_{yx}\delta_{wz})^2+(b_{wz}\delta_{yx})^2-2b_{yx}b_{wz}\delta_{yx}\delta_{wz}\cos 2\eta}}{2b_{yx}b_{wz}\sin 2\eta} \tag{3-7}$$

Thus, the source dynamics (course and speed) may be explicitly determined from the measured time scale-factor shifts, δ_{yx} and δ_{wz}, and a knowledge of the locations of the source and the receiving sensor stations. To avoid ambiguity, which may result from the "sign" of the trigonometric functions, some care should be exercised in the use of (3-6) and (3-7).

It will be noted in (3-7) that v will always be a real number; however, it is possible for v to take on negative values. In the event that v is negative, the simple interpretation is to take only the absolute value for v and add ± 180 degrees to the value of β to make it fall within the range $0 \leq \beta < 360$. To avoid the ambiguity of a negative speed, a simple precaution is to choose the sensor nomenclature; such that, b_{yx}, b_{wz} and $\sin 2\eta$ are all positive or that two of these terms are negative. For many applications this can be accomplished by insuring that

$$\beta_{ox} < \beta_{oy} \leq \beta_{oz} < \beta_{ow} \tag{3-8}$$

providing that,

$$\beta_{oz} + \beta_{ow} - \beta_{ox} - \beta_{oy} \leq 360^\circ \tag{3-9}$$

Since three receiving sensor stations are sufficient to produce two pairs of receiving sensors, we can let $\theta_z = \theta_y$ and $\phi_z = \phi_y$. In this event,

$$\beta_{oz} = \beta_{oy} \tag{3-10}$$

and (3-3) becomes,

$$\left.\begin{array}{l} \beta = \tfrac{1}{4}(\beta_{ox}+2\beta_{oy}+\beta_{ow}) \\ \\ \eta = \tfrac{1}{4}(\beta_{ow}-\beta_{ox}) \ . \end{array}\right\} \tag{3-11}$$

In all other respects the relations are unchanged.

IV

RESOLUTION IN SOURCE LOCALIZATION

In Section II we developed the algorithms (or analytical relations) for computing the location of a signal source, based on the time register measure between two pairs of receiving sensors whose locations were known. Before the practicality of these algorithms can be properly assessed, however, it will be necessary to determine the resolution of this localization in terms of the resolution of the basic time register measure τ. In other words, we wish to ascertain the sensitivity of the localization measure to the inherent resolution of the measure in time-difference-in-arrival of the source signal at the receiving sensor pairs. When this is accomplished, we can suitably outline an area on the surface of the sphere in which we can be assured that the source is known to exist within a definable degree of confidence. This we shall now proceed to do.

1.0 PROBLEM FORMULATION FOR A RECEIVING SENSOR PAIR

The approach to the problem will be one of determining the sensitivity of the equi-time-register curves to the nondimensional parameter μ. Since the parameter μ is directly related to the time-register measure τ, as given in (1-4) of Section II, we shall then be in a position to determine the sensitivity of localization to the measure τ. Our plan will be to ascertain both the translation distance, ds influenced by an error, $d\mu$, in the measure μ, and the direction of this translation. When this is accomplished for two pairs of receiving sensors, we shall then be in a position to outline an area on the surface of the sphere; in which, the source will be localized for a specified error in time-register measure.

Since the geometry of the problem is independent of the coordinate frame of reference of the sphere, we shall conveniently choose the reference frame given in Section II, 3.1.

1.1 Fundamental Equations

The fundamental equations which we wish to solve may readily be shown to be,

$$\frac{ds}{d\mu} = \frac{\rho \left| d\theta/d\mu \right|}{\sqrt{1 + (d\theta/d\phi)^2/\cos^2\theta}} \tag{1-1}$$

and,

$$\beta_\mu = \frac{d\theta/d\mu}{\left| d\theta/d\mu \right|} \tan^{-1} \left\{\frac{\cos\theta}{-d\theta/d\phi}\right\} \tag{1-2}$$

where ds is a measure of distance over the surface of the sphere and β_μ is the angle along which the distance, ds, is to be taken. Since the angle β_μ can be rather ambiguous due to the inherent nature of the transcendental functions, it will be best to determine this angle from a knowledge of the geometry of any specific problem. In essence, it is the direction normal to the tangent of the equi-time-register curve (at the point in question), and toward the curves of higher μ. Thus, the measures ds and β_μ define an error vector on the surface of the sphere; where ds is the scalar error magnitude and β_μ is the direction of the error vector. It should be evident that the error magnitude will be simply,

$$ds = \left| \frac{d\mu}{d\tau} \frac{ds}{d\mu} d\tau \right| \tag{1-3}$$

It will be noted that,

$$\tan^{-1} \left\{\frac{\cos\theta}{d\theta/d\phi}\right\} = \frac{\pi}{2} - \tan^{-1} \left\{\frac{d\theta/d\phi}{\cos\theta}\right\} \tag{1-4}$$

And for the geometry given in Section II, 3.1, β_μ will be,

$$\beta_\mu = \tan^{-1} \left\{\frac{d\theta/d\phi}{\cos\theta}\right\} \tag{1-5}$$

where β_μ is expressed in angular degrees relative to true North. Now, the slope of β_μ, as given in (1-5), is given in (3-14) of Section II. Consequently, it will be convenient to utilize the above expression for β_μ in the analysis to follow; in lieu of the expression given in (1-2). Since it will be well to examine the geometry of any specific problem to determine the true direction of β_μ, the actual form of this expression in the subject analysis is somewhat arbitrary; as long as, the final results

are not misapplied. Consequently, for convenience, we shall use the form given in (1-5) in the analysis to follow. In general, this will not lead to ambiguous results; as long as, care is taken in the employment of the results to any physical problem.

1.2 Graphical Interpretation of the Error Vector

At this point one may obtain a general feel for the quantity of the error vector through a study of the curves shown in Figures 2, 3, and 4 of Section II. For any given point on the family of curves, one may draw a vector from this point normal to the curve in the direction of increasing μ. The distance between two adjacent curves divided by the incremental difference in the values of μ will be the approximate magnitude of $ds/d\mu$. And for the subject geometry, the value of $d\mu/d\tau$ is simply,

$$\frac{d\mu}{d\tau} = \frac{c}{2\rho\theta_x} = c/D \tag{1-6}$$

where D is the great circle distance between the two receiving sensor stations and c is the velocity of signal propagation in the transmission medium.

2.0 SOLUTION OF THE BASIC ERROR EQUATIONS

2.1 General Solution

Making use of equations (3-4) and (3-14) in Section II, 3.1, we can solve the fundamental equations given in Section 1.1 above to yield the following relations.

$$\frac{d\theta}{d\mu} = \frac{[\sin^2\theta_x\cos^4\mu\theta_x - (\sin^2\theta_x - \sin^4\mu\theta_x)\cos^2\theta_x\cos^2\phi]\theta_x}{(\sin^2\theta_x\cos^4\mu\theta_x - \cos^2\theta_x\sin^2\mu\theta_x\cos^2\phi)\sqrt{(\sin^2\theta_x - \sin^2\mu\theta_x)(\cos^2\mu\theta_x - \cos^2\theta_x\cos^2\phi)}} \tag{2-1}$$

$$\sqrt{1+\frac{(d\theta/d\phi)^2}{\cos^2\theta}} = \sqrt{\frac{\sin^2\theta_x\cos^4\mu\theta_x - (\sin^2\theta_x - \sin^4\mu\theta_x)\cos^2\theta_x\cos^2\phi}{(\cos^2\mu\theta_x - \cos^2\theta_x\cos^2\phi)(\sin^2\theta_x\cos^2\mu\theta_x - \cos^2\theta_x\sin^2\mu\theta_x\cos^2\phi)}} \tag{2-2}$$

$$\frac{ds}{d\mu} = \rho\theta_x \sqrt{\frac{\sin^2\theta_x\cos^4\mu\theta_x - (\sin^2\theta_x - \sin^4\mu\theta_x)\cos^2\theta_x\cos^2\phi}{(\sin^2\theta_x - \sin^2\mu\theta_x)(\sin^2\theta_x\cos^2\mu\theta_x - \cos^2\theta_x\sin^2\mu\theta_x\cos^2\phi)}} \tag{2-3}$$

$$\beta_\mu = \tan^{-1}\left\{ \frac{\cos^2\theta_x \sin\mu\theta_x \sin\phi\cos\phi}{\sqrt{(\cos^2\mu\theta_x - \cos^2\theta_x\cos^2\phi)(\sin^2\theta_x\cos^2\mu\theta_x - \cos^2\theta_x\sin^2\mu\theta_x\cos^2\phi)}} \right\} \tag{2-4}$$

Although the above expressions are rather complex, they do simplify considerably for particular values of the variables μ and ϕ. For example, when μ is equal to zero, the two relevant relations become,

$$\left.\frac{ds}{d\mu}\right]_{\mu=0} = \sqrt{1+\cot^2\theta_x\sin^2\phi}\ \rho\theta_x$$

$$\left.\beta_\mu\right]_{\mu=0} = 0 \tag{2-5}$$

For ϕ equal to zero and ninety degrees, the expressions become,

$$\left.\frac{ds}{d\mu}\right]_{\phi=0} = \rho\theta_x$$

$$\left.\beta_\mu\right]_{\phi=0} = 0 \tag{2-6}$$

and

$$\left.\frac{ds}{d\mu}\right]_{\phi=\pi/2} = \frac{\rho\theta_x\cos\mu\theta_x}{\sqrt{\sin^2\theta_x - \sin^2\mu\theta_x}}$$

$$\left.\beta_\mu\right]_{\phi=\pi/2} = 0 \tag{2-7}$$

In all of the above situations, the vector direction, β_μ, is equal to zero relative to true North. That is, the slope of the equi-time-register curves is zero at the relevant points.

2.2 Solution for Small θ_x

Of particular interest will be the case where the angle θ_x is sufficiently small, so that, the sine of the angle can be replaced by the angle (expressed in radians) without undue error. This is not too great a restriction, since this criterion can be met for sensor pair spacings which are equal to or less than about 1,200 nautical miles over the earth's surface. With this assumption, then, equations (2-3) and (2-4) reduce to,

$$\frac{ds}{d\mu} = \rho \sqrt{\frac{(1-\mu^2)^2\theta_x^2+(1-\theta_x^2)(1-\mu^4\theta_x^2)\sin^2\phi}{(1-\mu^2)[1-\mu^2(\cos^2\phi+\theta_x^2\sin^2\phi)]}} \tag{2-8}$$

and,

$$\beta_\mu = \tan^{-1}\left\{ \frac{\mu(1-\theta_x^2)\sin\phi\cos\phi}{\sqrt{[1-\mu^2(\cos^2\phi+\theta_x^2\sin^2\phi)][\sin^2\phi+\theta_x^2(\cos^2\phi-\mu^2)]}} \right\} \tag{2-9}$$

For convenience, we can now study the problem in the near field (including the extremely far convergent zone) and the relatively far field (remote from the receiving sensors).

2.2.1 Near (and Convergent Zone) Field Solution: In the near field and in the extremely far field (or convergent zone), where the sine of the angle ϕ can be replaced by the angle itself (or π minus the angle), the relevant equations approximate,

$$\frac{ds}{d\mu} \approx \rho \sqrt{\theta_x^2+\phi^2/(1-\mu^2)^2} \tag{2-10}$$

$$\beta_\mu \approx \tan^{-1}\left\{ \frac{\mu\phi}{\sqrt{(1-\mu^2)[\phi^2+\theta_x^2(1-\mu^2)]}} \right\} \tag{2-11}$$

(NOTE: For the convergent zone area, the variable ϕ should be replaced by $\pi-\phi$.)

2.2.2 Far Field Solution: For the far field solution (remote from the sensor locations), the relevant relations may be approximated as,

$$\frac{ds}{d\mu} \approx \frac{\rho \sin \phi}{\sqrt{(1-\mu^2)(1-\mu^2\cos^2\phi)}} \tag{2-12}$$

$$\beta_\mu \approx \tan^{-1}\left\{\frac{\mu \cos \phi}{\sqrt{1-\mu^2\cos^2\phi}}\right\} \tag{2-13}$$

3.0 TRANSFORMATION OF THE COORDINATE FRAME OF REFERENCE

In the earlier analysis of the basic error relations, we developed the equations for a particular geometry of the receiving sensors in the normal spherical coordinates. Since we wish to apply these results to any geometry over the surface of the sphere, we shall now transform the specific spherical coordinate measures to a new measure space which is directly related to the physical geometry of the problem and independent of the frame of reference of the sphere.

To accomplish the above objective, the new coordinate frame of reference will be the midpoint of the great circle curve which joins the two receiving sensors. (In the above example, this point is the point $\theta=0,\phi=0$.) We then propose to employ two new variables, R and α, where R is the great circle range from the reference point to the source position, and α is the angle between the great circle path R and the normal to the great circle path between the two receiving sensors; taken at the reference point.

3.1 Transformation Equations

For the example problem, the normal to the great circle path between the two receiving sensors at the reference point is simply the equator, whose slope is zero. The slope of the great circle path R (at the reference point) may be obtained directly from (2-5), Section III. Thus, we have the relation

$$\tan \alpha = \tan\theta/\sin\phi \tag{3-1}$$

The great circle range R may be obtained directly from (1-5) of Section II, to give the relation,

$$\sin(R/2\rho) = \sqrt{\tfrac{1}{2}(1-\cos\theta\cos\phi)} \tag{3-2}$$

From the above two nonlinear equations in the new variables R and α, we may solve explicitly for the new variables. The useful interrelations between the four variables have been derived and, for convenience, they are displayed in Table 1.

TABLE 1 INTERRELATIONSHIP BETWEEN VARIABLES

ζ	$\sin^2\zeta$	$\cos^2\zeta$	$\tan^2\zeta$
$\frac{R}{\rho}$	$1-\cos^2\theta\sin^2\phi$	$\cos^2\theta\sin^2\phi$	$\frac{\tan^2\theta + \sin^2\phi}{\cos^2\phi}$
α	$\frac{\tan^2\theta}{\tan^2\theta+\sin^2\phi}$	$\frac{\sin^2\phi}{\tan^2\theta+\sin^2\phi}$	$\frac{\tan^2\theta}{\sin^2\phi}$
θ	$\sin^2(R/\rho)\sin^2\alpha$	$1-\sin^2(R/\rho)\sin^2\alpha$	$\frac{\sin^2(R/\rho)\sin^2\alpha}{1-\sin^2(R/\rho)\sin^2\alpha}$
ϕ	$\frac{\sin^2(R/\rho)\cos^2\alpha}{1-\sin^2(R/\rho)\sin^2\alpha}$	$\frac{\cos^2(R/\rho)}{1-\sin^2(R/\rho)\sin^2\alpha}$	$\tan^2(R/\rho)\cos^2\alpha$

3.2 Solution for the Parameter μ

With the introduction of the two new variables, the parameter μ is no longer independent, but implicitly defined by these variables. The solution for μ in terms of the new variables is, however, not a simple function, but fortunately can be derived explicitly.

From (3-2), Section II, we may write,

$$\lambda^4-(\sin^2\theta_x+\sin^2\theta+\cos^2\theta_x\cos^2\theta\sin^2\phi)\lambda^2+\sin^2\theta_x\sin^2\theta = 0 \qquad (3\text{-}3)$$

And using the relationships given in Table 2 we obtain,

$$\lambda^4-[\sin^2\frac{R}{\rho} + \sin^2\theta_x(1-\sin^2\frac{R}{\rho}\cos^2\alpha)]\lambda^2+\sin^2\theta_x\sin^2\frac{R}{\rho}\sin^2\alpha = 0 \qquad (3\text{-}4)$$

where, $\lambda^2 = \sin^2\mu\theta_x \leq \sin^2\theta_x$ (3-5)

Equation (3-4) has the solution,

$$\lambda^2 = \tfrac{1}{2}[b - \sqrt{b^2-4a}\,] \tag{3-6}$$

where,

$$\left.\begin{aligned} b &= \sin^2\frac{R}{\rho} + \sin^2\theta_x\left(1-\sin^2\frac{R}{\rho}\cos^2\alpha\right) \\ a &= \sin^2\theta_x\sin^2\frac{R}{\rho}\sin^2\alpha \end{aligned}\right\} \tag{3-7}$$

[NOTE: Only the smaller of the two solutions for λ^2 need be considered in (3-6), due to the restriction imposed by (3-5).]

When θ_x is sufficiently small so that $\sin\theta_x$ can be approximated as θ_x, equation (3-4) becomes,

$$\theta_x^2\mu^4 - \left[\sin^2\frac{R}{\rho} + \theta_x^2\left(1-\sin^2\frac{R}{\rho}\cos^2\alpha\right)\right]\mu^2 + \sin^2\frac{R}{\rho}\sin^2\alpha = 0 \tag{3-8}$$

This latter equation will be solved for both the near (including convergent zone) field and the far field.

3.2.1 Near (and Convergent Zone) Field Solution: For the situation where R/ρ (or $\pi - R/\rho$) is sufficiently small so that $\sin^2(R/\rho)\cos^2\alpha \ll 1$, equation (3-8) may be approximated as,

$$\mu^4 - (\xi^2+1)\mu^2 + \xi^2\sin^2\alpha = 0 \tag{3-9}$$

where,

$$\xi = \sin(R/\rho)/\theta_x = 2\rho\sin(R/\rho)/D \tag{3-10}$$

The solution to (3-9) is,

$$\mu^2 = \tfrac{1}{2}[1+\xi^2 - \sqrt{1+\xi^4+2\xi^2\cos 2\alpha}\,] \tag{3-11}$$

3.2.2 Far Field Solution: When $\sin(R/\rho)$ is sufficiently large so that,

$$\sin^2(R/\rho) \gg D^2/(4\rho^2+D^2\cos^2\alpha) \tag{3-12}$$

equation (3-8) may be approximated as,

$$\mu^4 - \xi^2\mu^2 + \xi^2\sin^2\alpha = 0 \qquad (3\text{-}13)$$

The solution in this case is

$$\mu^2 = \tfrac{1}{2}\,\xi^2\left[1-\sqrt{1-(2\sin\alpha/\xi)^2}\right]$$

$$= \sin^2\alpha\left[1+\frac{\sin^2\alpha}{\xi^2}+2\,\frac{\sin^4\alpha}{\xi^4}+\ldots\right] \qquad (3\text{-}14)$$

4.0 SOLUTION OF THE ERROR VECTOR FOR A RECEIVING SENSOR PAIR

Using the relations given in Table 2, and the solutions for μ given in the last section, we may readily compute the error vector (for a given receiving sensor pair) in terms of the new variables R and α. This will be done for both the near and far fields.

4.1 Near (and Convergent Zone) Field Solution

For the near field solution we shall assume that $\sin^2\frac{R}{\rho} \ll 1$ and employ the relations given in (2-10), (2-11), and (3-11) along with the data provided in Table 2, to obtain,

$$\frac{ds}{d\mu} = \frac{D}{2}\sqrt{\frac{1+\xi^4+2\xi^2\cos2\alpha+(1-\xi^2)\sqrt{1+\xi^4+2\xi^2\cos2\alpha}}{1+\xi^4-2\xi^2\sin^2\alpha+(1-\xi^2)\sqrt{1+\xi^4+2\xi^2\cos2\alpha}}} \qquad (4\text{-}1)$$

and,

$$\tan\alpha_\mu = \pm\sqrt{\frac{\xi^2\cos^2\alpha\,\left[1+\xi^2-\sqrt{1+\xi^4+2\xi^2\cos2\alpha}\,\right]}{1+\xi^4\sin^2\alpha+\xi^2(1-3\sin^2\alpha)+(1-\xi^2\sin^2\alpha)\sqrt{1+\xi^4+2\xi^2\cos2\alpha}}} \qquad (4\text{-}2)$$

(NOTE: Due to the change of variables, the angle specified as β_μ no longer will give the direction of the error vector relative to a true North reference. A new variable α_μ is therefore employed in place of the former variable β_μ which was applicable only to the earlier specific example. In the present analysis, the angle α_μ will be orthogonal to the measure of the error vector direction. The angle is measured relative to the slope of the great circle curve joining the point (R,α) and the midpoint between the two receiving sensors; the referenced slope to be taken at the point (R,α). The geometry will be demonstrated later in Figure 10.)

The above equations can be greatly simplified by considering limited ranges for the value of ρ.

4.1.1 Case Where $2 \leq \rho$: For the situation where the variable ρ is equal to or greater than two, equations (4-1) and (4-2) reduce to,

$$\frac{ds}{d\mu} \approx \frac{D}{2\cos\alpha} \sqrt{\rho^2+\cos^2\alpha} \tag{4-3}$$

and

$$\alpha_\mu \approx \pm \tan^{-1} \left\{ \frac{\rho \tan \alpha}{\sqrt{1+\rho^2+\sin^2\alpha}} \right\} \tag{4-4}$$

Making use of (1-6), equation (4-3) becomes,

$$\frac{ds}{d\tau} \approx \frac{c\rho \sin(R/\rho)}{D\cos\alpha} \sqrt{1+[D\cos\alpha/2\rho\sin(R/\rho)]^2} \tag{4-5}$$

It should also be noted that, when ρ is large, the direction of the error vector is approximately orthogonal to the angle α; since, under the circumstances, $|\alpha_\mu| \approx |\alpha|$.

4.1.2 Case Where $\rho = 1$: For the situation where the variable ρ is equal to unity, equations (4-1) and (4-2) become simply,

$$\frac{ds}{d_\mu} = D/\sqrt{2} \tag{4-6}$$

and,

$$\alpha_\mu = \alpha/2 \tag{4-7}$$

Thus, at the particular range R=D/2, the scalar magnitude of the error vector is independent of the angle α. In addition, the direction of the error vector is orthogonal to the angle $\alpha/2$.

4.1.3 Case Where $\rho \leq 1/2$: When the variable ρ^2 is small compared with unity, equations (4-1) and (4-2) reduce to,

$$\frac{ds}{d\mu} \approx \frac{D}{2}\sqrt{1 + \frac{\xi^2\cos^2\alpha}{1-2\xi^2\sin^2\alpha + \xi^4(1-\cos^4\alpha)}} \tag{4-8}$$

and,

$$\alpha_\mu \approx \pm \tan^{-1}\left\{\xi^2\sin\alpha\cos\alpha\sqrt{\frac{1-\xi^2\cos^2\alpha}{1+\xi^2(1-3\sin^2\alpha)+\xi^4\sin^2\alpha}}\right\} \tag{4-9}$$

Thus, in the limit as $\xi \to 0$, the magnitude of the error vector reduces to $(c/2)d\tau$ and the direction follows the great circle path between the two receiving sensors.

4.1.4 Graphical Presentation of the Error Vector Data: Graphical plots of the error magnitude and the angle α_μ are illustrated in Figures 6 and 7 for the near (and convergent zone) field. The data are displayed in convenient format for data abstraction, once the values of range and relative bearing to the source are known.

4.2 Far Field Solution

For the far field solution we shall assume that $D^2/4\rho^2 \ll \sin^2(R/\rho)$. Employing the relations given in (2-12), (2-13), and (3-14) along with the data given in Table 2, we obtain

$$\frac{ds}{d\mu} \approx \frac{2\rho^2\sin^2(R/\rho)}{\sqrt{4\rho^2\sin^2(R/\rho)\cos^2\alpha - D^2[1+\cos^2(R/\rho)]\sin^4\alpha}} \tag{4-10}$$

and,

$$\alpha_\mu \approx \pm \tan^{-1}\left\{\sqrt{\frac{\cos^2(R/\rho)[4\rho^2\sin^2(R/\rho)+D^2\sin^2\alpha]\sin^2\alpha}{4\rho^2\sin^2(R/\rho)\cos^2\alpha - D^2\cos^2(R/\rho)\sin^4\alpha}}\right\} \tag{4-11}$$

The above equations will be suitable approximations of the subject measures for,

$$|\alpha| \leq \tan^{-1}\left\{\frac{\rho\sin(R/\rho)}{D}\right\} \tag{4-12}$$

Over the indicated range of α, then, the error vector relations may be approximated as

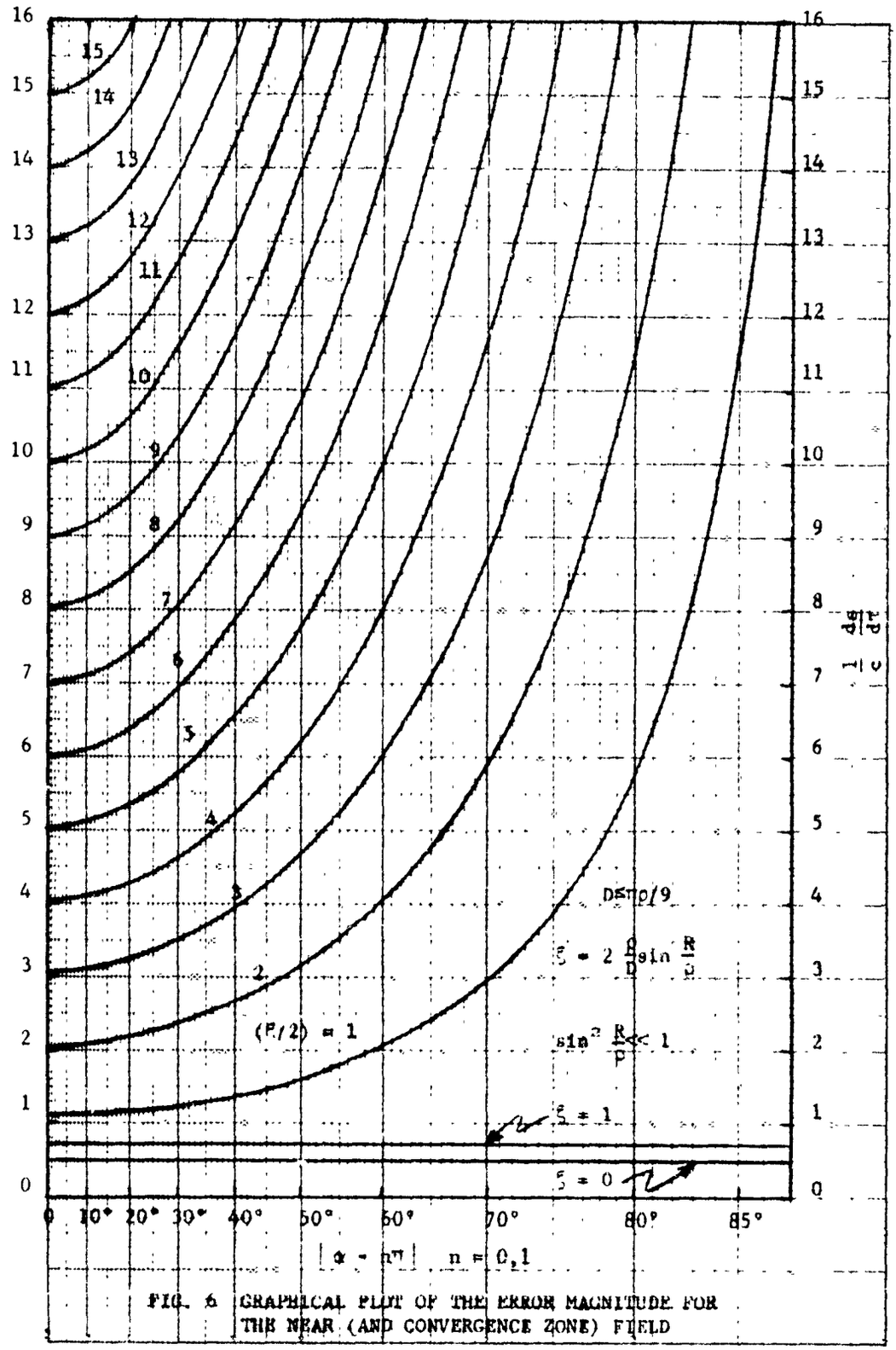

FIG. 6 GRAPHICAL PLOT OF THE ERROR MAGNITUDE FOR THE NEAR (AND CONVERGENCE ZONE) FIELD

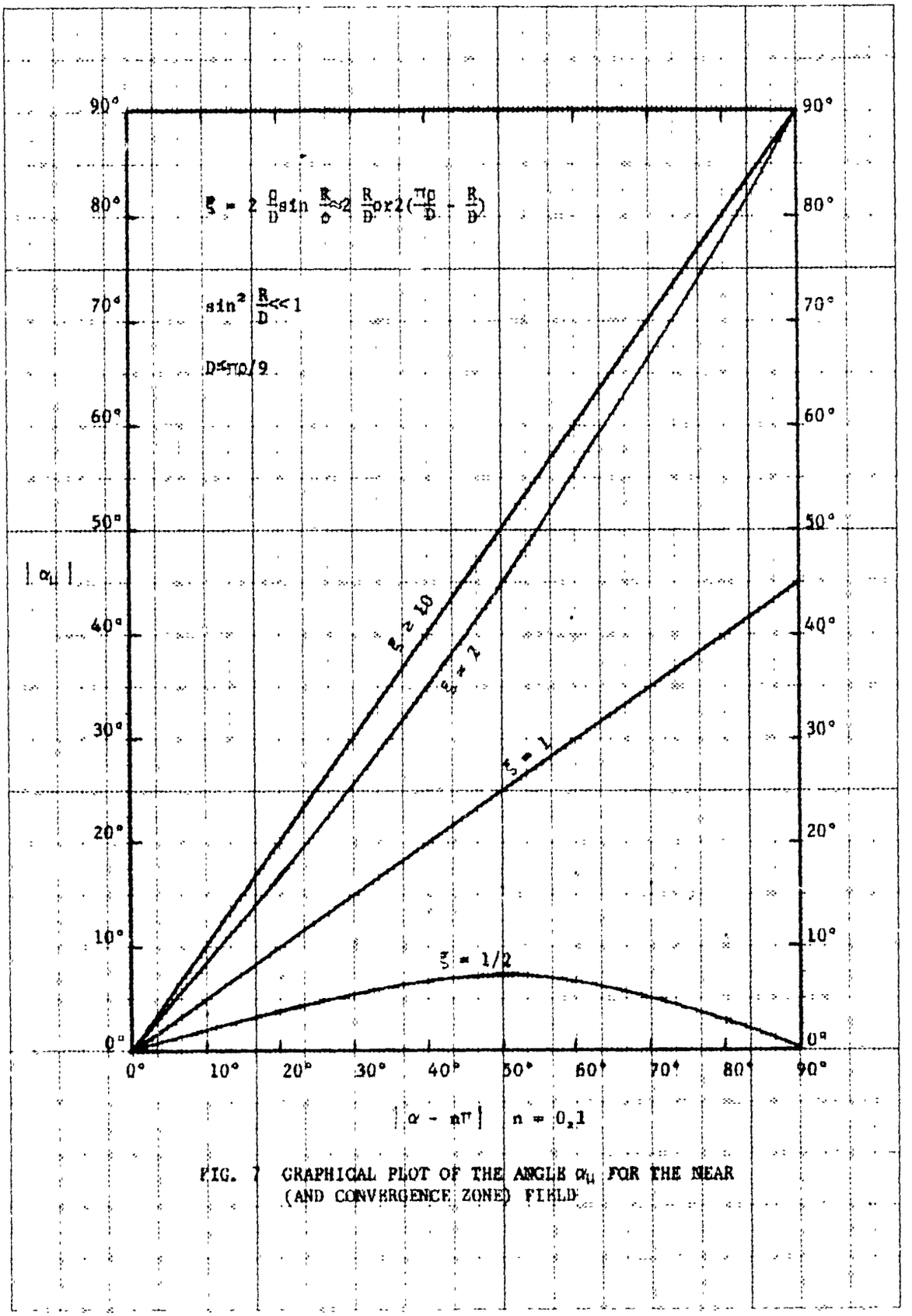

FIG. 7 GRAPHICAL PLOT OF THE ANGLE α_μ FOR THE NEAR (AND CONVERGENCE ZONE) FIELD

$$\frac{ds}{d\tau} \approx \frac{c\rho}{D} \frac{\sin(R/\rho)}{\cos\alpha} \tag{4-13}$$

$$\alpha_u \approx \pm \tan^{-1} \{\cos(R/\rho)\tan\alpha\} \tag{4-14}$$

Graphical plots of the above functions are illustrated in Figures 8 and 9 for convenience in data abstraction.

5.0 SOURCE LOCALIZATION ERROR ALGORITHMS

In this section we shall describe the general procedures; whereby, one may make use of the formulas and graphical illustrations developed in the earlier sections, to rather accurately define the area in which a source has been localized. This area-of-localization concept (rather than a single point) is based on the fact that the time register measure τ has a limit of resolution which will be $\pm\Delta\tau/2$. Since the measure of the variable τ is not precise, there will be some ambiguity about the exact location of the source which is directly related to the uncertainty (or resolution) in the measure of τ. It is, therefore, significant to be able to reasonably well define the influence of the τ measurement inaccuracy on the localization of the source.

5.1 General Description of the System Geometry

To define the source localization error, it will be necessary to know the location of the two (or more) receiving sensor pairs and the general location of the source relative to the receiving sensor pairs. In the subject problem, the precise location of all receiving sensors has been presumed to be known. The general location of the source will be simply the solution of the equations provided in Section II. This general location is based upon the actual measures of τ achieved at the two (or more) pairs of receiving stations. (Or, alternatively, a general location can be simply hypothesized for purposes of error analysis.)

Based on the location specifics described above, one may then construct a map (or diagram) of the general geometry as illustrated in Figure 10. The basic geometric orientation is illustrated in Figure 10(a), where the point 0

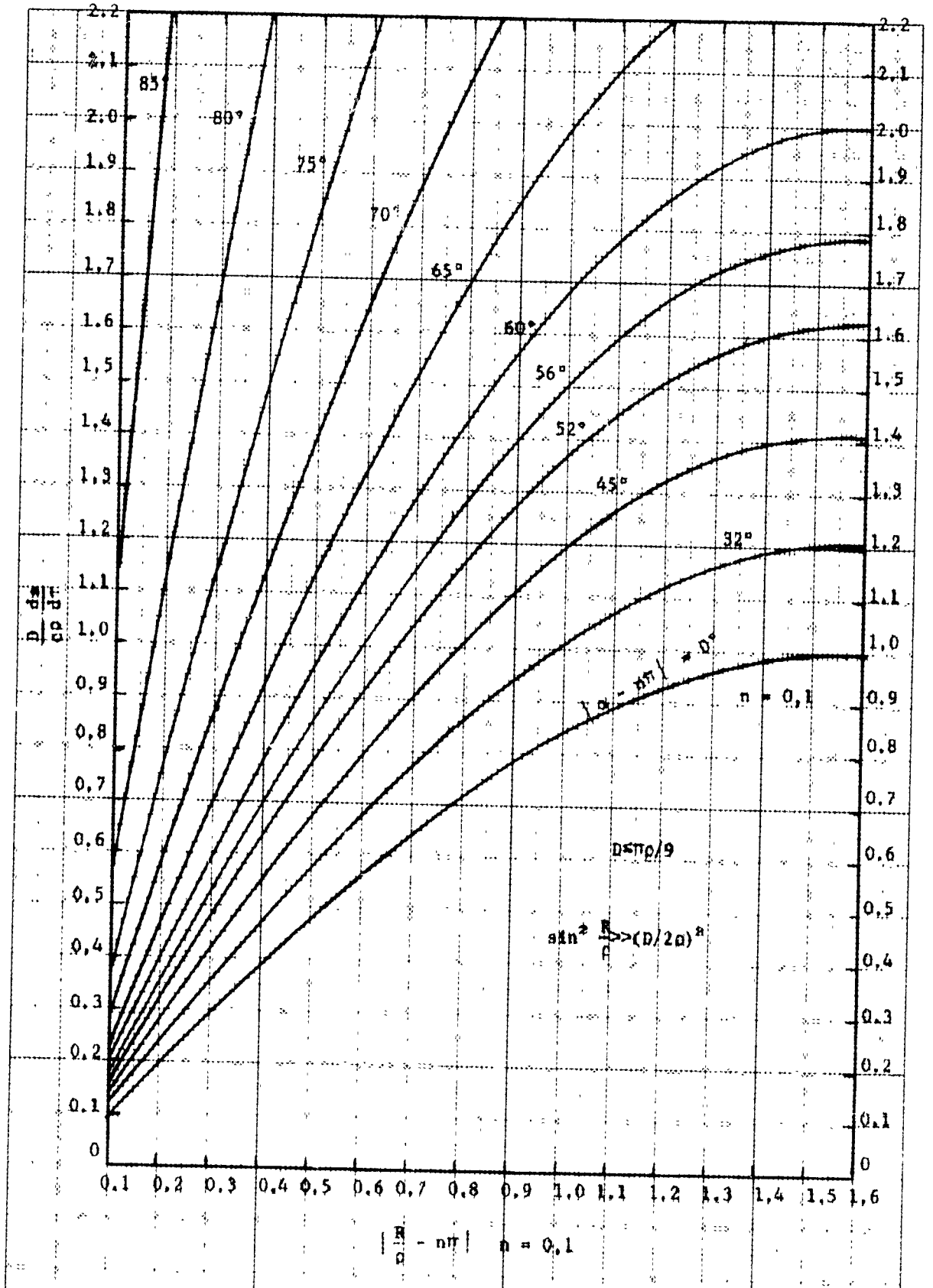

FIG. 8 GRAPHICAL PLOT OF THE ERROR MAGNITUDE FOR THE FAR FIELD

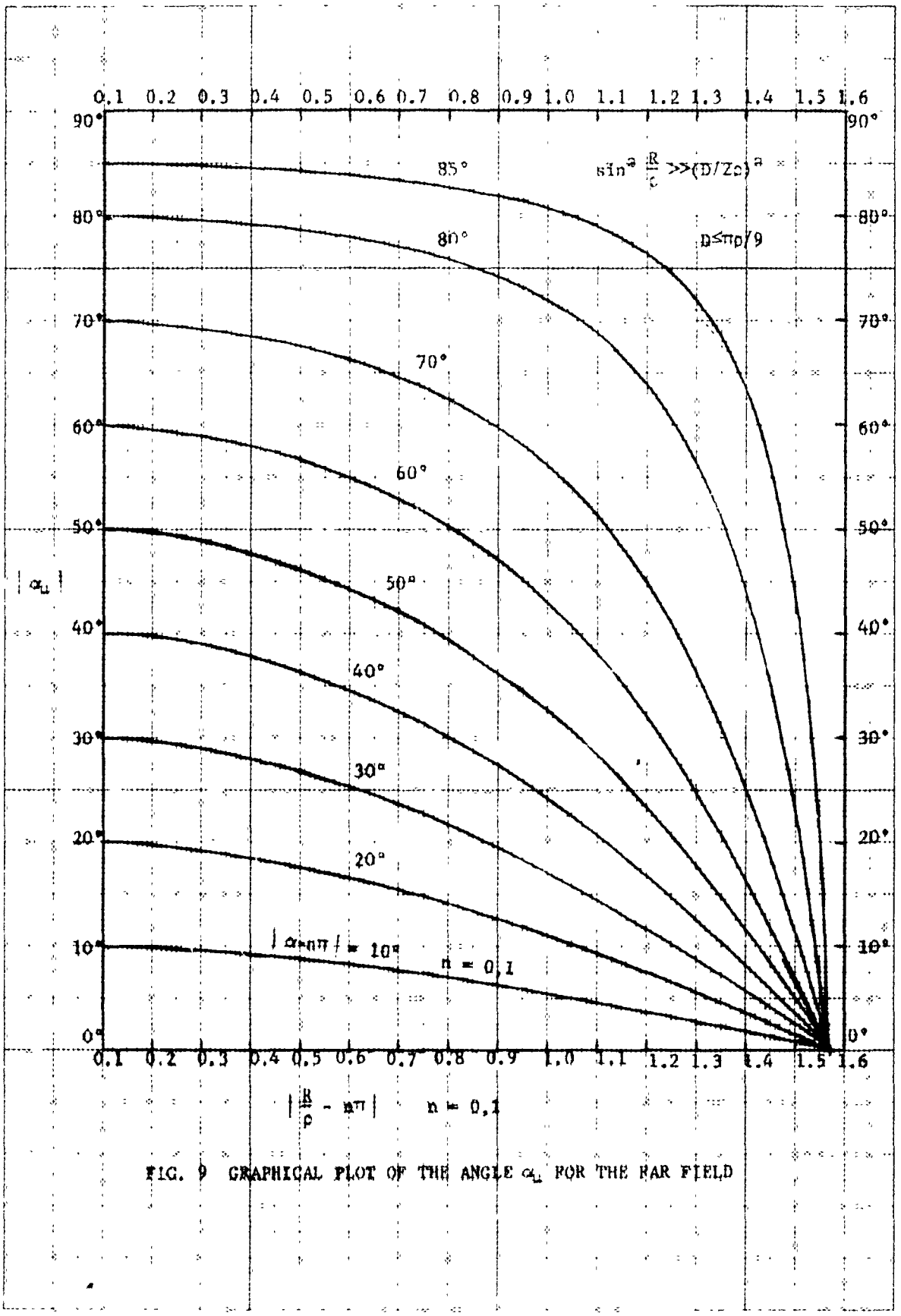

FIG. 9 GRAPHICAL PLOT OF THE ANGLE α_L FOR THE FAR FIELD

depicts the position of the source, and the points A_1 and A_2 depict the midpoint of the two sensor pairs. The lines OA_1 (or R_1) and OA_2 (or R_2) depict the great circle paths (and ranges) from the midpoints of the sensor pairs to the source. The lines A_1B_1 and A_2B_2 represent the great circle arcs through, and orthogonal to, the midpoints of the sensor pairs. The two angles α_1 and α_2 represent the angles to the source from the respective receiving sensor pairs. The two lines $A_1'B_1'$ and $A_2'B_2'$ are constructed to pass through the point 0 and parallel to the planes of the arcs A_1B_1 and A_2B_2 respectively. The angle Φ is the angle between the subject two reference axes.

Attention is now directed to Figure 10(b) which is a blow-up of the region about the point 0 with the two lines $A_1'B_1'$ and $A_2'B_2'$ as the appropriate reference axes. However, before proceeding further with the localization geometry, we shall first need to abstract the pertinent error vector data from the appropriate equations or graphs.

5.2 Error Vector Data Abstraction

From the system geometry, depicted in Figure 10(a), range and angle to the source (R_1,α_1 and R_2,α_2) from both pairs of receiving sensors may be determined (or computed). Using these data, along with the specified time register measurement resolution ($\pm\Delta\tau/2$)(or, alternatively, $\pm\sigma_\tau$), one may then employ the earlier equations (or graphs) to determine the magnitude of the respective error distances (Δs_1 and Δs_2), and the relevant angles (α_{u1} and α_{u2}) for each sensor pair. These data, along with the reference axes, $A_1'B_1'$ and $A_2'B_2'$ (illustrated in Figure 10) may then be employed to construct the localization error parallelogram.
(NOTE: A suitable measure for the time register resolution will be the standard deviation, σ_τ, of the time register measure τ. Either $\pm\sigma_\tau$ or a specific error increment, $\pm\Delta\tau/2$, can be employed in the error analysis.)

5.3 Construction of the Localization Error Parallelogram

Referring to Figure 10(b), the abstracted angles α_{u1} and α_{u2} are employed to construct a set of error axes C_1D_1 and C_2D_2. (NOTE: The direction of the error angles may readily be deduced, from the general

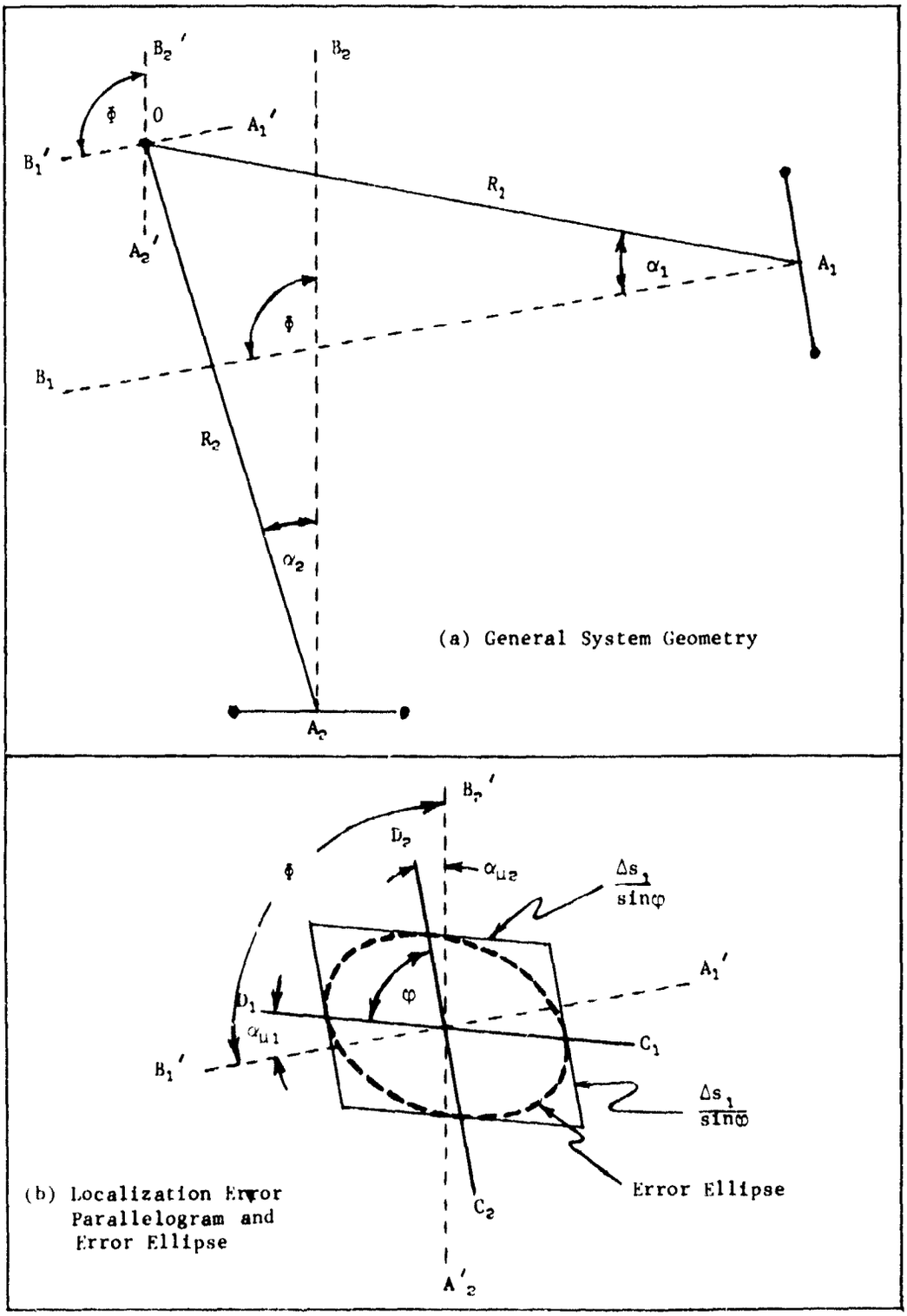

FIG. 10 DETERMINATION OF LOCALIZATION ERROR GEOMETRY FROM SYSTEM GEOMETRY AND ERROR VECTORS

system geometry, by noting which side of the great circle path, AB, that the source is located.) Using the error reference axes, then, we know that the direction of the error vector is orthogonal to these axes. As a consequence, one may construct the error parallelogram by drawing appropriate lines which are both; parallel to the error axes, and spaced a distance $\pm\Delta s/2$ from the error reference axes. The two sets of parallel lines are extended until they intersect; thus, forming the error parallelogram illustrated in Fig. 10(b). (NOTE: The commonly referred to error ellipse may be constructed within the error parallelogram as illustrated in the figure.)

Of great significance is the angle φ of intersection between the two error axes. This angle, along with the error magnitudes Δs_1 and Δs_2, will determine the dimensions and geometry of the localization error parallelogram.

From Figure 10(b) one may see that the angle φ is simply,

$$\varphi = \Phi - \alpha_{\mu 1} - \alpha_{\mu 2} \tag{4-15}$$

The lengths of the two sides of the parallelogram are respectively, $\Delta s_1/\sin\varphi$ and $\Delta s_2/\sin\varphi$. The area of the parallelogram, thus, becomes,

$$\text{Area} = \Delta s_1 \Delta s_2/\sin\varphi \tag{4-16}$$

and the length of the longest diagonal of the parallelogram is,

$$\ell = \frac{\sqrt{(\Delta s_1)^2+(\Delta s_2)^2+2\Delta s_1 \Delta s_2 \cos\varphi}}{\sin\varphi} \tag{4-17}$$

The importance of the angle φ should be quite evident. It can be seen that, the resolution of localization degrades as the angle φ approaches zero (or π), and improves as φ approaches $\pi/2$. Optimum localization resolution occurs when the source is located along the two great circle arcs A_1B_1 and A_2B_2, and when $\Phi = \pi/2 = \varphi$. From a study of the geometry considerations (illustrated in Figure 10), one may readily determine suitable sensor locations which will provide tolerable localization resolution over specified areas of the sphere.

For convenience, the dependence of the localization resolution area and the length of the long diagonal on the angle φ, is graphically displayed in Figure 11. The deterioration of localization resolution, for φ below about ten to twenty degrees, is quite apparent from the graph.

6.0 EXAMPLES OF THE USE OF THE LOCALIZATION ERROR DATA

To understand the use of the localization error data, and to develop a general "feel" for the magnitude of the localization resolution which is achievable in practice, several examples will be given in the areas of electromagnetic wave propagation and in underwater acoustic propagation.

6.1 Electromagnetic Localization Applications

In the following applications, it will be assumed that electromagnetic propagation, which essentially follows the curvature of the earth, is employed to locate a source at various positions with respect to strategically located receiving stations. The two pairs of receiving sensors will be assumed to each consist of sensors which are separated on great circle paths by a distance of one-thousand nautical miles. The source will be located at various distances from the pairs of receiving sensors to study the resulting localization resolution which might be achieved for typical geometries.

In the examples to be presented, we shall assume a mean global radius of 3,440 nautical miles and an electromagnetic propagation velocity around the earth surface of 161,500 nautical miles per second.

Three examples of source ranges (including angles) to the sensor pair centers (see Figure 10) are postulated. For convenience, all of the pertinent data on the source resolution are tabulated in Table 2 for easy reference. The upper part of the table gives the postulated data and the preliminary computations. The final results, illustrating the anti[illegible]ted source resolution parallelogram, are given in the lower five rows of the table.

The first example is a near field problem where the ranges to the source are less than the separation of the signal sensors. The second example is an

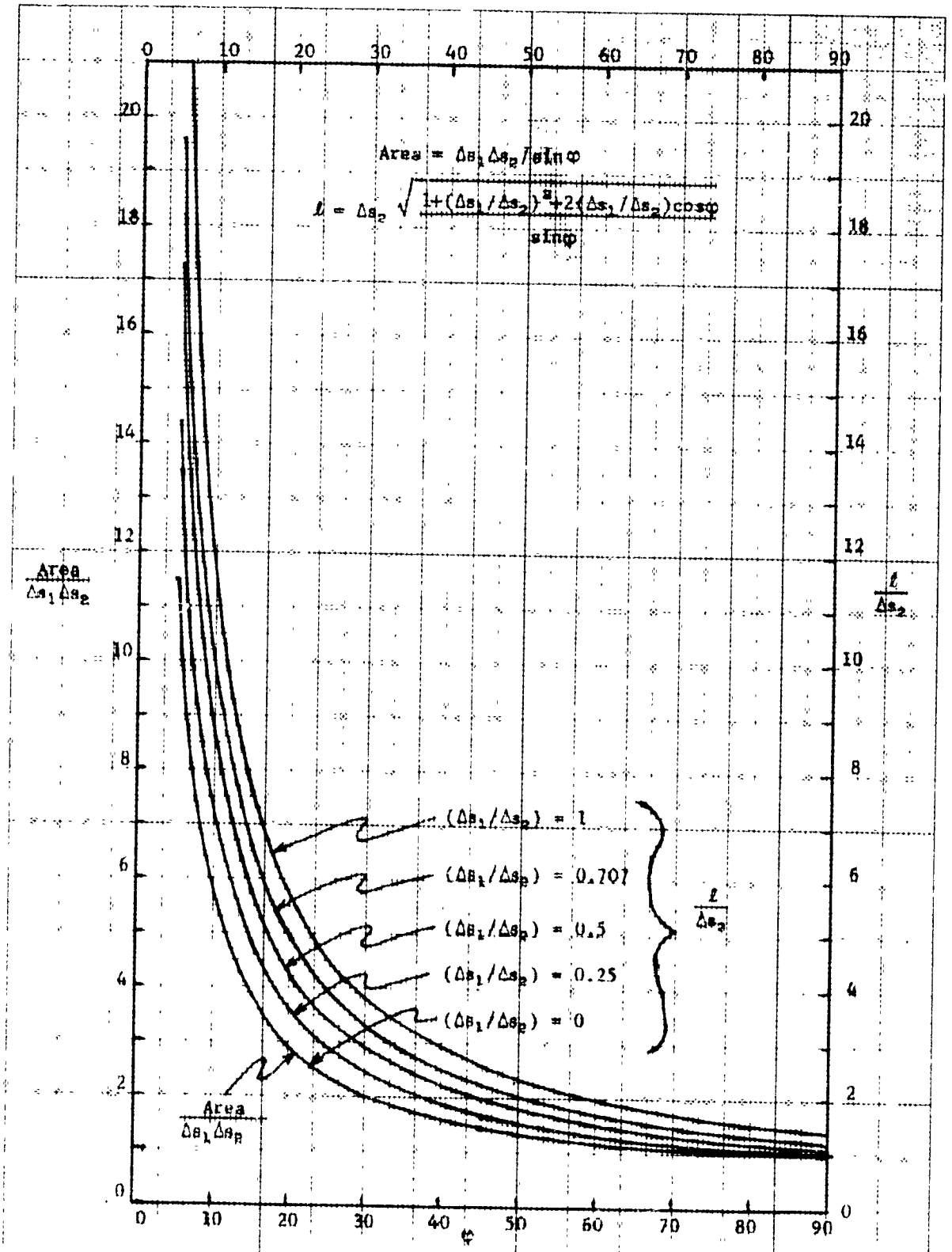

FIG. 11 DEPENDENCE OF LOCALIZATION RESOLUTION ON THE ANGLE φ

extremely long range problem where the source is located in the region of the extreme fa field convergence zone. In the third example the source is located in a region where the localization resolution is minimal. The first five rows of the table postulate the general geometry of the problem. The next five rows are basic data which are computed (or derived from the earlier graphs) on the basis of the individual sensor pair configurations. The final five rows illustrate the pertinent dimensions of the resolution error parallelogram which are computed from the earlier data. (NOTE: In the subject examples, the angle φ has been postulated as 60° in all cases. To compute this angle, additional information regarding the relative position of the two sensor pairs and the source would need to have been specified.)

In all three examples, the results are given in terms of the time difference resolution, $\Delta\tau$, (or, alternatively, $2\sigma_\tau$) measured in microseconds. For a one microsecond time difference resolution, then, the final answer is achieved by simply letting $\Delta\tau$ be equal to unity. For other time difference resolutions, the final answers may be readily derived. It is significant to note that the localization resolution, for examples 1 and 2 are identical; in spite of the fact that the relative ranges to the source are vastly different. This is a result of the convergent zone properties of the spherical geometry. Of course, the subject calculations do not take into account propagation anomalies (which must appear in the factor $\Delta\tau$); but even so, the relative accuracies of the measurement error would be as shown. This means that although, for the extremely long ranges the absolute accuracy of localization may be somewhat greater than shown (due to uncertainties in propagation paths and velocities), the relative position of two (or more) sources, for station keeping purposes, would be as normally computed.

6.2 Underwater Acoustic Localization Applications

In addition to electromagnetic propagation applications, the subject theory is also applicable to the field of underwater acoustics. In these latter applications, low frequency sound will travel over long distances in essentially great circle paths at a propagation velocity of approximately 0.8 nautical miles per second. These examples of underwater acoustic applications are considered in the same manner as was given for the electromagnetic

TABLE 2 RESULTS OF THREE EM LOCALIZATION EXAMPLES

		EXAMPLE		
		#1	#2	#3
D_1, D_2	(NMi.)	1,000	1,000	1,000
R_1	(NMi.)	500	10,300	6,000
α_1	(deg.)	75°	75°	20°
R_2	(NMi.)	400	10,400	4,000
α_2	(deg.)	45°	45°	15°
σ_{s_1}	(NMi.)	$0.114\Delta\tau$	$0.114\Delta\tau$	$0.600\Delta\tau$
α_{u1}	(deg.)	37.5°	37.5°	3.5°
σ_{s_2}	(NMi.)	$0.114\Delta\tau$	$0.114\Delta\tau$	$0.527\Delta\tau$
α_{u2}	(deg.)	18°	18°	3.0°
$\sigma_{s_1}\sigma_{s_2}$	(Sq. NMi.)	$0.013(\Delta\tau)^2$	$0.013(\Delta\tau)^2$	$0.316(\Delta\tau)^2$
RESOLUTION ▱	Φ	(deg.)	60°	60°	60°
	Side 1	(NMi.)	$0.132\Delta\tau$	$0.132\Delta\tau$	$0.693\Delta\tau$
	Side 2	(NMi.)	$0.132\Delta\tau$	$0.132\Delta\tau$	$0.600\Delta\tau$
	ℓ(diag.)	(NMi.)	$0.228\Delta\tau$	$0.228\Delta\tau$	$1.054\Delta\tau$
	Area	(Sq. NMi.)	$0.015(\Delta\tau)^2$	$0.015(\Delta\tau)^2$	$0.365(\Delta\tau)^2$

* NOTE: $\Delta\tau$ measure of ambiguity is given in microseconds

applications discussed in the previous section. The pertinent data for these examples are displayed in Table 3.

The first example is a near field problem where the ranges to the signal source are comparable to the sensor separation distance, D=200 NMi. In the second example, the ranges to the signal source have been increased to ranges of approximately 1000 nautical miles. It can, therefore, be anticipated that the resulting localization resolution will degrade appreciably. In the third example, the ranges to the source are the same as for example 2, and the sensor separation distance has been increased to 500 NMi. This last example is intended to illustrate the improvement in localization resolution which can be realized by employing more widely separated sensors in the sensor pair configuration. In all of the underwater

TABLE 3 RESULTS OF THREE UNDERWATER ACOUSTIC LOCALIZATION EXAMPLES

		EXAMPLE		
		#1	#2	#3
D_1, D_2	(NMi.)	200	200	500
R_1	(NMi.)	300	1200	1200
α_1	(deg.)	20°	15°	15°
R_2	(NMi.)	250	900	900
α_2	(deg.)	30°	20°	20°
$*\Delta s_1$	(NMi.)	$1.36\Delta\tau$	$5.08\Delta\tau$	$2.04\Delta\tau$
α_{u1}	(deg.)	18°	14.5°	14.5°
Δs_2	(NMi.)	$1.20\Delta\tau$	$3.85\Delta\tau$	$1.54\Delta\tau$
α_{u2}	(deg.)	26°	19.5°	19.5°
$\Delta s_1 \Delta s_2$	(Sq.NMi.)	$1.63(\Delta\tau)^2$	$19.56(\Delta\tau)^2$	$3.14(\Delta\tau)^2$
RESOLUTION φ	(deg.)	60°	60°	60°
RESOLUTION Side 1	(NMi.)	$1.57\Delta\tau$	$5.87\Delta\tau$	$2.36\Delta\tau$
RESOLUTION Side 2	(NMi.)	$1.39\Delta\tau$	$4.45\Delta\tau$	$1.78\Delta\tau$
RESOLUTION ℓ(diag.)	(NMi.)	$2.72\Delta\tau$	$8.89\Delta\tau$	$3.57\Delta\tau$
RESOLUTION Area	(Sq.NMi.)	$1.88(\Delta\tau)^2$	$26.6(\Delta\tau)^2$	$3.62(\Delta\tau)^2$

* NOTE: $\Delta\tau$ measure of ambiguity given in seconds

acoustic examples, the time difference resolution measure, $\Delta\tau$, is given in seconds.

7.0 OPTIMUM LOCALIZATION RESOLUTION SYSTEMS

In following the analysis of localization resolution, one may note that there exists an optimum geometry for source localization; beyond which, the resolution cannot be improved by geometric considerations. This optimum geometry is realized when the source is located anywhere on the great circle path joining the two sensor locations. On this line, the source localization resolution becomes, simply,

$$\Delta s = (c/2)\Delta\tau \qquad (7\text{-}1)$$

As the source deviates from this line, the localization resolution will degrade from that given in (7-1). However, the amount of degradation will be dependent on the great circle distance between the two sensor locations and the relation of the source to the two points. It can readily be shown that, if the source lies within a circle which passes through the two sensor points and is orthogonal to the great circle path between the two sensor points (that is, the straight line joining the two sensor points forms the diameter of the circle), then the localization resolution will be bounded by the following relation,

$$(c/2)\Delta\tau \leq \Delta s \leq (c/\sqrt{2})\Delta\tau \qquad (7\text{-}2)$$

This fact is readily evident in Figure 6. Thus, it appears that for, at least, limited regions of surveillance, the source localization resolution can be optimized and made essentially independent of source range and sensor spearation distance. Two applications of this optimum resolution phenomenon will now be considered.

7.1 Channel Navigation Application

Consider a relatively narrow channel through which vehicles; such as, ships, aircraft, etc. may wish to transit under controlled navigation conditions. By placing a pair of sensors (or sources) across and orthogonal to the channel, then, the optimum in localization resolution could be achieved for vehicles passing through the channel. If the length of the channel is short compared to the channel span, one pair of sensors (sources) would suffice for the navigation system. Otherwise, appropriately coded sets of sensors could be placed along the channel to guide the traffic along the entire length. The lateral localization resolution that is realizable by such a system is given by equation (7-2). For example, if an underwater acoustic system is employed across a relatively narrow straight, the localization resolution within the straight would be,

$$\begin{aligned} \Delta s &\approx 0.4\Delta\tau \quad \text{(nautical miles)} \\ &\approx 800\Delta\tau \quad \text{(yards)} \end{aligned} \qquad (7\text{-}3)$$

where $\Delta\tau$ is measured in seconds. Thus, if the measurement of time register, τ, is accurate to 0.1 second, the cross-channel resolution would be 80 yards. Shipping lanes (through the straight) of about 200 yards in width, appear readily assignable for the control of local traffic in this application. Such a system might be feasible for traffic control during times of relatively poor visibility to supplement or augment electromagnetic means of navigation.

7.2 Global Navigation Application

A most interesting application for the use of optimum localization resolution arises in the case where the sensor (or source) locations are spaced one hundred and eighty degrees apart, on opposite sides of the sphere. This situation was described in Section II, 3.1.1. In this circumstance, the source (or single receiver) will always lie on a great circle path which joins the two sensor (or source) points. Thus, equation (7-1) represents the localization resolution achievable everywhere on the surface of the globe. In this situation, all of the equi-time-register curves will be circles around the sphere, similar to the circles of constant Latitude on the earth. It is therefore intriguing to consider three orthogonal sets of sensors (sources), located on orthogonal axes and spaced one hundred and eighty degrees about the sphere, in an ideal type of global navigation scheme.

As an example of the proposed global navigation system, consider that three pairs of electromagnetic transmitters are located at the following earth coordinates relative to true North.

1. (90°N,0°W) and (90°S,0°W) True North and True South Poles.
2. (0°N,90°W) and (0°N,90°E) Equator at 90°West and 90° East Longitude.
3. (0°N,0°W) and (0°N,180°W) Equator at zero and 180° West Longitude.

The frequency of the transmissions will need to be such that the EM propagation will effectively circle the earth and be receivable around the globe.

For the hypothesized system, the localization equations will be, simply,

$$\theta_o = u_1\pi/2 = \sin^{-1}\left\{\sqrt{\cos^2(u_2\pi/2)-\sin^2(u_3\pi/2)}\right\}$$

$$= \cos^{-1}\left\{\sqrt{\sin^2(u_2\pi/2)+\sin^2(u_3\pi/2)}\right\} \qquad (7\text{-}4)$$

$$\phi_o = \sin^{-1}\left\{\frac{\sin(u_2\pi/2)}{\cos(u_1\pi/2)}\right\}$$

$$= \cos^{-1}\left\{\frac{\sin(u_3\pi/2)}{\cos(u_1\pi/2)}\right\}$$

$$= \tan^{-1}\left\{\frac{\sin(u_2\pi/2)}{\sin(u_3\pi/2)}\right\} \qquad (7\text{-}5)$$

where (θ_o, ϕ_o) is the location of the receiving station and,

$$\left.\begin{aligned} u_1 &= c\tau_1/\pi\rho \\ u_2 &= c\tau_2/\pi\rho \\ u_3 &= c\tau_3/\pi\rho \end{aligned}\right\} \qquad (7\text{-}6)$$

The subscripts, in the above indicated measures, represent the three listed transmitter pairs given previously.

For the postulated navigation system, the localization resolution in each of two dimensions will be,

$$\begin{aligned} \Delta s &= 0.081\Delta\tau \quad \text{(nautical miles)} \\ &= 162\Delta\tau \quad \text{(yards)} \end{aligned} \qquad (7\text{-}7)$$

where $\Delta\tau$ is the time register resolution in microseconds. Thus, for about a ten microsecond time register resolution, the positional resolution of receiver location will be within an area less than one square nautical mile. Of course, due to EM propagation anomolies, the absolute precision of location may be less than this. However, for the same general area, the propagation conditions should be identical; so that, the above localization resolution is applicable to relative position control for station keeping purposes, etc.

V

RESOLUTION IN SOURCE DYNAMICS

In Section III, we developed the algorithms or relations for computing the source dynamics (heading and speed) from a knowledge of the system geometry and the time scale-factor measures between two pairs of receiving sensors. Before the value of these computations can be assessed, however, it is essential to know the confidence or trust that can be placed in the computed results. That is, how accurate are the resulting dynamic calculations? If we can assume a negligible geometry and computational error, the principal contributor to error (or uncertainty in the computed results) will be the accuracy or inherent resolution of the basic time scale-factor measure, δ. Thus, what we intend to develop in this section is the influence of errors in the time scale-factor measure on the computed values for the source speed and heading. That is, we shall determine the resolution in the measures of the source dynamics in terms of the resolution of the basic time scale-factor measures.

The problem we are confronted with is quite complex and involved since it is intuitively evident that the answers we are seeking will be dependent, not only on the rather extensive geometry of the source and multisensor receiving system, but also on the interrelation of the dynamic variables themselves. Never-the-less, by a careful selection of system parameters which convey physical meaning within the geometric system, we shall be able to present the final data in a form readily interpretable and useful in physical applications.

1.0 BASIC RELATIONS

To begin our solution, we shall develop the basic differential equations which relate the sensitivity of the source dynamics to variations in the time scale-factor measure.

1.1 Source Velocity Relation

The basic differential equation for the source velocity will be,

$$dv = \frac{\partial v}{\partial \delta_1} d\delta_1 + \frac{\partial v}{\partial \delta_2} d\delta_2 \tag{1-1}$$

where, in the present study, the subscript 1 will be employed to denote the time scale-factor measure for the first pair of receiving sensors, and the subscript 2 will denote the time scale-factor measure for the second pair of receiving sensors. Previously (in Section III) the subscripts for these measures were xy and zw respectively. (For convenience, the subscripts 1 and 2 will be used to replace the earlier subscript notation for all of the system parameters dealing with the two pairs of receiving sensors.)

Using equation (3-7) in Section III, we may readily carry out the differential operations called for in (1-1) to obtain,

$$dv = \frac{c[b_2(b_2\delta_1 - b_1\delta_2\cos 2\eta)d\delta_1 + b_1(b_1\delta_2 - b_2\delta_1\cos 2\eta)d\delta_2]}{2b_1b_2\sin 2\eta\sqrt{(b_2\delta_1)^2+(b_1\delta_2)^2-2b_1b_2\delta_1\delta_2\cos 2\eta}}$$

$$= \frac{c^2[b_2(b_2\delta_1 - b_1\delta_2\cos 2\eta)d\delta_1 + b_1(b_1\delta_2 - b_2\delta_1\cos 2\eta)d\delta_2]}{4\ vb_1^2b_2^2\sin^2 2\eta} \tag{1-2}$$

1.2 Source Heading Relation

Following the same procedure as for the source velocity, the source heading differential relation may be derived from (3-6), Section III, as,

$$d\beta = \frac{\partial \beta}{\partial \delta_1} d\delta_1 + \frac{\partial \beta}{\partial \delta_2} d\delta_2$$

$$= \frac{-b_1b_2(\delta_2 d\delta_1 - \delta_1 d\delta_2)\sin 2\eta}{(b_2\delta_1)^2+(b_1\delta_2)^2-2b_1b_2\delta_1\delta_2\cos 2\eta}$$

$$= \frac{-c^2(\delta_2 d\delta_1 - \delta_1 d\delta_2)}{4v^2b_1b_2\sin 2\eta} \tag{1-3}$$

2.0 RELATIONS EXPRESSED IN INTERPRETABLE FORM

Although the basic relations, derived above, are correct, they are not

in a form that is readily interpretable. We shall therefore proceed to define some new parameters which transform the parameters given in (1-2) and (1-3) into ones which are readily interpretable in terms of the physical geometry of the system under consideration.

2.1 Definition of Geometric Parameters

In Section III, we defined a number of parameters; including, ξ, η, b_1, and b_2, which were convenient in developing the solution for the velocity, v, and heading, θ, of the source. We shall now proceed to define a new set of parameters which will better illustrate the geometry of the problem we are dealing with and provide an insight into the effect of the system geometry on the resolution of the measures for v and β.

Referring to equation (3-3), Section III, let,

$$\left.\begin{aligned} \bar{\beta}_1 &= \xi - \eta = \tfrac{1}{2}(\beta_{ox}+\beta_{oy}) \\ \bar{\beta}_2 &= \xi + \eta = \tfrac{1}{2}(\beta_{oz}+\beta_{ow}) \end{aligned}\right\} \qquad (2\text{-}1)$$

The above two new parameters represent the mean angles of the source rays to the first and second pairs of sensors respectively.

From (2-1), then, it is seen that,

$$2\eta = \bar{\beta}_2 - \bar{\beta}_1 = \Delta\bar{\beta}_{21} \qquad (2\text{-}2)$$

where, $\Delta\bar{\beta}_{21}$ is a new parameter representing the angle between the two mean angles defined in (2-1).

From equation (3-2), Section III, we may write,

$$\left.\begin{aligned} b_1 &= \sin\tfrac{1}{2}(\beta_{oy}-\beta_{ox}) = \sin(\Delta\beta_1/2) \\ b_2 &= \sin\tfrac{1}{2}(\beta_{ow}-\beta_{oz}) = \sin(\Delta\beta_2/2) \end{aligned}\right\} \qquad (2\text{-}3)$$

where $\Delta\beta_1$ and $\Delta\beta_2$ represent, respectively, the angle between the rays emanating from the source to the two sensors in each pair (that is, they represent the respective pair aperture angles).

It will also be convenient to define one additional new parameter as follows. Let,

$$\bar{\beta}_{21} = \tfrac{1}{2}(\bar{\beta}_1 + \bar{\beta}_2) = \xi \qquad (2\text{-}4)$$

The above parameter represents the mean of the two mean angles $\bar{\beta}_1$ and $\bar{\beta}_2$, given in (2-1) (which is also the mean of all four sensor rays).

To obtain a better understanding of the geometric significance of the new parameters, they are presented diagramatically in Figure 12. (Although the subject diagram is, of necessity, drawn on a plane, one should keep in mind that the lines and angles are intended to represent what would be realized geometrically on the surface of a sphere.)

For a number of applications, one may approximate the angles $\Delta\beta_1/2$ and $\Delta\beta_2/2$ by the following equations,

$$\left.\begin{aligned} |\,\Delta\beta_1/2\,| &\approx \tan^{-1}\{D_1\cos\alpha_1/2R_1\} \\ |\,\Delta\beta_2/2\,| &\approx \tan^{-1}\{D_2\cos\alpha_2/2R_2\} \end{aligned}\right\} \qquad (2\text{-}5)$$

where, D_1 and D_2 represent the great circle distance between the two sensors for each sensor pair, and the ranges (R_1 and R_2) and angles (α_1 and α_2) are as shown in Figure 10. The suitability of the above approximations will need to be examined for the specific application under consideration.

2.2 Dynamic Error Relations

We may now employ the new parameters, defined in the last section, in the error relations given in (1-2) and (1-3). To do this, we will make use of equation (3-4), Section III, and the following two identities,

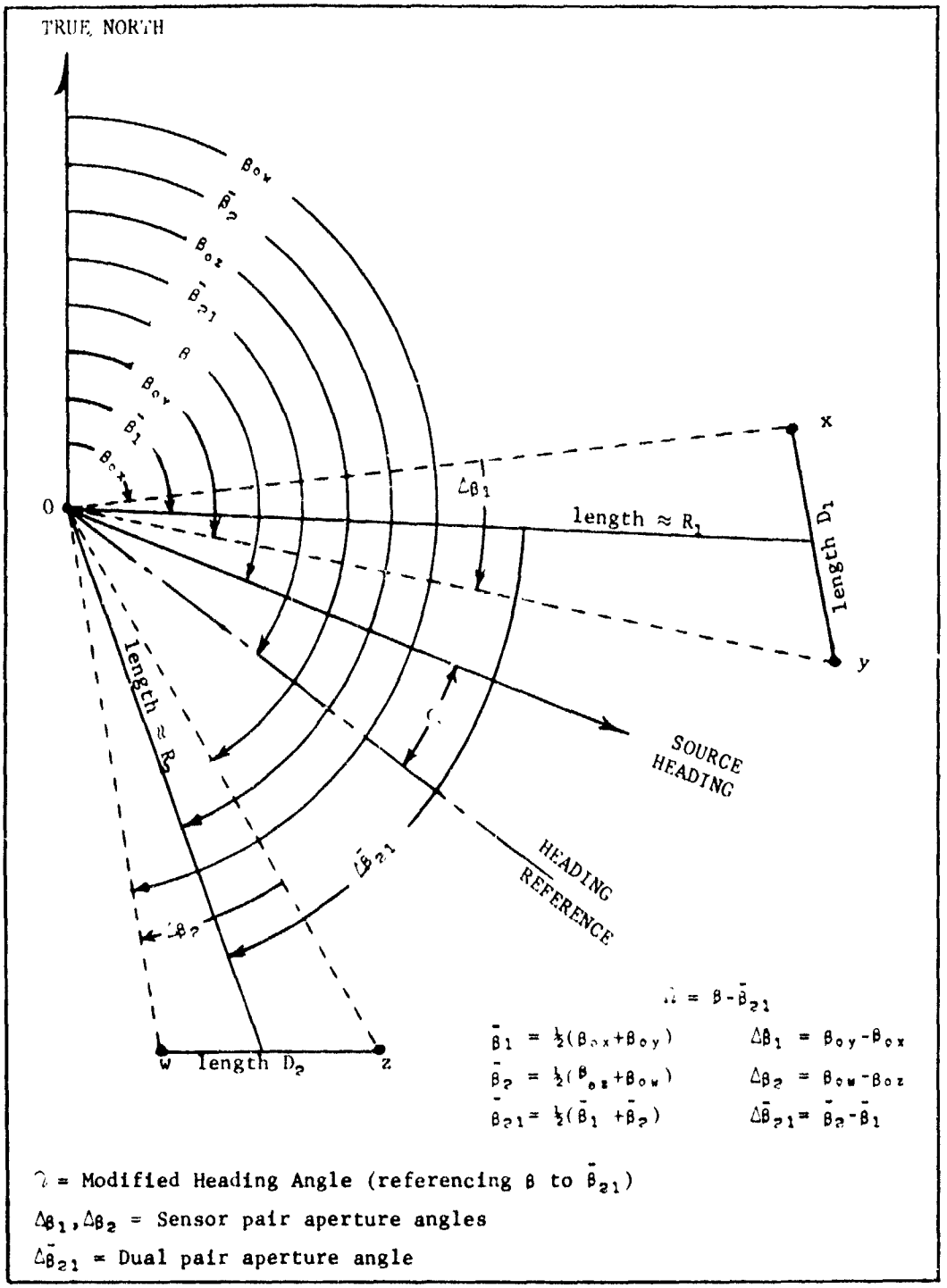

FIG. 12 GEOMETRIC DIAGRAM ILLUSTRATING THE SIGNIFICANT PARAMETERS INVOLVED IN THE SOURCE DYNAMIC ERROR RELATIONS

$$\left.\begin{aligned} \sin(\bar{\beta}_1-\beta)-\sin(\bar{\beta}_2-\beta)\cos\Delta\bar{\beta}_{21} &= -\sin\Delta\bar{\beta}_{21}\cos(\bar{\beta}_2-\beta) \\ \sin(\bar{\beta}_2-\beta)-\sin(\bar{\beta}_1-\beta)\cos\Delta\bar{\beta}_{21} &= \sin\Delta\bar{\beta}_{21}\cos(\bar{\beta}_1-\beta) \end{aligned}\right\} \qquad (2\text{-}6)$$

Carrying out the resulting algebra, we obtain for the dynamic error functions,

$$dv = \frac{c}{2\sin\Delta\bar{\beta}_{21}}\left[\frac{\cos(\bar{\beta}_2-\beta)}{\sin(\Delta\beta_1/2)}\,d\delta_1 - \frac{\cos(\bar{\beta}_1-\beta)}{\sin(\Delta\beta_2/2)}\,d\delta_2\right]$$

$$= \frac{c}{2\sin\Delta\bar{\beta}_{21}}\left[\frac{\cos(\Omega-\Delta\bar{\beta}_{21}/2)}{\sin(\Delta\beta_1/2)}\,d\delta_1 - \frac{\cos(\Omega+\Delta\bar{\beta}_{21}/2)}{\sin(\Delta\beta_2/2)}\,d\delta_2\right] \qquad (2\text{-}7)$$

and,

$$d\beta = \frac{c}{2v\sin\Delta\bar{\beta}_{21}}\left[\frac{\sin(\bar{\beta}_2-\beta)}{\sin(\Delta\beta_1/2)}\,d\delta_1 - \frac{\sin(\bar{\beta}_1-\beta)}{\sin(\Delta\beta_2/2)}\,d\delta_2\right]$$

$$= \frac{-c}{2v\sin\Delta\bar{\beta}_{21}}\left[\frac{\sin(\Omega-\Delta\bar{\beta}_{21}/2)}{\sin(\Delta\beta_1/2)}\,d\delta_1 - \frac{\sin(\Omega+\Delta\bar{\beta}_{21}/2)}{\sin(\Delta\beta_2/2)}\,d\delta_2\right] \qquad (2\text{-}8)$$

where,

$$\Omega = \beta-\bar{\beta}_{21} \qquad (2\text{-}9)$$

That is, the variable Ω is the measure of the source heading relative to the mean angle of all rays from the source to the four receiving sensors (see Figure 12).

(NOTE: The heading error, $d\beta$, given in (2-8) is in radians. To convert to degrees, this relation should be multiplied by the factor $180/\pi$.)

2.3 Properties of the Dynamic Error

From (2-7) and (2-8) it is evident that,

$$d\beta = -dv/v \qquad (2\text{-}10)$$

for the heading angle advanced ninety degrees. It is further evident that the resolution in source heading will be inversely proportional to the source velocity. This is to be expected intuitively; since, for a source velocity of zero, the heading becomes completely ambiguous.

It is further evident that for some particular source heading, the dynamic error will be inversely proportional to the sine of the angle $\Delta\bar{\beta}_{21}$. Consequently, the dynamic error tends to minimize when $\bar{\beta}_1$ is orthogonal to $\bar{\beta}_2$ (see Figure 12). (NOTE: The fact that this is not true for all source headings will be discussed later. At this point we are confining our remarks only to the general trend where all heading angles need to be considered.) The error also minimizes as $\sin(\Delta\beta_1/2)$ and $\sin(\Delta\beta_2/2)$ approaches unity. Thus, the error reduces as the sensor separation distance D_1 and D_2 increases and the range to the source (from the sensor midpoints) decreases (see Figures 10 and 12). These results appear intuitively acceptable based upon geometric considerations.

3.0 DYNAMIC ERROR MEASURE STATISTICS

Equations (2-7) and (2-8) can be used to determine the error in the source dynamics for specified error in the measures of δ_1 and δ_2 (providing the errors are quite small.) Of greater significance will be the expected values of these errors and their standard deviations. These statistical measures of error will now be computed in terms of the standard deviation of the measure of the time scale-factor shift variable δ.

3.1 Probability Density Function for the Dynamic Error Measures

From (2-7) and (2-8) it is evident that the dynamic error measures, dv and $d\beta$, take the form,

$$\epsilon = A\Delta\delta_1 + B\Delta\delta_2 \qquad (3\text{-}1)$$

where ϵ represents the dynamic error statistic (dv or $d\beta$), A and B are parameters, and $\Delta\delta_1$ and $\Delta\delta_2$ are independent statistical samples of the time scale-factor shift error statistic. We wish to determine the mean or expected value of ϵ and also the variance of ϵ about this expected value.

To accomplish our objective, we shall assume that the time scale-factor error statistics, $\Delta\delta_1$ and $\Delta\delta_2$, are independent and have a zero mean Gaussian distribution. For this assumption (which is quite reasonable), it is a simple matter to show that the dynamic error statistic, ϵ, also has a zero

mean Gaussian distribution. The expected value of ϵ will, therefore, be zero, and it may readily be shown that the variance of ϵ will be,

$$\sigma_\epsilon^2 = (A^2+B^2)\sigma_\delta^2 \tag{3-2}$$

where, σ_δ is the standard deviation of the time scale-factor shift variable δ.

3.2 Standard Deviation of the Dynamic Error Measures

Using the results of (3-2) in (2-7) and (2-8) we obtain the standard deviation of the dynamic errors as,

$$\sigma_v = \frac{c\sigma_\delta}{2\,|\sin\Delta\bar{\beta}_{21}|}\sqrt{\frac{\cos^2(\Omega-\Delta\bar{\beta}_{21}/2)}{\sin^2(\Delta\beta_1/2)} + \frac{\cos^2(\Omega+\Delta\bar{\beta}_{21}/2)}{\sin^2(\Delta\beta_2/2)}} \tag{3-3}$$

and

$$\sigma_\beta = \frac{90c\sigma_\delta}{\pi v\,|\sin\Delta\bar{\beta}_{21}|}\sqrt{\frac{\sin^2(\Omega-\Delta\bar{\beta}_{21}/2)}{\sin^2(\Delta\beta_1/2)} + \frac{\sin^2(\Omega+\Delta\bar{\beta}_{21}/2)}{\sin^2(\Delta\beta_2/2)}} \tag{3-4}$$

where the standard deviation of the source heading is given in degrees.

3.3 Properties of the Standard Deviations

The following properties of the standard deviations given in (3-3) and (3-4) will be found useful.

$$\sigma_\theta(\Omega;\Delta\bar{\beta}_{21},\Delta\beta_1,\Delta\beta_2) = \frac{180}{\pi v}\,\sigma_v(\Omega-90;\Delta\bar{\beta}_{21},\Delta\beta_1,\Delta\beta_2) \tag{3-5}$$

$$\sigma_v(-\Omega;\Delta\bar{\beta}_{21},\Delta\beta_1,\Delta\beta_2) = \sigma_v(180-\Omega;\Delta\bar{\beta}_{21},\Delta\beta_1,\Delta\beta_2)$$

$$= \sigma_v(\Omega;-\Delta\bar{\beta}_{21},\Delta\beta_1,\Delta\beta_3) = \sigma_v(\Omega;\Delta\bar{\beta}_{21},\Delta\beta_2,\Delta\beta_1) \tag{3-6}$$

and,

$$\sigma_v(\Omega;180-\Delta\bar{\beta}_{21},\Delta\beta_1,\Delta\beta_2) = \sigma_v(\Omega-90;\Delta\bar{\beta}_{21},\Delta\beta_2,\Delta\beta_1)$$

$$= \sigma_v(90-\Omega;\Delta\bar{\beta}_{21},\Delta\beta_1,\Delta\beta_2) \qquad (3\text{-}7)$$

Equation (3-5) illustrates the simple relationship between the standard deviations of the two dynamic measures, and equations (3-6) and (3-7) demonstrate the symmetries that exist between the modified heading variable, Ω, and the parameters $\Delta\bar{\beta}_{21}$, $\Delta\beta_1$ and $\Delta\beta_2$.

3.3.1 Non-Dimensional Equation Form: For convenience, the following nondimensional form will be used to express the source dynamics errors. Let,

$$r_v(\Omega;\Delta\bar{\beta}_{21},b) = \left|\sin(\Delta\beta_a/2)\right| \frac{\sigma_v}{c\sigma_\delta}$$

$$= \frac{\sqrt{\cos^2(\Omega'-\Delta\bar{\beta}_{21}/2)+b^2\cos^2(\Omega'+\Delta\bar{\beta}_{21}/2)}}{2\left|\sin(\Delta\bar{\beta}_{21})\right|} \qquad (3\text{-}8)$$

and,

$$r_\beta(\Omega;\Delta\bar{\beta}_{21},b) = \left|\sin(\Delta\ell_a/2)\right| \frac{v\sigma_\beta}{c\sigma_\delta}$$

$$= \frac{180}{\pi}\, r_v(\Omega-90;\Delta\bar{\beta}_{21},b) \qquad (3\text{-}9)$$

where,

$$\left.\begin{aligned} b &= \frac{\sin(\Delta\beta_a/2)}{\sin(\Delta\beta_b/2)} \\ \left|\Delta\beta_a\right| &\le \left|\Delta\beta_b\right| \end{aligned}\right\} \qquad (3\text{-}10)$$

and where,

$\Delta\beta_a$ is the smaller of the absolute values of $\Delta\beta_1$ and $\Delta\beta_2$

$\Delta\beta_b$ is the larger of the absolute values of $\Delta\beta_1$ and $\Delta\beta_2$

Ω' is a new modified source heading angle related to the modified source heading angle Ω in a manner defined in Table 5.

The above functions are plotted graphically in Figures 13 through 17 for convenience in data abstraction. Selection of the appropriate scales (on the graphs), as a function of the variables and the range on the pertinent parameters, is given in Table 4 for ready reference.

TABLE 4 INTERPRETATION OF SCALES ON THE ACCOMPANYING GRAPHS

		$\Gamma_v = \lvert\sin(\Delta\beta_a/2)\rvert\,\sigma_v/(c\sigma_\delta)$ (Use left hand ordinate scale)		$\Gamma_\beta = \lvert\sin(\Delta\beta_a/2)\rvert\, v\sigma_\beta/(c\sigma_\delta)$ (Use right hand ordinate scale)	
		$\lvert\Delta\beta_1\rvert \le \lvert\Delta\beta_2\rvert$	$\lvert\Delta\beta_2\rvert < \lvert\Delta\beta_1\rvert$	$\lvert\Delta\beta_1\rvert \le \lvert\Delta\beta_2\rvert$	$\lvert\Delta\beta_2\rvert < \lvert\Delta\beta_1\rvert$
		$(\Delta\beta_a = \Delta\beta_1)$	$(\Delta\beta_a = \Delta\beta_2)$	$(\Delta\beta_a = \Delta\beta_1)$	$(\Delta\beta_a = \Delta\beta_2)$
$\lvert\Delta\bar{\beta}_{21}\rvert \le 90°$	$0 < \Delta\bar{\beta}_{21}$	$\Omega' = \Omega$ (lower scale)	$\Omega' = -\Omega$ (lower scale)	$\Omega'-90 = \Omega$ (upper scale)	$\Omega'-90 = -\Omega$ (upper scale)
	$\Delta\bar{\beta}_{21} < 0$	$\Omega' = -\Omega$ (lower scale)	$\Omega' = \Omega$ (lower scale)	$\Omega'-90 = -\Omega$ (upper scale)	$\Omega'-90 = \Omega$ (upper scale)
$90° \le \lvert\Delta\bar{\beta}_{21}\rvert$	$0 < \Delta\bar{\beta}_{21}$	$\Omega'-90 = -\Omega$ (upper scale)	$\Omega'-90 = \Omega$ (upper scale)	$\Omega' = -\Omega$ (lower scale)	$\Omega' = \Omega$ (lower scale)
	$\Delta\bar{\beta}_{21} < 0$	$\Omega'-90 = \Omega$ (upper scale)	$\Omega'-90 = -\Omega$ (upper scale)	$\Omega' = \Omega$ (lower scale)	$\Omega' = -\Omega$ (lower scale)

NOTE: See Figure 12 for geometric interpretation of variable and parameters

3.3.2 Analysis of the Graphical Data: A study of the standard deviations displayed graphically in Figures 13 through 17 reveals the following:

(1) The dynamic error (or standard deviation) will be directly proportional to the sine of one-half the aperture angle of the smallest sensor-pair aperture ($\Delta\beta_a$). (The aperture angle of a sensor pair is taken as the angle between the two great circle rays emanating from the source to the two individual sensors forming the sensor pair.) Therefore, the larger that the smallest of the two aperture angles becomes, the better will be the resolution of the dynamic measures. The optimum aperture angle will, of course, be 180 degrees. This aperture angle occurs when the source is located on the great circle path between the sensor pair.

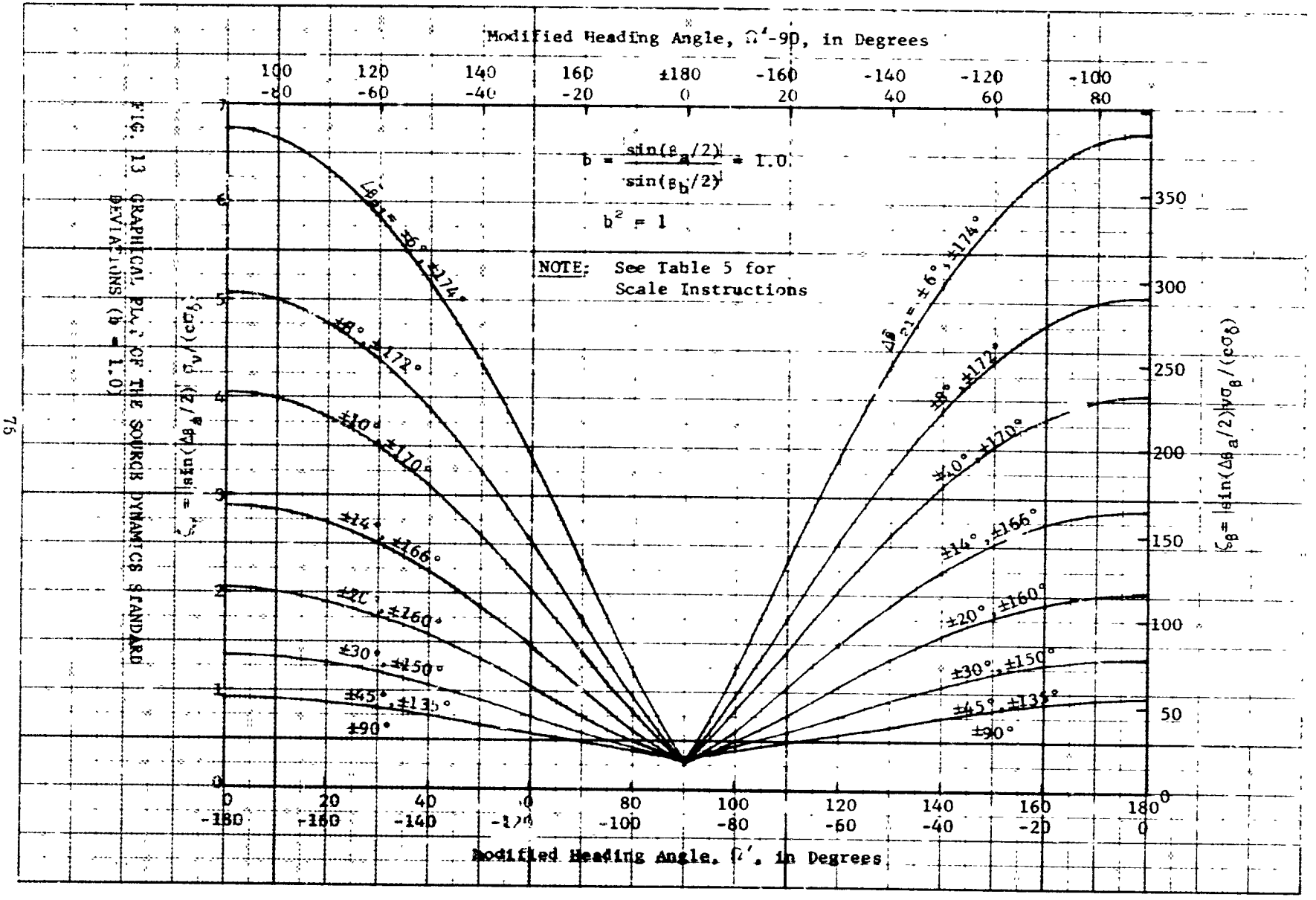

FIG. 13 GRAPHICAL PLOT OF THE SOURCE DYNAMICS STANDARD DEVIATIONS (b = 1.0)

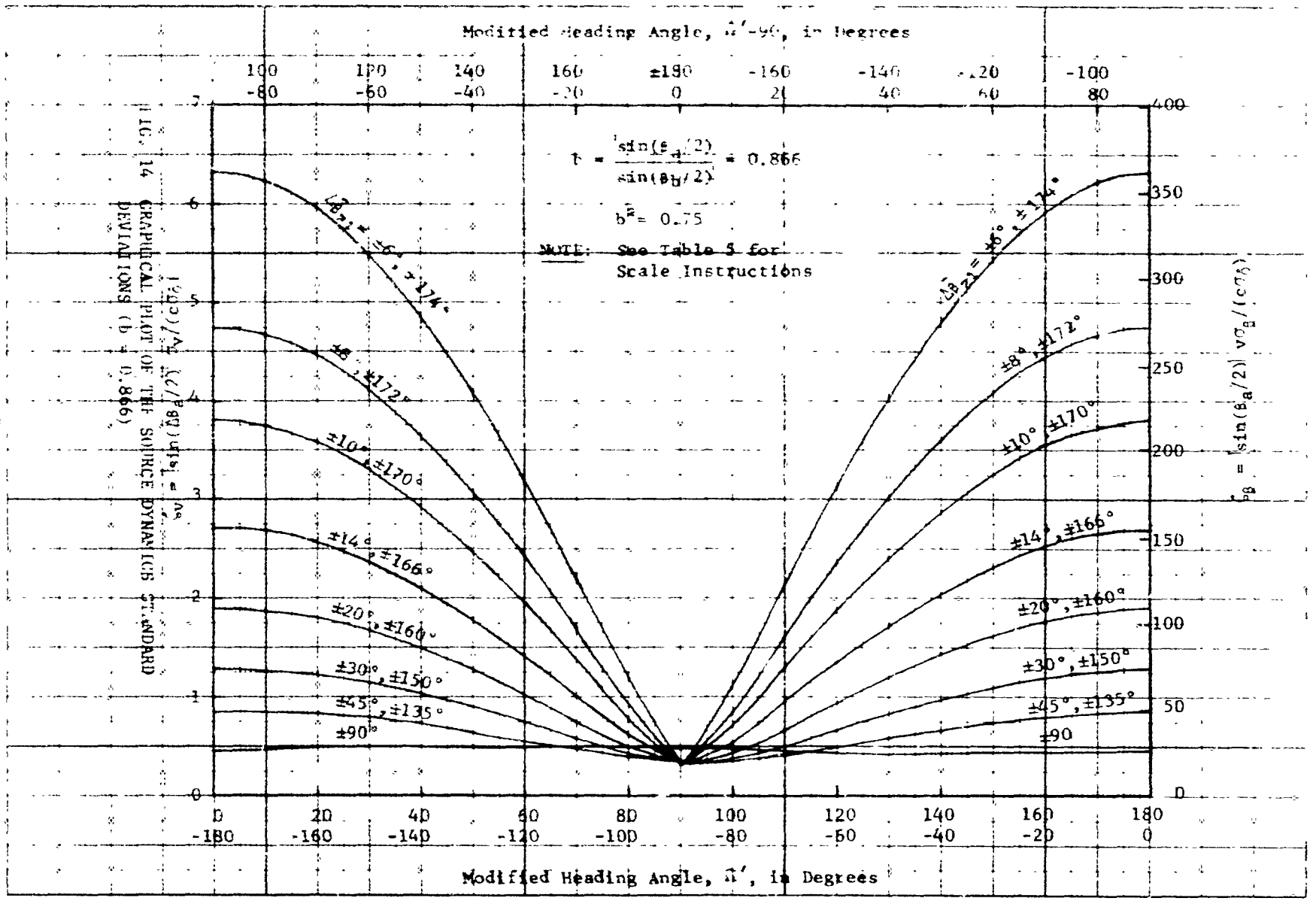

FIG. 14 GRAPHICAL PLOT OF THE SOURCE DYNAMICS STANDARD DEVIATIONS (β_d = 0.866)

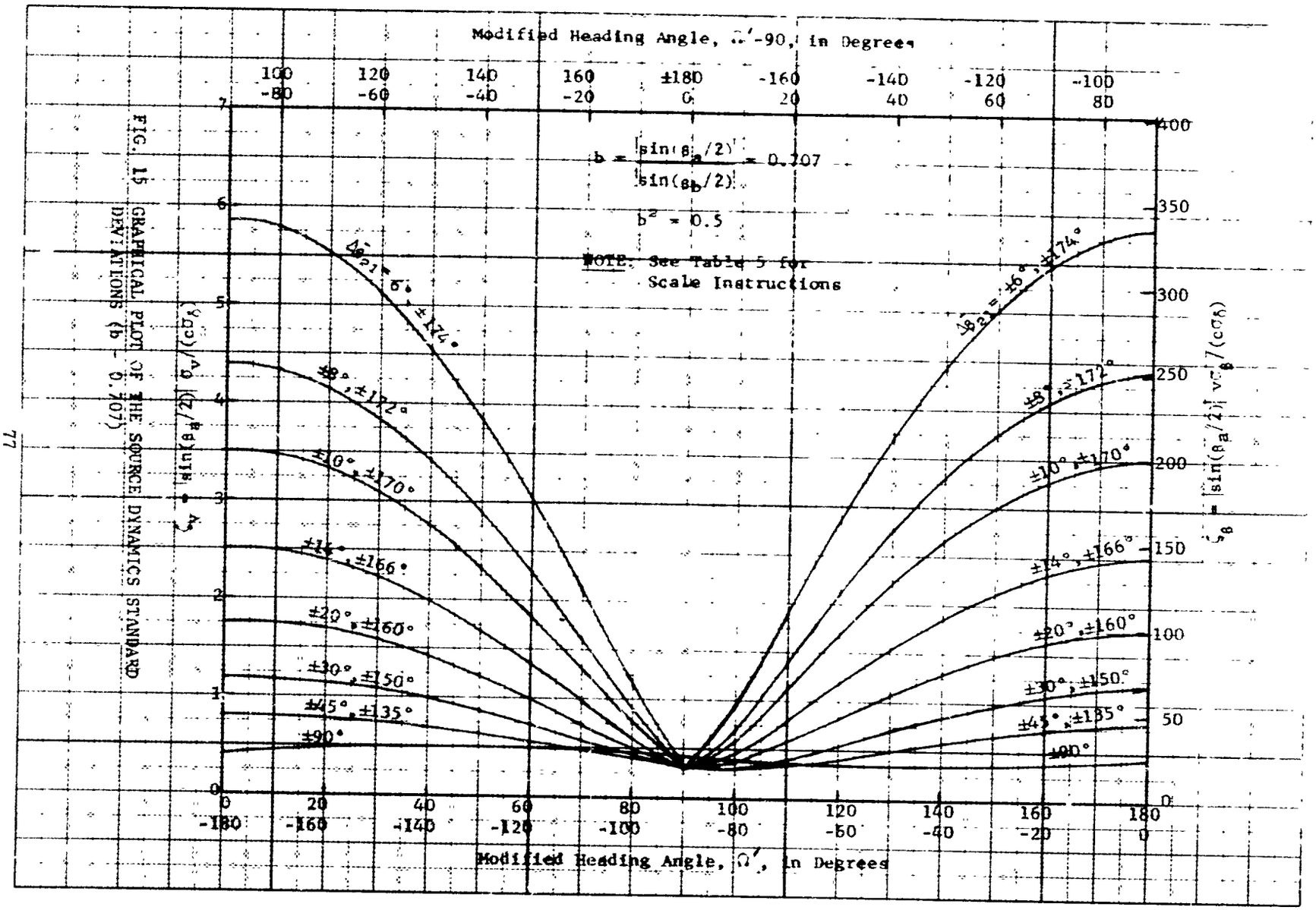

FIG. 15 GRAPHICAL PLOT OF THE SOURCE DYNAMICS STANDARD DEVIATIONS (b = 0.707)

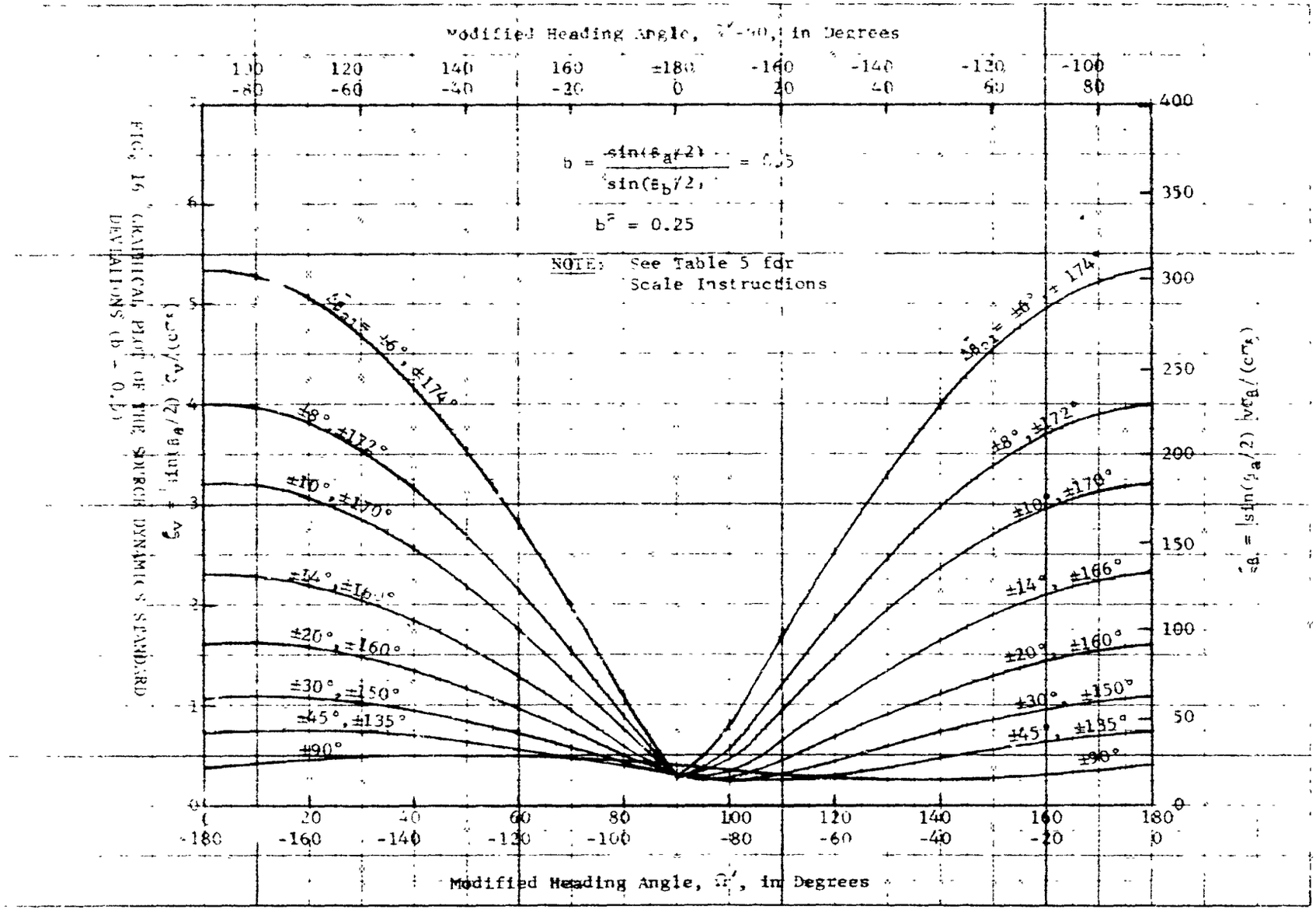

FIG. 16 GRAPHICAL PLOT OF THE SURFACE DYNAMIC STANDARD DEVIATIONS (ε_a = 0.1)

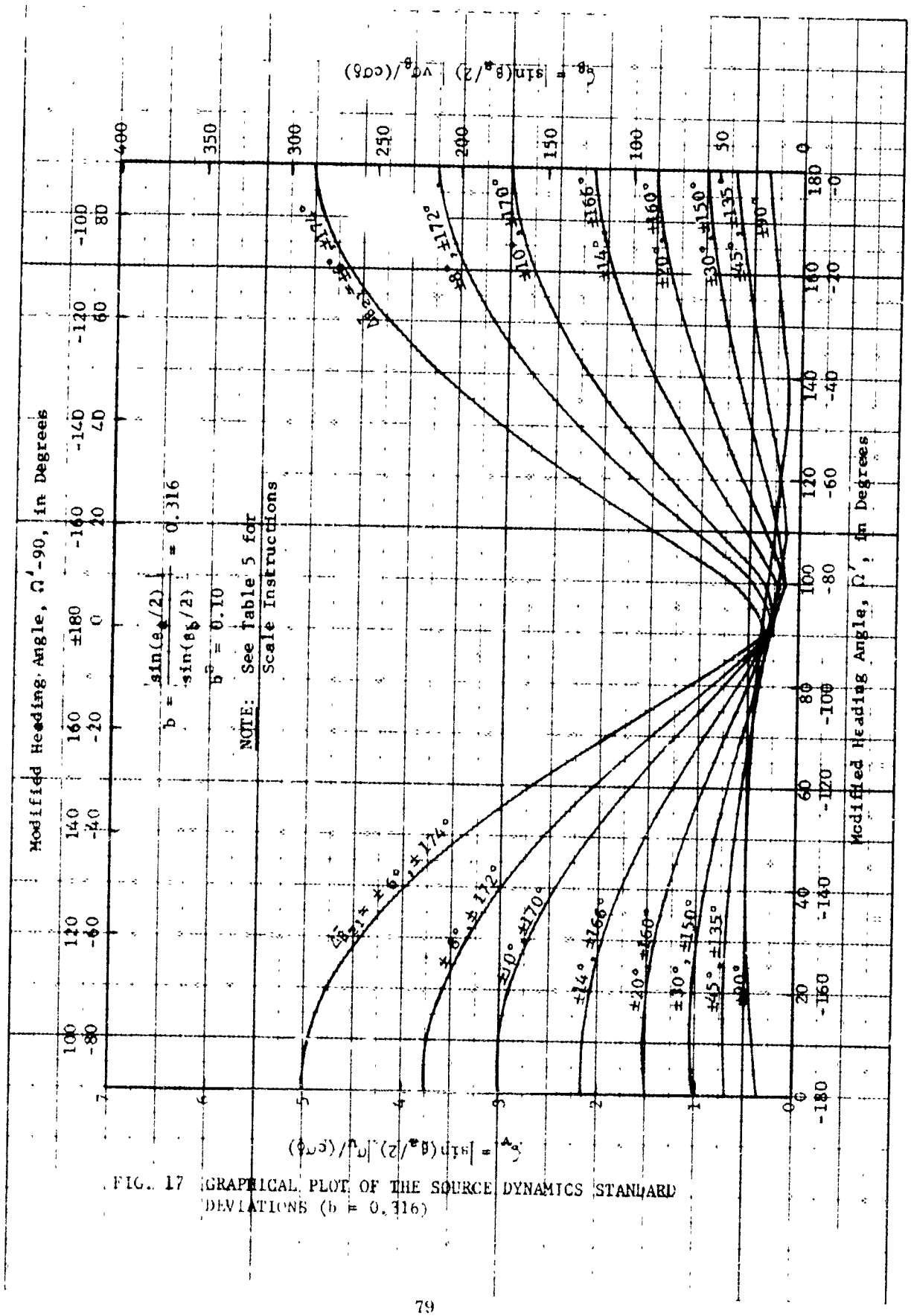

FIG. 17 GRAPHICAL PLOT OF THE SOURCE DYNAMICS STANDARD DEVIATIONS (b = 0.316)

(2) The dynamic error will be relatively insensitive to the parameter b (the ratio of the sines of the two sensor pair aperture half angles). Given the fact that the minimum of the two aperture angles is fixed, the fact that the larger of the two aperture angles is about equal to the smaller, or is very much larger, is of only minor significance. Naturally, the greater the difference, the better will be the source dynamics resolution. But, the improvement will be relatively small.

(3) The dynamic error sensitivity to the dual pair aperture angle, $\Delta\bar{\beta}_{21}$, will be strongly dependent on the source heading angle relative to the mean sensor angle $\bar{\beta}_{21}$ (see Figure 12). Over most heading angles, the dynamic error increases as the dual pair aperture angle becomes smaller, but the increase in error does not become excessive until this dual pair aperture angle reduces to something less than about fifteen degrees. For dual pair aperture angles below about five or six degrees, the loss in source dynamics resolution can become prohibitively large. An interesting and unexpected result is that, over a particularly narrow range of heading angles, the source dynamic resolution will be relatively independent of the dual pair aperture angle $\Delta\bar{\beta}_{21}$, and can even improve with a decrease in $\Delta\bar{\beta}_{21}$. The overall effect, though, is that a decrease in the dual pair aperture angle will result in a decrease in the source dynamic resolution (increased dynamic measure error).

(4) It was mentioned above that, for dual pair aperture angles, $\Delta\bar{\beta}_{21}$, different from ninety degrees, the resolution of the dynamic measures will be dependent on the source heading. An interesting facet of this phenomenon is that the velocity error and the heading error are in quadrature in this regard. That is, for those headings which minimize the velocity error, the heading error will be maximized. And, conversely, where the heading error is a minimum, the velocity error will be maximum. Thus, there appears to be a trade-off in resolution between the velocity measure and the heading (or course) measure as a function of the source heading. Naturally, there exists source headings which result in about equal resolution of both dynamic measures (where neither is maximum or minimum).

(5) Another interesting phenomenon is that when the absolute value of the dual pair aperture angle, $\Delta\bar{\beta}_{21}$, is less than ninety degrees, the minimum error for source velocity is

realized for source headings which are normal to the mean sensor direction, $\bar{\beta}_{21}$ (see Figure 12). Thus, the minimum error for source heading will occur for source headings along the mean sensor direction, $\bar{\beta}_{21}$. On the other hand, when the absolute value of the dual pair aperture angle, $\Delta\bar{\beta}_{21}$, becomes greater than ninety degrees, the converse will be true. That is, in this circumstance, the minimum error for source velocity will occur for source headings along the mean sensor direction, $\bar{\beta}_{21}$, and the minimum error for source heading will occur for source headings orthogonal to this direction.

(6) As an overall observation, it can be concluded that the source dynamics resolution will be near optimum when the two sensor pair aperture angles, $\Delta\beta_1$ and $\Delta\beta_2$, are large (preferably near 180 degrees) and the dual pair aperture angle, $\Delta\bar{\beta}_{21}$, is in the neighborhood of 90 degrees. As a consequence, when the source is located in the near field of the sensors; so as, to be effectively surrounded by the sensors, the resolution of the dynamic measures will be high. As the source location becomes remote from the general sensor configuration, the source dynamic resolution can be expected to decrease. But, this decrease in source dynamic resolution will continue only to the point where the source is removed approximately one-quarter of the way around the spherical globe from the geometric center of the sensor configuration. As the source location becomes further removed, the source dynamic resolution can be expected to improve again. And, as the source reaches the extreme far field, on the opposite side of the globe from the sensor configuration, the relevant aperture angles will, once again, achieve the same values they took on in the near field. Thus, the convergent zone properties discussed in regard to the sensor location resolution, will also apply to the sensor dynamics resolution. Consequently, it appears possible to achieve an unbelievably high heading and speed resolution for a source located at extremely long great circle ranges from the relevant sensor configuration when we are working in a spherical geometry. The practicality of this seeming paradox will be dependent on the ability to realize reliable signal propagation over the extremely long propagation paths.

4.0 EXAMPLES OF THE USE OF THE DYNAMICS ERROR DATA

To understand the use of the source dynamics error data, and to develop a general "feel" for the magnitude of the velocity and heading resolution which is achievable in practice, several examples will be given in the areas of electromagnetic wave propagation and in underwater acoustic propagation.

4.1 Electromagnetic Source Dynamics Application

In the following applications, it will be assumed that electromagnetic propagation, which essentially follows the earth's curvature, is employed to measure the source dynamics (heading and speed) of an aircraft in motion. The location and dynamics of the aircraft will be varied with respect to strategically located receiving stations. The geometry of the receiving stations will also be varied to demonstrate the effect of these parameters.

Four examples have been chosen for study, and the results are tabulated in Table 5 for easy reference. The upper portion of the table gives the postulated geometry and source dynamics. The central position of the table lists the results of the preliminary computations. And, the lower portion of the table illustrates the final results for the resolution of the target dynamics. The standard deviation of the target dynamics is first given in terms of the standard deviation for the basic time scale-factor measure, and then followed by actual numbers based upon an assumed value for $c\sigma_\delta$ which appears reasonable to achieve.

The first example (see Table 5) depicts a near field situation where the ranges to the source are less than the separation distance (D_1 and D_2) between sensor stations. The source velocity (speed of the aircraft) is given as 500 KTS. The second problem is identical to the first, except that the source has been translated to the extreme far convergence zone field on the opposite side of the globe. It will be noted that the resolution of the source (aircraft) dynamics is the same in both cases.

In the third and fourth examples, the sensor separation distance has been reduced to two hundred nautical miles. In the third example, the source ranges can be considered as intermediate, and in the fourth example they would be considered as reasonably long. The standard deviation of the source dynamics can be expected to degrade measurably due to the decrease in the source pair aperture angles. This is moderated, somewhat, by the fact that the dual pair aperture angle has been increased to ninety degrees. In addition, the higher source speed (600 KTS as compared with 250 KTS) has resulted in a higher resolution for the source heading.

TABLE 5 RESULTS OF FOUR EM DYNAMIC EXAMPLES

			EXAMPLE			
			#1	#2	#3	#4
D_1, D_2		(NMi)	1,000	1,000	200	200
R_1		(NMi)	500	10,300	400	1,200
α_1		(deg.)	30°	30°	18°	5°
r_2		(NMi)	400	10,400	300	800
α_2		(deg.)	45°	45°	30°	15°
v		(KTS.)	500	500	250	600
$\Omega=\beta-\bar{\beta}_{21}$		(deg.)	40°	40°	60°	20°
$\Delta\beta_1$		(deg.)	82°	82°	27°	9.5°
$\Delta\beta_2$		(deg.)	83°	83°	32°	13.8°
$\sin(\Delta\beta_1/2)$			0.66	0.66	0.233	0.083
$\sin(\Delta\beta_2/2)$			0.66	0.66	0.277	0.120
b^2			1	1	0.707	0.478
$\Delta\bar{\beta}_{21}$		(deg.)	45°	45°	30°	90°
σ_v		(KTS)	$1.14(c\sigma_\delta)$	$1.14(c\sigma_\delta)$	$3.22(c\sigma_\delta)$	$5.78(c\sigma_\delta)$
σ_β		(deg.)	$0.114(c\sigma_\delta)$	$0.114(c\sigma_\delta)$	$1.06(c\sigma_\delta)$	$0.437(c\sigma_\delta)$
$(c\sigma_\delta)$	σ_v	(KTS)	11.4 KTS	11.4 KTS	32.2 KTS	57.8 KTS
= 10 KTS	σ_β	(deg.)	1.14°	1.14°	10.6°	4.37°

The above examples illustrate that quite useful results should be achievable over a variety of system geometries and source dynamics.

4.2 Underwater Acoustic Applications

Since the subject theory is applicable to underwater acoustic propagation, we have considered four examples in this area for demonstration. The examples are presented in the same manner as for the electromagnetic propagation applications described in the last section. The resulting data are tabulated in Table 6 for convenient reference. (In the case of the

TABLE 6 RESULTS OF FOUR UNDERWATER ACOUSTIC DYNAMIC EXAMPLES

			EXAMPLES			
			#1	#2	#3	#4
D_1, D_2		(NMi.)	180	180	200	500
R_1		(NMi.)	200	380	1200	1200
α_1		(deg.)	30°	13°	15°	15°
R_2		(NMi.)	250	400	900	900
α_2		(deg.)	20°	10°	20°	20°
v		(KTS.)	10	20	25	25
$\delta = \beta - \bar{\beta}_{21}$		(deg.)	20°	45°	-30°	-30°
$\Delta\beta_1$		(deg.)	42°	26°	9.2°	22.8°
$\Delta\beta_2$		(deg.)	37°	25°	12.0°	29.2°
$\sin(\Delta\beta_1/2)$			0.363	0.225	0.080	0.198
$\sin(\Delta\beta_2/2)$			0.321	0.216	0.105	0.252
b'			0.78	0.925	0.589	0.617
$\angle\bar{\beta}_{21}$		(deg.)	40°	53°	60°	60°
σ_v		(KTS.)	2.96($c\sigma_\delta$)	2.92($c\sigma_\delta$)	5.63($c\sigma_\delta$)	2.27($c\sigma_\delta$)
σ_β		(deg.)	11.6($c\sigma_\delta$)	11.2($c\sigma_\delta$)	14.9($c\sigma_\delta$)	6.03($c\sigma_\delta$)
($c\sigma_\delta$)	σ_v	(KTS.)	0.44 KTS.	0.44 KTS.	0.84 KTS.	0.34 KTS.
= 0.15 KTS.	σ_β	(deg.)	1.74°	1.68°	2.24°	0.90°

underwater acoustic applications, a value for $c\sigma_\delta$ of 0.15 was assumed to be realizable and is employed in the last two rows of the table.)

In the first two examples a sensor separation distance (D_1 and D_2) of 180 nautical miles was chosen and source ranges in the near to intermediate field are presumed The resulting standard deviation for the dynamic variables

(source speed and heading) are comparable and fall within a range which appears quite attractive.

In the latter two examples, the source range has been increased to the neighborhood of one thousand nautical miles. The two examples are identical with the exception that the sensor separation distances (D_1 and D_2) have been increased from 200 nautical miles (in example #3) to 500 nautical miles (in example #4). The results demonstrate the improvement achieved by the wider sensor separation at the longer ranges.

The above examples demonstrate the usefulness of time scale-factor measure to determine source dynamics in underwater acoustic applications, providing the resolution of the time scale-factor measure, δ, can be made sufficiently high.

5.0 OPTIMUM SOURCE DYNAMICS RESOLUTION SYSTEMS

In following the analysis of source dynamic resolution, one may note that there exists a near optimum geometry for source dynamics resolution; beyond which, the resolution cannot be improved by geometric considerations. This optimum geometry is realized when $\Delta\beta_1$ and $\Delta\beta_2$ are both 180 degrees, and $\Delta\bar{\beta}_{21}$ is 90 degrees (see Figure 12). When this situation exists, equations (3-3) and (3-4) reduce simply to,

$$\sigma_v = \tfrac{1}{2}(c\sigma_\delta) \tag{5-1}$$

and,

$$\sigma_\rho = \frac{90}{\pi v}(c\sigma_\delta) = \frac{28.65}{v}(c\sigma_\delta) \tag{5-2}$$

The above relations will be realized when the source is located on the great circle paths which join the sensors in both pairs of receiving stations and when these great circle paths are orthogonal. When the latter requirement is not fully met, the result will not be seriously changed providing $\Delta\bar{\beta}_{21}$ does not become significantly less than about 45 degrees (see Figure 13). As a consequence, relations (5-1) and (5-2) will be applicable for the global navigation system described in Section IV, 7.2.

For a more localized situation, where a particular area is to be covered, the optimum sensor geometry would be as illustrated in Figure 18.

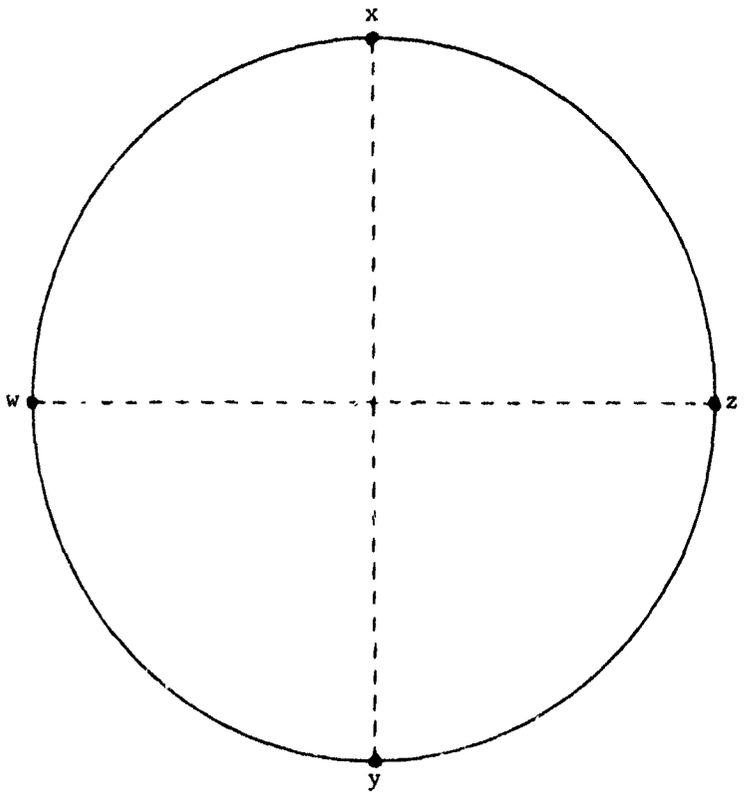

Fig. 18 Optimum Sensor Geometry for a Localized Area Coverage

In Figure 18 the sensor pairs are xy and zw, and the desired area of coverage lies within the circle joining all of the sensors. Naturally, the closer the source is to the center of the circle, the more nearly optimum will be the resolution. However, it can be shown that for the source located anywhere within the indicated circle, the standard deviation of the velocity error will be bounded by the relation,

$$0.5(c\sigma_\delta) \leq \sigma_v < 1.3(c\sigma_\delta) \qquad (5\text{-}3)$$

As it turns out, the same general system geometry which optimizes the source localization resolution will also be optimum for the source dynamics resolution.